UNIVERSITA' DEGLI STUDI DI MESSINA

Dipartimento di Scienze Chimiche, Biologiche, Farmaceutiche ed Ambientali

Dottorato di Ricerca in Scienze Chimiche

Ciclo XXXIII (2017 – 2020)

Engineered Biomaterials based on Hyaluronic Acid and Cyclodextrin Supramolecular Assemblies for Therapy and Diagnosis

Annalaura Cordaro

Supervisor

Prof. Anna Piperno

Co-supervisor

Dr. Antonino Mazzaglia

Coordinator

Prof. Paola Dugo

Indice

Aim of the work

Contemporary technological progress is essential for the development of modern medicine, providing knowledge, tools and materials to achieve more advanced and ambitious objectives. In the field of biomedical technologies, the study of *biomaterials* has become one of the cornerstones of research, due to its multiple applications and the vital importance they cover in the manufacture of prostheses or biomedical devices with various functions, both for internal and external use.

The so-called **biopolymers** are a set of materials, of natural or synthetic origin, which, due to a series of peculiar characteristics such as biocompatibility, biodegradability and non-immunogenicity, well suit for use in the biomedical field.

Recent advances in nanotechnology are greatly encouraging the design of new sophisticated biomaterials-based platforms with increasingly complex functions. Such fine materials are often designed to mimic a subset of the physicochemical properties of natural materials. Knowledge gained from fundamental studies is being used in conjunction with fabrication methods such as self-assembly to design biomaterials that optimally interface with the biology of the host.

This thesis focuses the attention on the development of new biomaterials based on cationic poly-cyclodextrin (PolyCD) and hyaluronic acids (HA). Physico-chemical properties of such engineered platforms were tailored by chemical modification using covalent and/or not covalent approaches. Complementary techniques including UV/Vis, steady-state, time-resolved fluorescence, DLS, zeta potential measurements, ^{1}H and ^{13}C NMR, Maldi-TOF etc. have been employed for the characterization of the functionalized polymers. Figure 1 reports a general overview of different nanodevices developed during PhD research activity. These engineered systems have revealed a broad versatility for their potential biological applications and have been investigated as carriers for drug delivery, hydrogel components and biosensing materials (Figure 1).

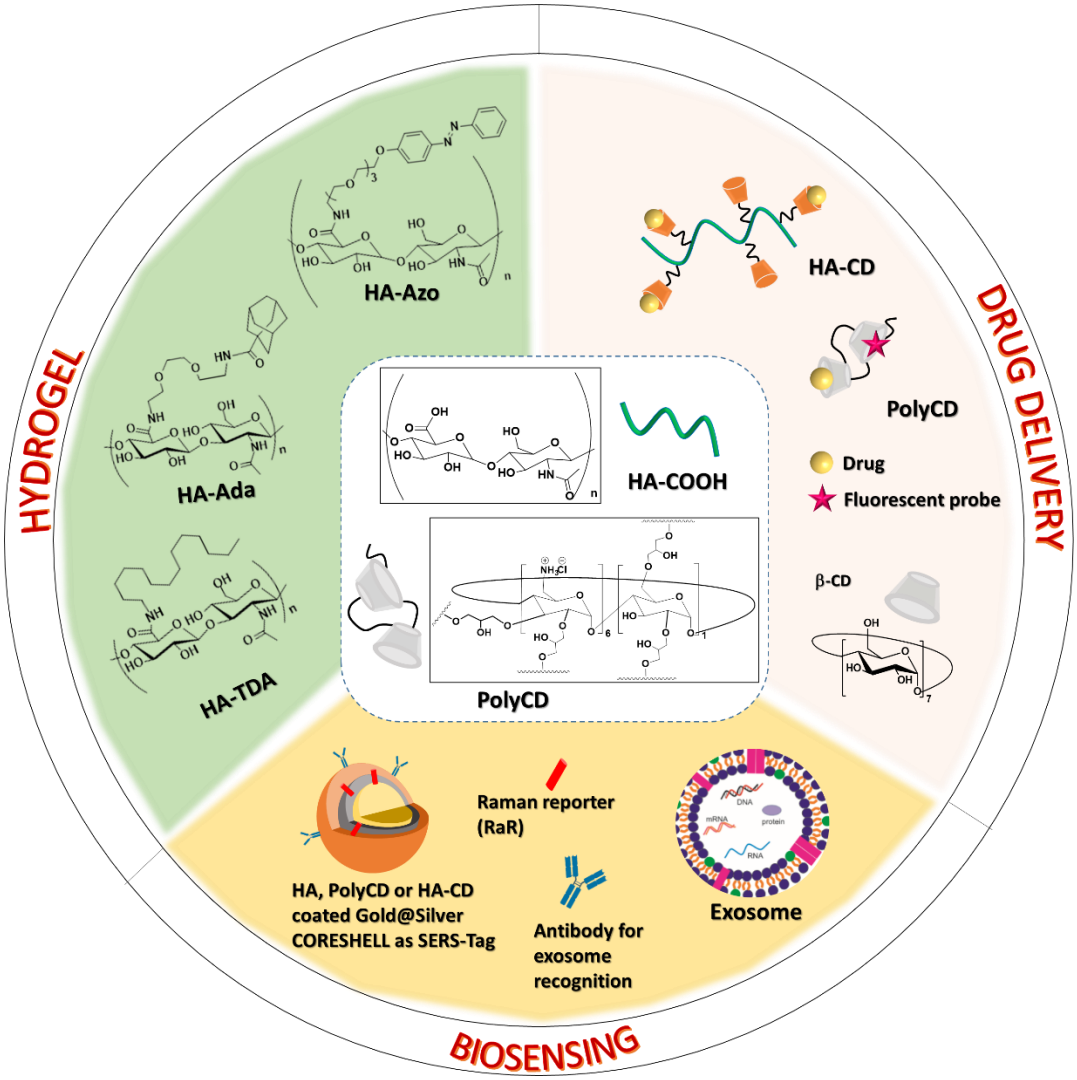

Figure 1 General overview of engineered platforms based on HA and PolyCD

The thesis is structured in four chapters. Chapter I reports an overview of the main characteristics of hyaluronic acid derivatives and cyclodextrin polymers: selected examples of literature data summarize the main biological applications describing the currently available procedures for their functionalization. Chapter II deals about the nanoassemblies based on PolyCD loaded with the non-steroidal anti-inflammatory drug Diclofenac (DCF) and linked by supramolecular interactions with a fluorescent probe (adamantanyl-Rhodamine conjugate, Ada-Rhod). PolyCD-based nanoassemblies (Figure 2) were investigated as anti-inflammatory nanomedicines to tackle critical pathological inflammation in osteoarticular diseases.

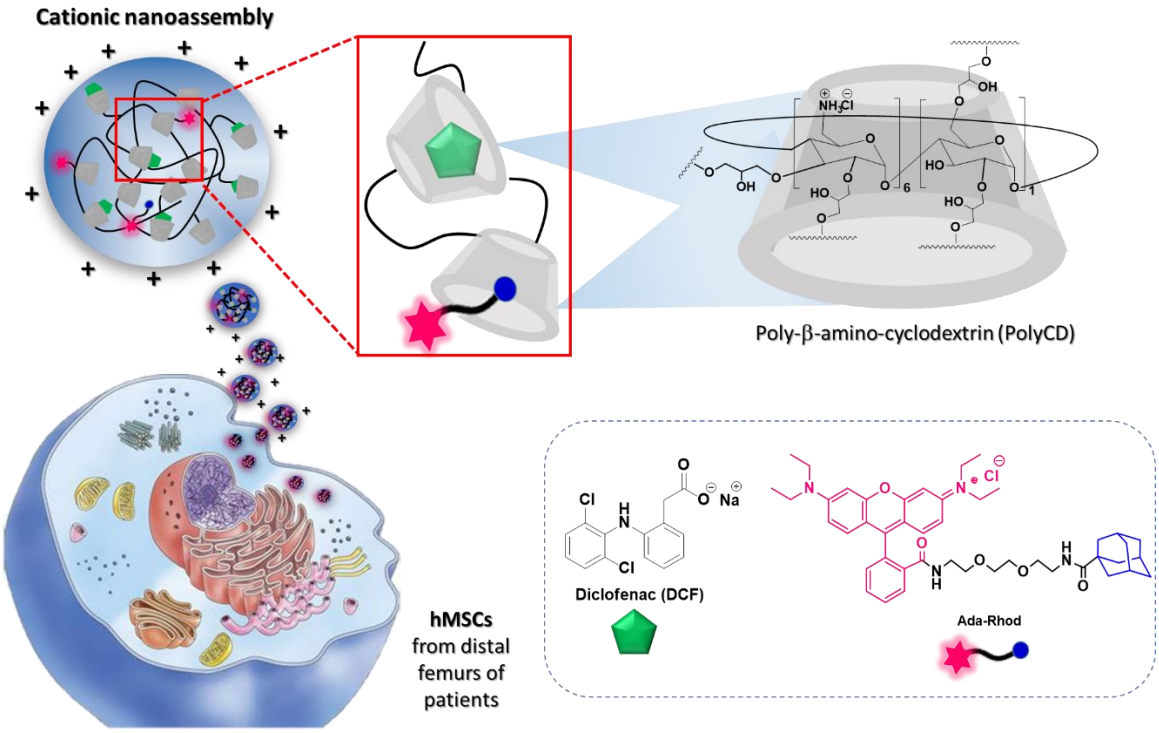

Figure 2 Sketched view of PolyCD@Ada-Rhod/DCF nanoassemblies

Chapter III reports the synthesis of new hyaluronic acid derivatives obtained by conjugation and click chemistry reactions. HA derivatives have been investigated as hydrogel components and as platforms for the delivery of antiviral drugs (Figure 3). Specifically, this section reports the results of the research project about supramolecular hydrogels obtained during an abroad research period carried out at the Institute of Soft Nanoscience of the Westfälische Universität in Münster (Germany), under the supervision of Prof. Bart Jan Ravoo.

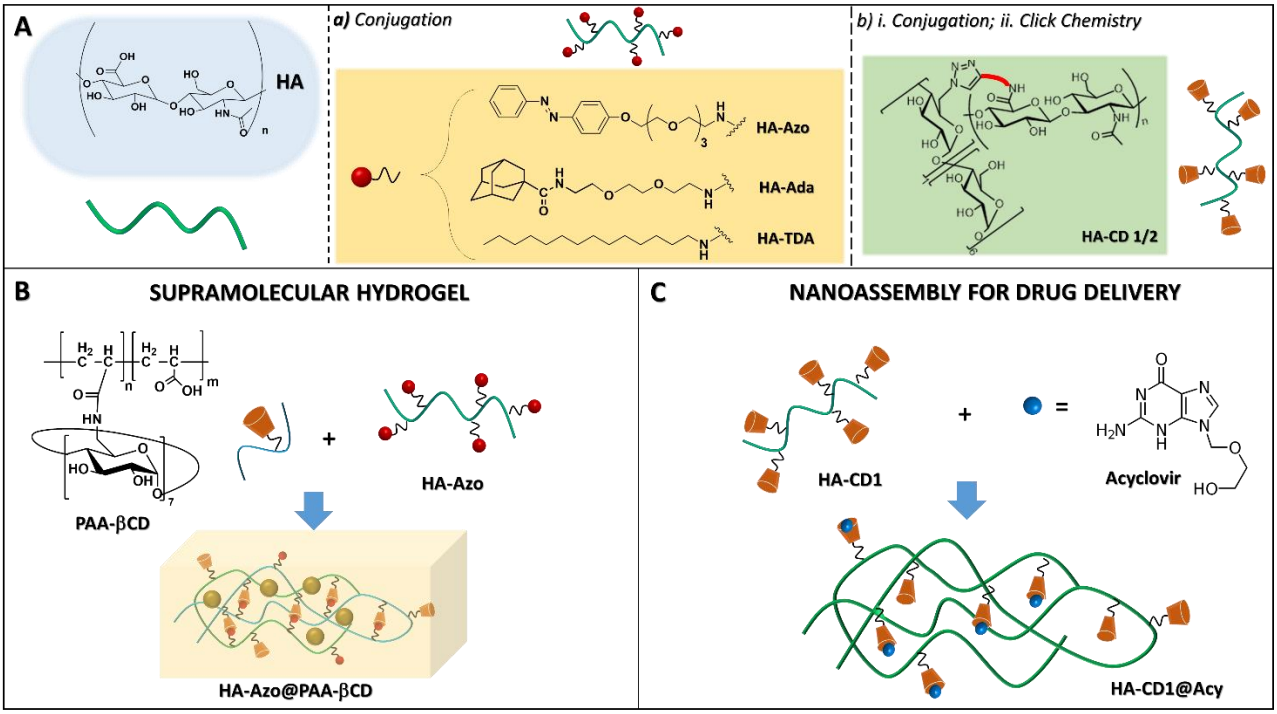

Figure 3 Derivatized HAs investigated as hydrogel components and drug delivery platforms

Finally, Chapter IV describes the preliminary results about the synthesis and characterization of Gold@Silver Core-Shell nanoparticles (Au@Ag NPs), coated by a polymeric matrix. Specifically, the synthesis, the physicochemical properties and the interaction with selected Raman reporters (RaRs) of Gold@Silver Core-Shell NPs obtained from cationic poly-cyclodextrin (PolyCD), Hyaluronic Acid (HA), and Hyaluronic acid modified with β-cyclodextrins (HA-CD) will be discussed. Gold@Silver NPs are proposed as SERS-Tag for exosomes recognition (Figure 4).

Exosomes are a subgroup of cell-derived nanosized extracellular vesicles that have been recently recognized as new mediators for many cellular processes. They emerged as potential biomarkers for non-invasive disease diagnosis and monitoring of treatment response, especially in cancer therapy.

This research project is carried out in collaboration with Prof. Simion Astilean and Dr. Alexandru Hada from the Interdisciplinary Research Institute in BioNano-Sciences, Babes-Bolyai University (Romania).

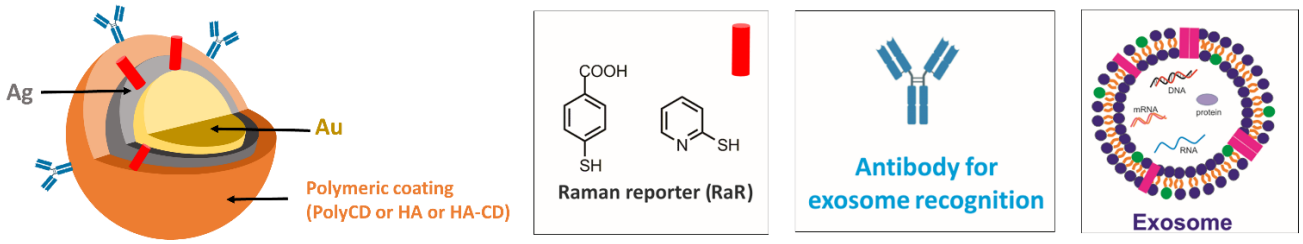

Figure 4 Schematized view of materials used for the preparation of Gold@Silver Coreshell NPs

Chapter 1

Biomaterials

Biomaterials were firstly defined as: "... substances systematically and pharmacologically inert, designated for implantation within living tissues or for their incorporation into them."[1] Subsequently in November 1982, during the Consensus Development Conference on the Clinical Application of Biomaterials (Bethesda, USA) a group of experts elaborated the following definition: “Any substance or combination of substances, other than a drug, of synthetic or natural origin, which can be used for any period of time, alone or as part of a system that treats, make it grow or replaces any tissue or organ in the body.” The latter definition was changed a few years later in a second Consensus Development Conference in 1986, this time in Chester, into a different and more concise explanation of the term biomaterial: “... a non-living substance, used in the manufacture of a medical device that has in some point an interface with a living tissue ...” [2]. Hence, the need for contact between biomaterial and tissue of the recipient organism becomes a fundamental aspect: the “coexistence” of these is the basis for the survival of any prosthesis or artefact. This ability of the biomaterial to coexist within the body takes the name of **compatibility**, or **biocompatibility**. By compatibility we generally mean the ability of an object, an artifact, a material, to coexist, cohabit, integrate with a tissue, an organ, a receiving site in a living organism. A material is compatible if, inserted in a host site, it does not induce significant adverse effects and does not even suffer from it.[3]

The major problem encountered in the design of a biomaterial is having to cope with the various and severe conditions to which the material must undergo in a very complicated and aggressive environment such as the human body. In fact, when we talk about compatibility we refer to a *biological compatibility* (biocompatibility) understood as the attitude of the material not to determine adverse reactions in the organism, which reacts to every foreign body implanted in a tissue recognizing it as "non-self", in non-specific and specific ways.[4]

By *chemical compatibility*, we mean the property of the biomaterial to not undergo, once placed in its biological context of use, such chemical processes that could make its function impossible or make it lose its biological compatibility, or those chemical metabolic processes that could determine the generation of toxic products for the organism. Finally, for *mechanical or physical compatibility*, is intended the suitability of the biomaterial to perform the function for which it is intended, therefore, to present characteristics (such as hardness, modulus of elasticity, etc.) similar to the microenvironment as it must face the forces applied in the administration site. [5] The chemical composition of biomaterials has been the focus of their design for the past few decades, but there is growing appreciation of the importance of other properties, because they have significant effects on how cells perceive, interact and internalize the material, which affects the efficacy of those used as drug carriers or vehicles to target specific cells and tissues in the body. In addition to mechanical properties and size, external and environmental stimuli, such as temperature, electromagnetic fields or light irradiation are increasingly being used to modulate the performance of biomaterials, often by dynamically altering their structure. Hydrogels, for example, can be designed to change their swelling behavior and stiffness in response to particular cues.

1.1 Biomaterials in drug delivery

A major focus in biomaterials research regards the development of effective strategies to deliver pharmacologically active agents to manage, treat or cure diseases. It is well known that the modality of delivery affects numerous factors that contribute to therapeutic efficacy, including pharmacokinetics, distribution, cellular uptake and metabolism, excretion and clearance, as well as toxicity. Furthermore, drugs can lose their pharmacological activity due to changes in environmental factors such as humidity, temperature, and pH, which can occur in the body or during storage.[6] Recent advances in the study of biomaterials for drug delivery are enabling significant progress both in biology and medicine. Multidisciplinary collaborations between physical scientists, engineers,

chemists, biologists and clinicians have generated major breakthroughs for a range of diseases and in particular for cancer therapy and autoimmune diseases. Despite these efforts, drug delivery still remains a prominent challenge because of the limited understanding of biological barriers and physiological mechanisms, that is why there is an urgent need for the design, implementation and translation of biomaterials in this field (Figure 1).

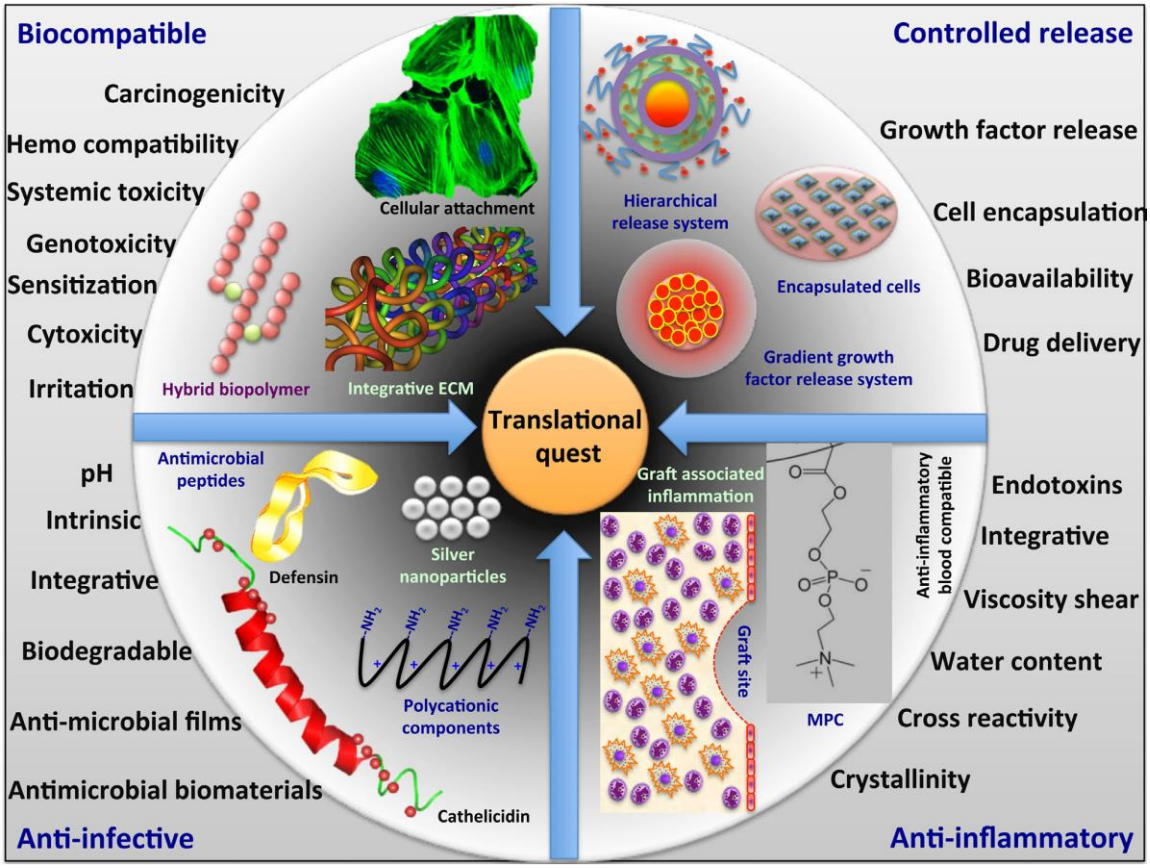

Figure 1 Translational quest for next generation biomaterials[7]

Biomaterials have improved the delivery and efficacy of a range of pharmaceutical compounds including antibodies, peptides, vaccines, drugs and enzymes, among others.[8] In particular, the polymer and lipid-based materials development for drug delivery has been driven by advances in organic and synthetic chemistry, materials science, genetic engineering, and biotechnology.[9] Many of these materials have been designed to release therapeutics for extended periods of time and can be

further modified to target specific sites within the body, thereby reducing the amount of drug to achieve the desired therapeutic effect along with reduced toxicity. The physicochemical properties of biomaterials and their intended route of administration can be systematically tailored to maximize therapeutic benefits, always considering that each route has its own advantages and limitations, thus requiring the design of biomaterials to be uniquely suited for the intended administration route.[10] New "smart" or responsive biomaterials which have the potential to exploit and respond to these mechanisms are also in demand. Nevertheless, compatibility remains a key factor to avoid the immune responses, thus for the development of implantable devices for long-term controlled drug release, cell-based therapies, implantable sensors, as well as tissue engineering and regenerative medicine.

1.2 Polysaccharide-based biomaterials

Polysaccharides are an important class of biomaterials with significant research interest for a variety of drug delivery and tissue regeneration applications. These polymers, belonging to the carbohydrates family, are often isolated and purified from renewable natural sources including plants, animals and microorganisms. Thanks to their biochemical similarity with human extracellular matrix components they are rapidly recognized and "accepted" by the body. Among their numerous advantages they benefit of natural abundance, relative ease of isolation and various sites for chemical modification. In fact, polysaccharide structure offers freely available hydroxyl, carboxylic and amine functionalities (Figure 2) that make it possible to alter and tune their physicochemical properties by modifying their structure.[11]

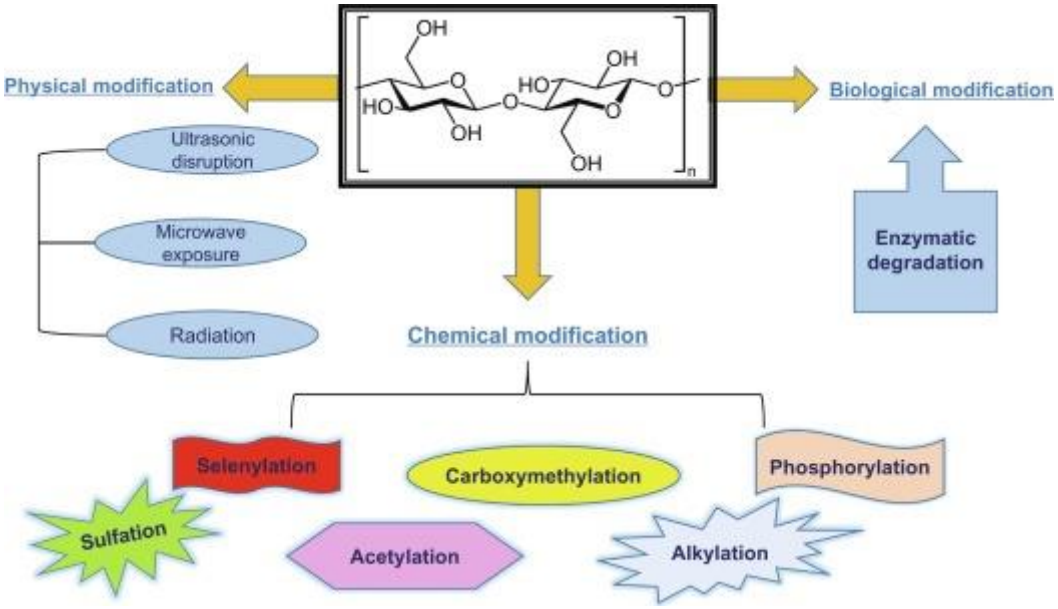

Figure 2 General structure of polysaccharide-based polymers and common modification approaches [12]

In addition, these polymers undergo enzymatic degradation in biologic environments into non-toxic byproducts and they are generally components of the extracellular matrix (ECM) in the organisms, thus they participate in inter and intracellular signaling pathways, contributing to cell growth. In spite of many merits as biomaterials, these polysaccharides suffer from drawbacks including variations in material properties based on source, microbial contamination, uncontrolled water uptake, poor mechanical strength, and unpredictable degradation patterns. For these reasons, by combination with appropriate hydrophobic counterparts, polysaccharide-based porous scaffolds, fiber matrices, hydrogels and micro/nano particles have been developed for a variety of tissue regeneration and drug delivery applications (Figure 3).[13, 14]

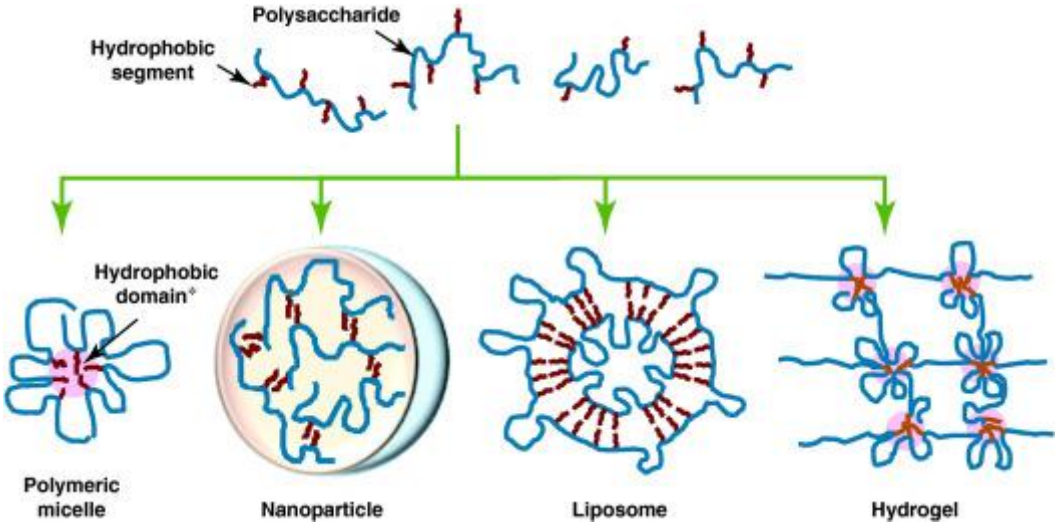

Figure 3 Schematic depiction of different drug delivery systems formed by self-association of amphiphilic polysaccharides in aqueous solution. Hydrophobic domain due to the association of hydrophobic groups[15]

1.3 Cyclodextrins

Cyclodextrins (CDs) are a series of oligosaccharides, consisting of 6 (αCD), 7 (βCD) or 8 (γCD) glucopyranose units attached by $\alpha(1\rightarrow4)$ glucosidic bonds. Also known as cycloamyloses or cyclomaltoses, they can be obtained by enzymatic degradation of starch or by metabolism of a certain bacteria, *Bacillus macerans.* [16, 17] First isolated in 1891 by the French scientist Villiers, they were initially identified as "cellulosine" because of the characteristics similar to cellulose, such as resistance towards hydrolysis and absence of reducing power.[18] Concerning the tridimensional structure, although CDs are ring molecules, due to the lack of free rotation between the glucopyranose units, they are not cylindrical but, rather, they can be considered shaped as a truncated cone (Figure 4).[19] Structural studies have revealed that secondary hydroxyl groups (C2 and C3) are located on the wider edge of the ring, whereas the primary hydroxyls (C6) are located at the narrow side. The C3 and C5 hydrogens are located at the inside of the torus-like structure, together with the ether-like oxygen. As a result, these molecules assume a peculiar conformation, owing a hydrophilic exterior which makes them relatively water soluble, and a hydrophobic inner cavity (with an internal diameter

of ca. 4.5, 7.0 and 8.5 Å for α-, β- and γ-CD, respectively) able to entirely or partially accommodate suitably sized lipophilic low molecular weight molecules.[20]

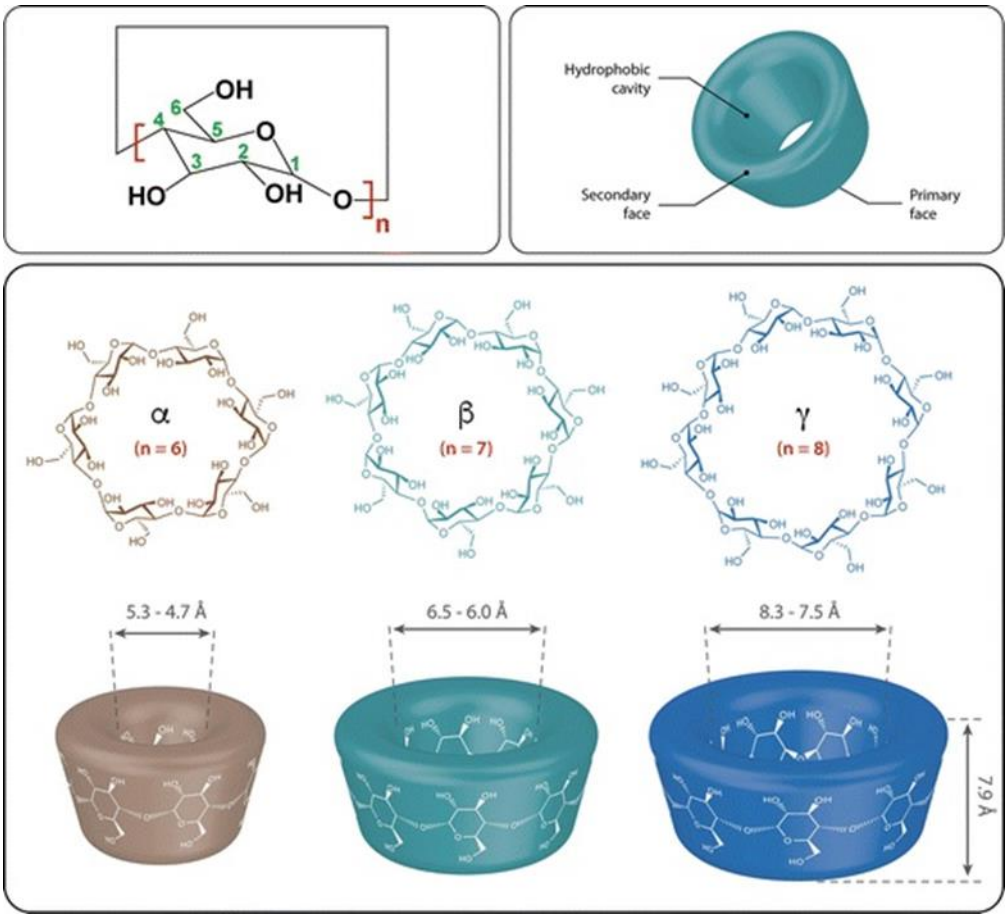

Figure 4 Structures of α, β and γ cyclodextrins[21]

The driving forces behind the formation of these so-called *host-guest* inclusion complexes are mainly hydrophobic van der Waals interactions, although other factors also play a role, including pH and ionization state, temperature and method of preparation.[22] In aqueous solutions, the non-polar cavity of CDs is occupied by water molecules. Thus, the inclusion complex formation is thermodynamically associated with an increase of entropy related to the displace of water molecules from the cavity in favor of an apolar-apolar association and a lower, more stable, energy state.[23] The binding of guest molecules within the host cavity is not permanent, but rather a dynamic equilibrium. So, formation of an inclusion complex is the result of a thermodynamic equilibrium between the free guest, CD molecules and the complex. Besides 1:1 interactions, many other host-guest stoichiometries have

been identified and studied, with guest molecules encapsulated by more than one CD (1:2) or lower order complexes where one CD interacts with multiple guests (2:1). Many methods are reported for the preparation of inclusion complexes, such as: co-evaporation, co-precipitation, spray-drying, freeze-drying, kneading, sealed-heating and supercritical fluid technology.[24-27] Techniques such as scanning electron microscopy (SEM), ultraviolet spectroscopy, differential scanning calorimetry (DSC), thermogravimetric analysis (TGA), infrared spectroscopy and X-ray diffraction are commonly used to demonstrate inclusion complex formation.[20, 28] Thanks to these peculiar properties, CDs have been widely used as models to understand the mechanisms of molecular recognition. Therefore, for their good solubility, bioavailability, safety and stability, their use has a long history in pharmacy, analytical sciences, separation processes, pesticides, foodstuffs, cosmetic and packaging industries.[29, 30] In the pharmaceutical field, CDs have been applied as solubilizers for lipophilic drugs to enhance their bioavailability and/or reduce adverse effects after oral, parenteral or other routes of administration, as safe excipients in some formulations and as effective carriers to vehicle drugs. In fact, after administration of a drug/CD complex, its dissociation leads to drug release in relevant body compartments, which is mediated by dilution effects, competitive replacement by tissue/serum components (e.g., lipids or cholesterol), and drug binding to cellular membranes or other tissue structures. Parenteral administration is generally preferred because of their poor absorption from the gastrointestinal tract (ca. 3%). However, they are poorly susceptible to hydrolytic action of body enzymes and mainly excreted unaltered by renal filtration. [31]

Depending on the CD subtype, dose and route of administration, some adverse effects have been reported occasionally. For example, at high concentrations, CDs can extract cholesterol and other lipid membrane components from cells (e.g., erythrocytes), leading to disruption of cell membranes.[32] In addition, related to internal hydrogen bonding between CD's hydroxyl groups, unmodified CD has a relatively low aqueous solubility (18.5 $mg \cdot mL^{-1}$),[33] consequently after parenteral administration of

high doses of CDs, crystalline precipitates of CDs or their complexes with, for example, cholesterol can be formed in the kidneys, leading to nephrotoxicity.

1.3.1 Chemically modified cyclodextrins

Natural cyclodextrins have some drawbacks, such as a limited solubility in most of the commonly used solvents and the limited reactivity due to the presence of only one type of functional group. Thus, to maximize their utilization possibilities, derivatization of one or more of their hydroxyl groups is necessary. For practical purposes, the CD derivatives can be classified according to their intended use as: carriers for active substances (as solubilizers or stabilizers), separating agents in chromatography, catalysts, enzyme models, additives, detergents or viscosity modifiers.[34]

Another reason for CD structural modification is to achieve specific binding behavior. Attachment of one or more substituents on the macrocycle backbone can significantly modify the strength of non-covalent interaction with specific guest. Due to the highly-functionalized and symmetrical nature, selective modification of CD remains very challenging task.[35] The preparation of selectively substituted CD derivatives often involves extensive purification procedures to recover pure single isomer compound. This is indisputable justification for the effort put in developing new synthetic strategies which would allow synthesis of pure derivatives in reasonable yields.

1.3.2 Cyclodextrins in the pharmaceutical field

CDs have been extensively utilized to form inclusion complexes with drugs through host-guest interactions both in pharmaceutical science and technologies. Actually, there are over 30 marketed pharmaceutical products based on CD complexes.[36] The major applications include: increasing drug solubility and stability,[33] masking odor and tastes,[37] controlling drug release profiles and improving drug permeability across biological barriers (absorption enhancers).[38] Conventional pharmaceuticals formulated using CDs can be dosed by oral, nasal, ocular, rectal and dermal delivery. To further

improve the pharmaceutical features of native CDs with respect to solubility, inclusion capability, controlled drug delivery capacity and toxicity, chemically modified CDs have been synthesized, including highly soluble,[39] amphiphilic, and hydrophobic derivatives.[40-42] The excellent biocompatibility and unique inclusion capability as well as powerful functionalization capacity of cyclodextrins and their derivatives makes them especially attractive for engineering novel functional materials for biomedical applications.[30, 43-45] Recently, the interest towards CDs as building blocks to construct functional materials has grown. In fact, they can lead, via supramolecular interactions, to the formation of novel higher order structures (Figure 5) which properties can be tuned with a series of external stimuli, e.g. enzyme activation, light, temperature, pH changes, redox reactions and competitive binding.

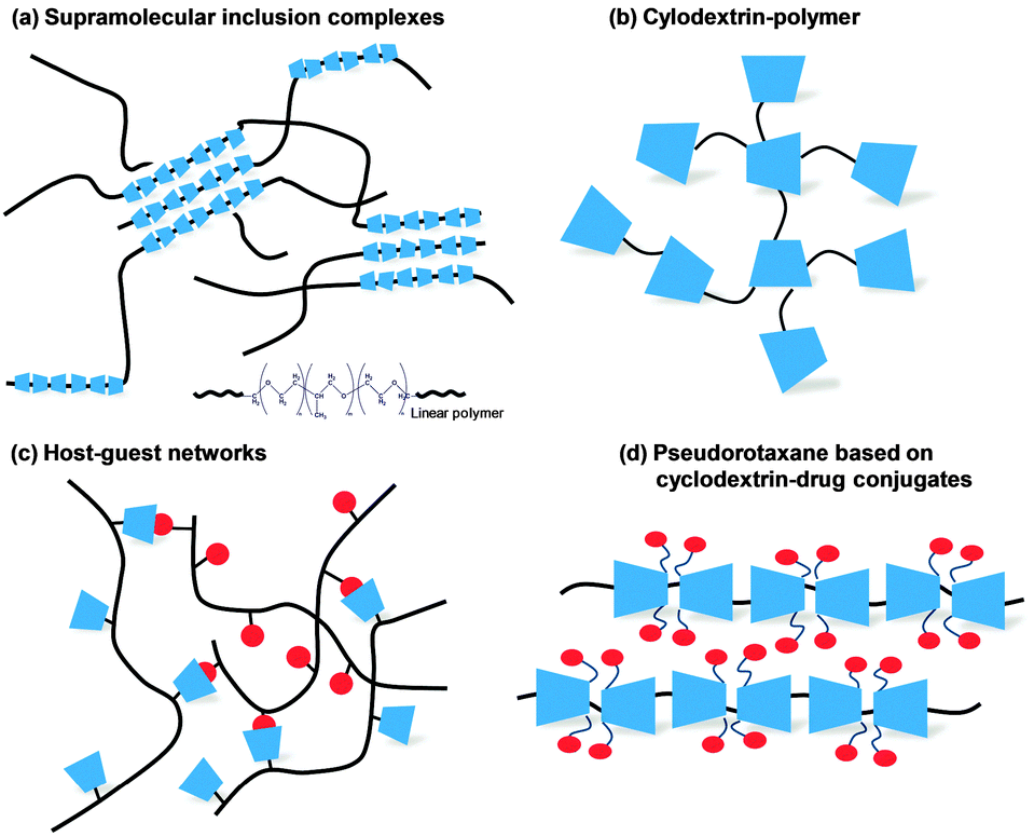

Figure 5 (a) Schematic structure of supramolecular CD-based inclusion complexes, (b) representative structure of a CD–polymer, (c) supramolecular host– guest networks and (d) pseudorotaxanes based on CD–drug conjugates[46]

1.4 Cyclodextrin polymers

A broad spectrum of CD-containing polymers with versatile architectures has been synthesized to assemble functional platforms.[16, 47-50] These assemblies have found wide applications in drug delivery,[51] gene therapy,[52] and medical imaging. [16] These polymers possess diverse architectures varying from linear, grafted, block, branched, to hyper-branched and dendritic, while the CD units can be either covalently linked in the main chains or conjugated as flanking side groups (Figure 6).

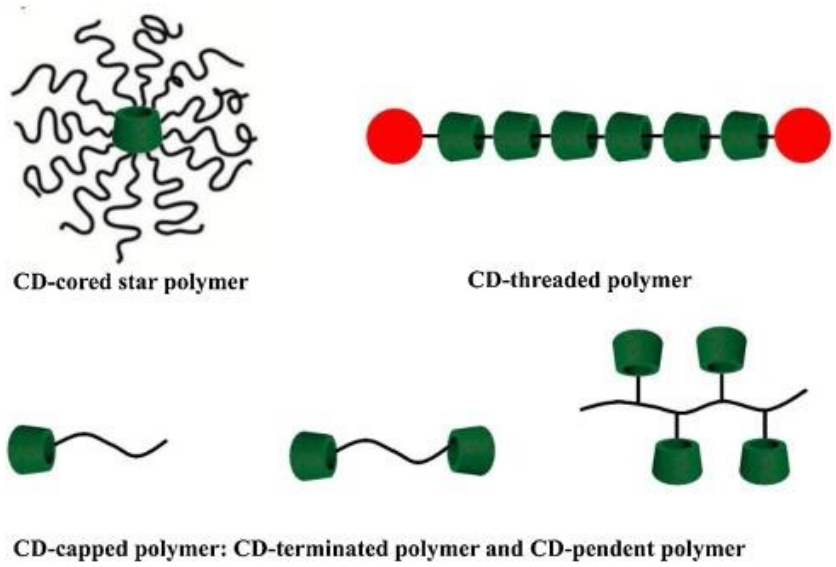

Figure 6 Some examples of CD-based polymer architectures[53]

A facile approach to prepare CD-containing polymers is the polycondensation of CDs with epichlorohydrin (EPI) in alkaline solution of NaOH.[54] To improve swelling properties, reduce toxicity (e.g., membrane disruption) and increase drug loading efficacies, EPI cross-linking has also been performed in the presence of cationic or anionic compounds. Although the encapsulation efficiency and release may be reduced respect to neutral EPI cross-linked systems, the cationic networks show improved internalization efficiency, which, if it is counterbalanced by reduced toxicity, is beneficial for their application as drug carriers.[16, 55] Moreover, compared with nonionic counterparts, charged CD polymers have additional electrostatic interactions with oppositely charged guest molecules to

achieve a synergistic effect.[56] Nevertheless, polymers thus obtained generally exhibit branched structure and broad molecular weight distribution. This type of CD-based polymers has been widely employed to construct nanospheres, nanogels or hydrogels and nanocapsules, via host-guest interaction in the presence of appropriate guest molecules (Figure 7). Besides EPI, examples of other cross-linking agents commonly used to create CD-based networks are diepoxides (e.g., alkyleneglycoldi(epoxypropyl)ethers),[57, 58] diisocyanates (e.g., hexamethylene diisocyanate (HMDI)),[59, 60] and anhydrides.[61]

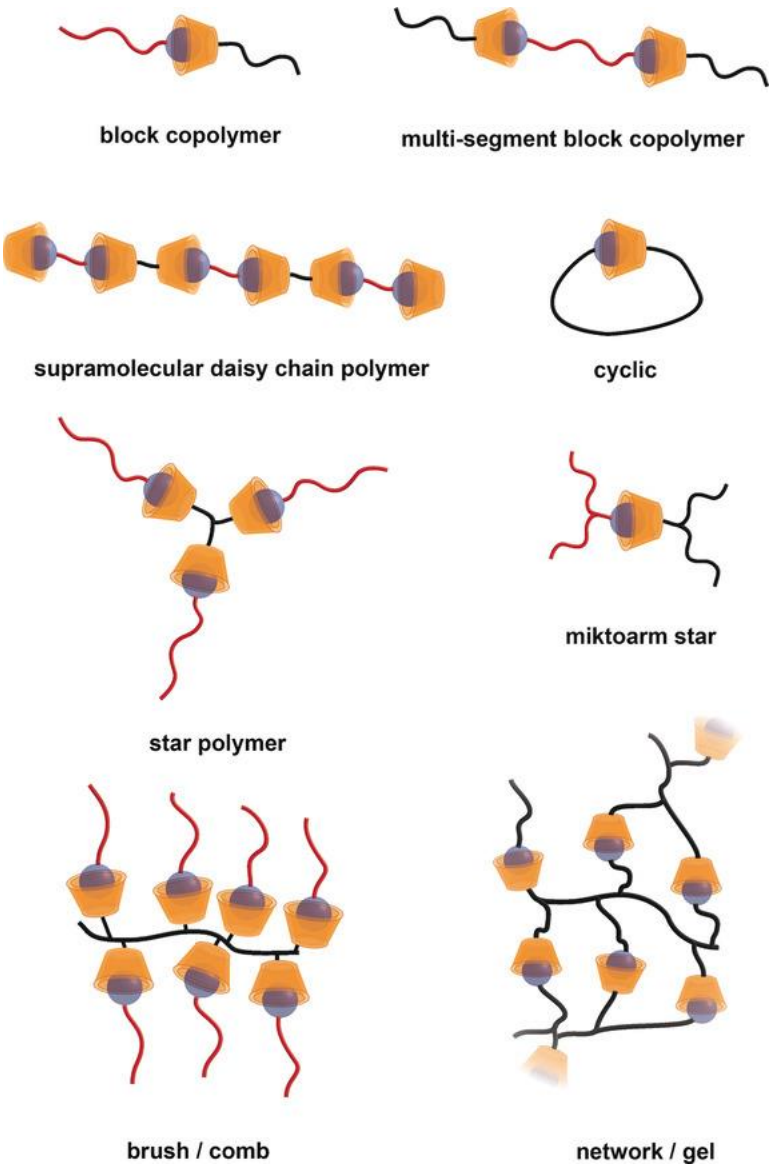

Figure 7 Higher level supramolecular structures obtained via host-guest interactions with cyclodextrins.[62]

Besides polymerization of CDs using low molecular weight cross-linking agents, covalently cross-linked systems have also been developed by coupling either modified or unmodified CDs to a wide variety of pre-existing polymers.[63] Many cyclodextrin-containing polymer networks have been prepared for example by using CD itself as a cross-linking agent. CDs have been covalently conjugated onto various polymers to modify physicochemical properties, to improve biocompatibility, to enhance drug/gene delivery capabilities,[64] or to impart macromolecular hosts with multiple binding sites. These CD-containing polymers were utilized to fabricate supramolecular assemblies across nano, micro, and macro-scales. Generally, two approaches are employed to synthesize CD-pendant polymers: a) direct polymerization of CD-containing monomers or copolymerization with other monomers, which is frequently used to prepare CD-pendant acrylate polymers (PAA-CD); b) coupling the functionalized CDs to the target polymers or their derivatives, which is generally applied to polymers with terminal functional groups. In many cases, this may significantly reduce the CDs' rotational freedom and their accessibility toward guest molecules. In this kind of strategy, CD derivatives that contain only one reactive group are often preferred. Synthesis of these monosubstituted CD derivatives requires a careful control of reaction conditions and extensive purification steps, because of the inherent polyfunctionality of CD (multiple hydroxyl groups). Among all the hydroxyl groups present on CD molecule, the ones at position 6 are the most basic, most nucleophilic and considerably accessible. Thus, under standard conditions, the electrophile will attack this position predominantly. As an example, *tert*-butyldimethylsilyl chloride will selectively give substitution toward position 6, whereas the more reactive trimethylsilyl chloride reacts with all the hydroxyls indiscriminately. The most commonly applied method to prepare monofunctionalized CD involves a reasonably selective reaction of *p*-toluenesulfonyl chloride (*p*-TsCl) or tosylimidazole with a primary hydroxyl group at the 6-position of CD,[65, 66] followed by purification via crystallization (from water) or chromatography. The resulting mono-6-tosylated CD can then be converted into other mono-6-substituted CD derivatives by attack of suitable nucleophiles, including azides, amines (e.g., alkyl amines and hydroxylamine), iodide, and

thioacetate (Figure 8).[42, 67] Monotosylation of unmodified CDs in the position 6 is a typical starting reaction leading to a reactive CD intermediate, which can be easily converted to a range of useful derivatives.

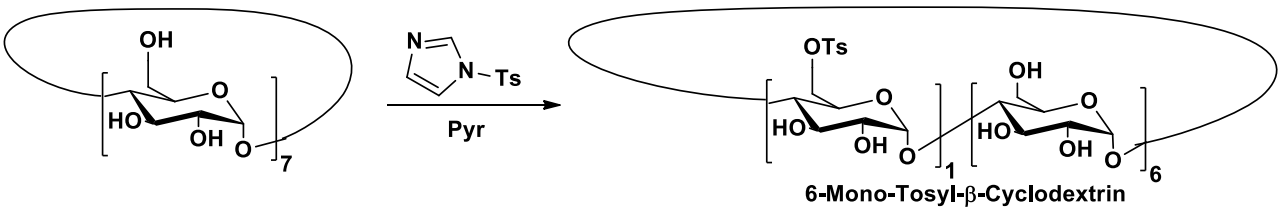

Figure 8 Synthesis of intermediate Ts-CD via direct monotosylation at primary position.

1.4.1 Synthetic strategies

Among other CDs, especially βCD is extensively studied because of the optimal size of its cavity that allows inclusion complexes formation with a wide range of drugs. Use of βCD as a drug carrier notoriously helps increasing water solubility, chemical stability and bioavailability of the encapsulated drug. However, the presence of intramolecular hydrogen bonding between OH-2 and OH-3 of CD wider rim has been considered as the main cause for the low water solubility (with respect to α and γ CD) and consequent toxicity of this compound.[68]

Polymerized β-cyclodextrins (β-CDP) combine the advantageous properties of polymers (high molecular weight and higher solubility) with the formation of inclusion complexes due to cyclodextrins. This justifies the superiority of β-CDP over parent cyclodextrins and some other chemically modified and non-polymerized derivatives. In fact, several phase solubility studies made upon different drugs have proved that β-CDP possess better physical and chemical properties compared to native βCD and some of its derivatives in terms of both complexing capacity and solubilizing power. To synthesize such polymerized structures, different routes can be investigated:

1) direct cross-linking of the CD rings; 2) polymerizing functional monomers containing CDs; 3) grafting of CDs to other pre-constituted polymer networks.

Based on the method of synthesis, β-CDP can be linear or branched. Linear polymers are generally prepared by co-polymerization of CD vinyl derivatives,[69-71] whereas branched polymers are prepared by polycondensation of CD with bifunctional reactants [72] leading to formation of high molecular weight polymers. Synthesis of CD polymers is currently a very demanding task considering the high number of functional groups per CD unit and the difficulties in the purification due to the presence of undesidered byproducts after polycondensation. Chemical cross-linking with epichlorohydrin (EPI, 1-chloro-2,3-epoxypropane) is the basic method to produce β-cyclodextrin-based polymers, with different grades of solubility. This cross-linking agent is known from past 50 years and is relatively easy to use. It is the most common cross-linker used in polysaccharide chemistry [73] and it contains two reactive functional groups, an epoxide group and a chloroalkyl moiety, which can form bonds with βCD molecules (cross-linking step) and/or itself (polymerization step). The polymers prepared are purified before use and the presence of free/unreacted EPI can be discarded.[74]

Polymerized cyclodextrins can be cationic, anionic or non-ionic. In particular, charged polymerized cyclodextrins assume peculiar properties; as an example, CDs functionalized with weak acid or base may exhibit reversible supramolecular complexation behaviors induced by pH changes. Indeed, they may form stronger complexes with oppositely charged molecules and weaker complexes with molecules of same charge.

Synthesis of water soluble β-CDP via epichlorohydrin cross-linking [75]

This strategy provides a single step condensation and polymerization reaction in alkaline medium (Figure 9). The raw product is a mixture of monomeric unreacted species and polymeric fractions with different MWs. Briefly, a mixture of βCD and ~50% w/w of NaOH solution is stirred at 25°C

for 24 h. The mixture is then heated to 30°C and EPI is added rapidly and stirred vigorously for 6h. Finally, the reaction is stopped by addition of acetone. After decantation, acetone is removed and the solution is kept at 50°C overnight. After cooling, the solution is neutralized with HCl and dialyzed in order to eliminate salts and low molecular weight compounds. The obtained solution is evaporated and precipitated by adding dehydrated ethanol. Concentrations of EPI, NaOH and CD are key factors to avoid undesired gelation processes.

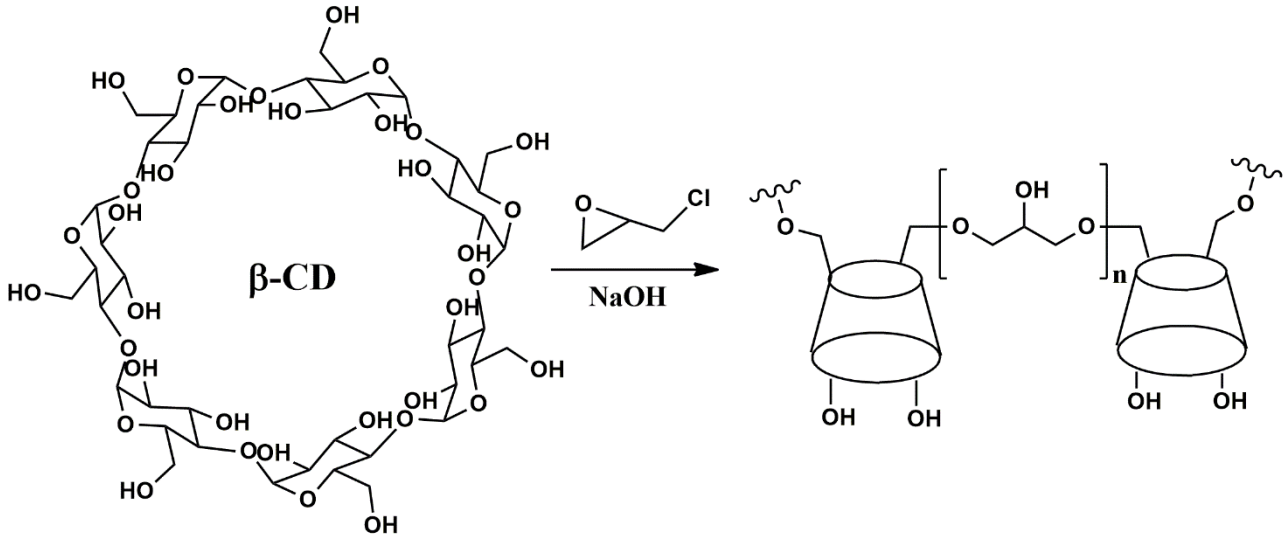

Figure 9 Cross-linking mechanism via epichlorohydrin

Synthesis of charged β-CDP

Malanga et al.[76] reported an effective strategy that allows appending ionic functional groups on cyclodextrin polymers either before (pre-branching) or after (post-branching) polymerization via EPI. In both cases, the synthesis consists in two following steps: 1) introduction of azido groups (N_3) on β-CD polymer/monomer via iodination and azidation reactions and 2) reduction of the azido groups to amino moieties. The final aim is to introduce one single amino moiety (in chlorohydrate form) per CD ring. The most challenging part are the control over the iodination degree and the purification steps over the polymerized product, that is not suitable for chromatography. Briefly, Ph_3P is dissolved in dry DMF and I_2 is added by keeping the temperature of the reaction

mixture below 40°C. Dried pre-formed poly-β-CD is added to the solution, temperature is increased to 50°C and the mixture is stirred for 1h. Then, the solution is cooled down to 30°C, $CH_3OH/NaOCH_3$ are added and left over stirring for 30 min. After removal of methanol under vacuum, DMF and NaN_3 in excess are added and the solution is again heated at 80°C for 2h. Finally, solvents are removed under reduced pressure and addition of water results in the precipitation of a white solid. The solid is filtered off, the filtrate is extracted with DCM and the aqueous phase is dialyzed over deionized water for 24 h. The final product is obtained by freeze drying and characterized by FT-IR (Figure 10). The reduction step follows a hydrogenolytic method based on a combination of hydrazine and Pd/C as catalyst. The overall progression of the reaction is also evaluated by FT-IR spectroscopy.

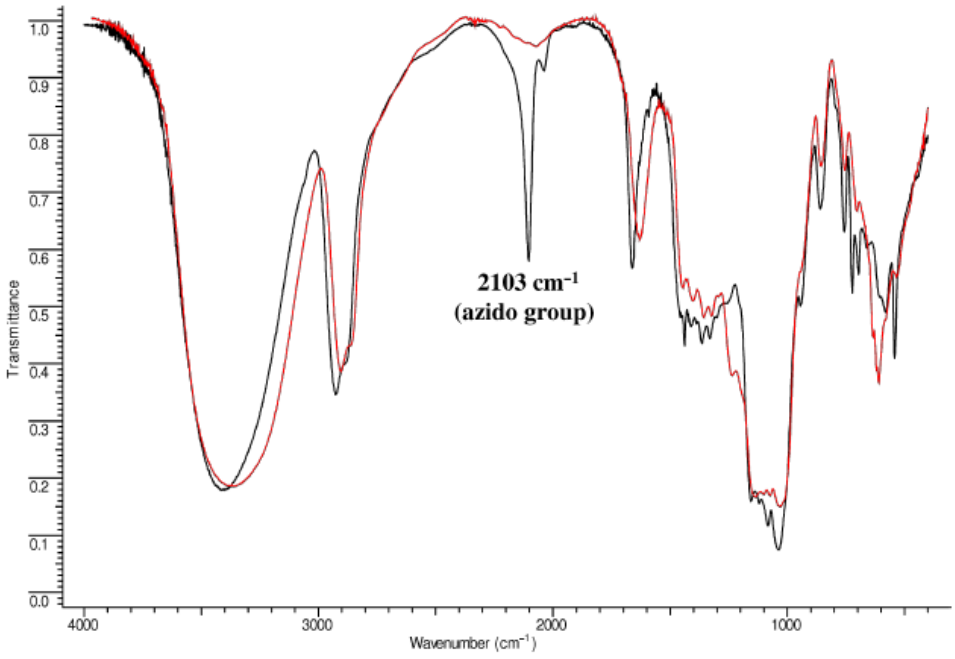

Figure 10 FT-IR analysis of the product before (black line) and after (red line) reduction[76]

The mono-azido-poly-β-CD compound is first dissolved in water. Pd/C suspension and then hydrazine hydrate are gradually added and heated to reflux for 1 h. The reaction mixture is cooled to r.t. and filtered with a glass filter to remove the charcoal. The mother liquor is repetitively centrifuged, filtered and finally dialyzed in water for 24 h. The pH of the solution is adjusted at 4-5 with HCl 1N and the final product is obtained by freeze drying as a white powder.

The pre-branching method provides exactly the same procedure on the β-CD monomer, before the cross-linking reaction.

The group of Yang et al[77] reported another method to prepare cationic and anionic cyclodextrin oligomers via one-step polycondensation with EPI, with a slight change in the reaction conditions. Moreover, this strategy requires the addition of choline chloride to obtain cationic polymers and chloroacetic acid for anionic ones. Both synthetic strategies allow the introduction of additional pendant groups into the polymeric structures thus enriching the properties of the compound. The polycondensation via EPI of water insoluble β-CDP has also been reported, but their utility is mainly associated, thanks to their exceptional separation efficiency, with environmental applications as purifying agents towards impurities, pollutants and toxins from waste waters.[73, 78]

Table 1 Types of polymerized cyclodextrins [75]

Type of CD	Polymer	Charge	Solubilty	Cross linking agent
α	Epichlorohydrin-α-cyclodextrin polymer	Non-ionic	Soluble	Epichlorohydrin
β	Epichlorohydrin-β-cyclodextrin polymer	Non-ionic	Soluble	Epichlorohydrin
	Carboxymethyl epichlorohydrin-β-cyclodextrin	Anionic	Soluble	Epichlorohydrin
	Branched cationic-β-cyclodextrin polymer	Cationic	Insoluble	Epichlorohydrin and choline chloride
	Sulfated β-cyclodextrin polymer	-	Soluble	Epichlorohydrin
	β–Cyclodextrin epichlorohydrin polymer	-	Insoluble	Epichlorohydrin
γ	Epichlorohydrin–γ–cyclodextrin	Non-ionic	Soluble	Epichlorohydrin

1.4.2 Current Applications

Cyclodextrin polymers, as well as parent CDs, possess a well-established safety profile in terms of biocompatibility and biodegradability and have played a significant role in pharmaceutical and biomedical applications over the past decades. The non-covalent interactions that underlie their ability to form inclusion complexes have been extensively investigated using the combined efforts of spectroscopic techniques such as UV, CD, NMR and fluorescence spectroscopy, to develop various nanosystems. Particular attention has been put in the fabrication of smart drug delivery systems to overcome or minimize the drawbacks associated with conventional formulations such as non-specific drug distribution and inadequate control over release patterns which may lead to serious overdose related side effects.[79]

Polycondensation with epichlorohydrin leads to the generation of cyclodextrin polymers able to self-assemble, forming improved therapeutic carriers compared to native CDs. Examples of these interconnected molecular assemblies are polyrotaxanes, polypseudorotaxanes and polycatenane.[46, 80] Moreover, another possibility is to exploit the supramolecular interaction, grafting such polymers with other linear or branched polymeric frameworks such as chitosan, polyethylenimine, alginate, poly(N-isopropylacrylamide) and hyaluronic acid. Nevertheless, major attention has been destined to the creation of cyclodextrin-based intelligent and stimuli-responsive biomaterials for many biomedical applications (i.e. tissue eingeneering, medical devices, biosensing and imaging). These *smart* polymers, are developed to trigger the drug release in response to changes in environmental factors, including physical stimuli (temperature, light, electrical, magnetic or ultrasonic), chemical stimuli (pH, ionic, and redox) and biological stimuli (enzymes, inflammation or biomarkers).[81, 82] Typically, stimuli-responsive nanosystems are based on the reversible association/dissociation of guest molecules with the CDs, controlled by applying specific external triggers (Figure 11). Moreover, cyclodextrins are interesting materials for the design of medical devices because they can encapsulate dyes that are clinically relevant in diagnosis. Multi-functional polymeric CD-based

networks can contemporary vehicle both probes and therapeutic agents, with any competitive effect, realizing, in fact, a theranostic strategy.

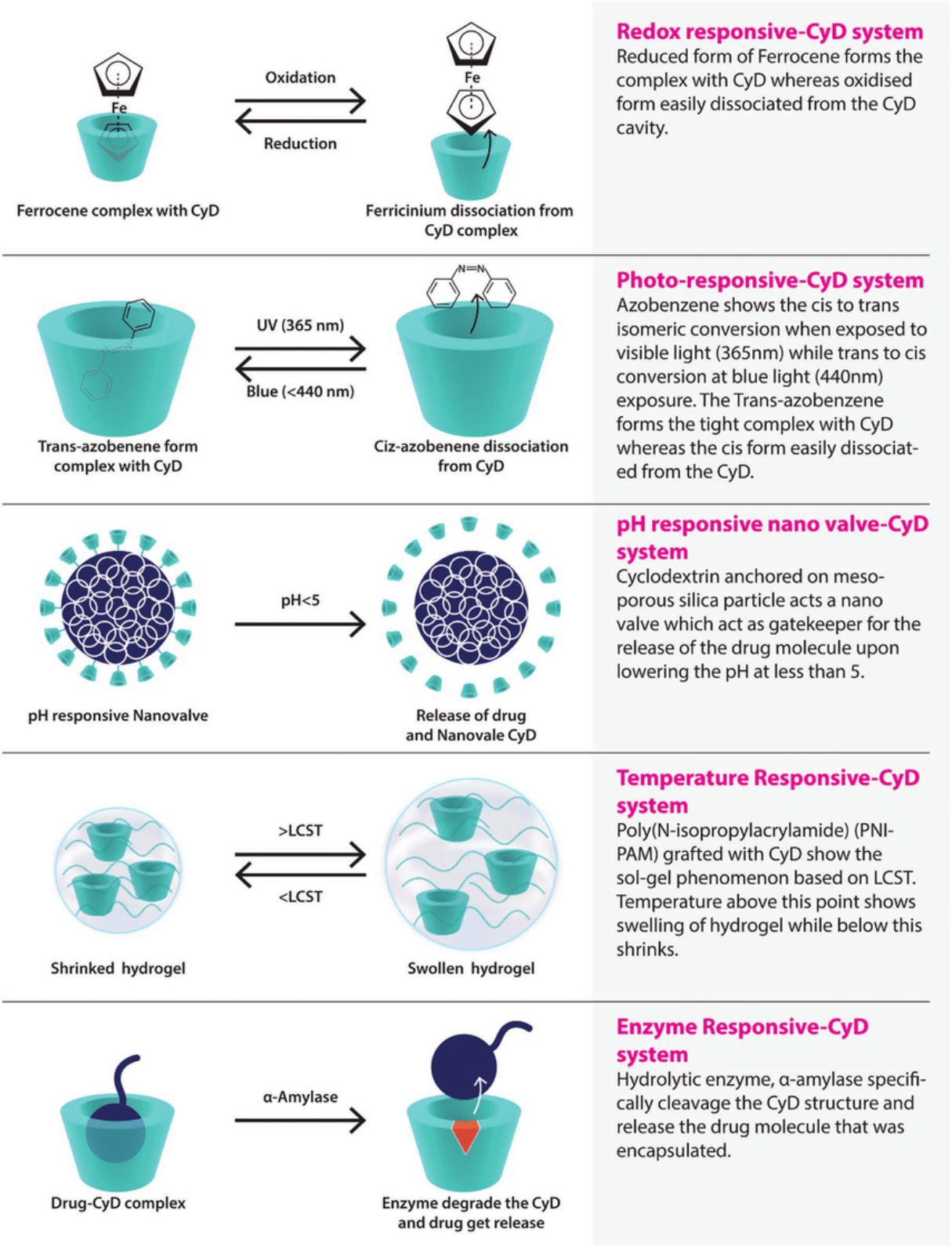

Figure 11 Examples of stimuli-responsive CD-based systems[79]

1.5 Hyaluronic Acid

Hyaluronic acid (HA), or hyaluronan, is a linear polysaccharide formed by alternating units of β-1,4-D-glucuronic acid and β-1,3-N-acetyl-D-glucosamine, linked together by $\beta(1\rightarrow3)$ linkages (Figure 12). This polyanionic glycosaminoglycan is typically observed in the extracellular matrix of epithelial, connective and nerve tissue of vertebrates, but is present throughout the whole body in a wide range of molecular weights.[83] It belongs to the family of glycosaminoglycans, a group of heteropolysaccharides that also comprises chondroitin sulfates, dermatan sulfate, heparin and heparin sulfates. Unlike the others, HA is not sulfated and it is not associated with any protein. It was first isolated in 1934 by Meyer and Palmer from bovine vitreous humor.[84]

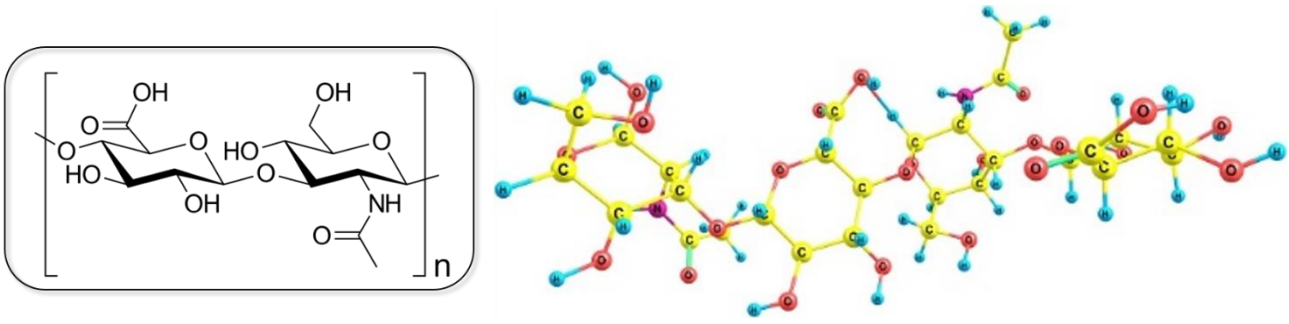

Figure 12 Chemical and molecular structure of hyaluronic acid

Among its physiological functions it is known for playing an important role in cell migration, proliferation and differentiation,[85] thus mediating cellular signaling, wound repair, morphogenesis, and matrix organization.[86] Furthermore, it's been demonstrated that HA and its receptors are involved in the processes of tumor cell motility and invasion. Proteins capable of interaction with HA are designated as hyaloadherines and act in the stabilization of tissue integrity. Some of these proteins are associated with cell membranes and act as cell-receptors, by activating different intracellular signaling pathways.[87] One of these membrane receptors it's called CD44 and has been found in almost

all human cell types, in many isoforms.[88] Besides, hyaluronan also interacts with fibronectin and other growth factors. The binding of HA to CD44 isoforms is implicated in angiogenesis, migration, proliferation and aggregation stimuli, also affecting cell adhesion to ECM components.[89, 90] Moreover, CD44 was found to be over-expressed in a variety of solid tumors, such as pancreatic,[91] breast and lung cancer.[92] For this reason, HA has been recently studied as targeting agent for the selective delivery of chemotherapeutics to improve discrimination between healthy and malignant tissues.[93, 94] Hyaluronan degradation is accomplished by two basic mechanisms: a) enzymatic degradation performed by hyaluronidases (HYALs) and b) non-specific mechanisms, represented mainly by oxidation-reduction degradation reaction caused by reactive oxygen species (ROS).[85] HA normally acts as a jelly coating which serves as a sort of protective "shield" to the cells. When there is an inflammation occurring, a higher rate of hyaluronan degradation is expected for many reasons: presence of pathogens producing hyaluronidase, decrease of pH and presence of ROS. This leads to a decrease of HA molecular weight together with the polymer water binding capacity and consequent formation of edema.[95] Moreover, decrease in thickness and viscosity of the hyaluronan jelly-like coat that surrounds the cells results in a higher accessibility of the cell toll-like receptors (TLR) to their ligands, normally involved in the cascade activation of innate immunity, thus amplifying the inflammatory reaction.[96] Hyaluronic acid in its natural form has many interesting uses in biomedical applications and its chemical modifications may extend this biopolymer range of use. The presence of carboxylic and hydroxyl groups in the structure allows several chemical modifications. The main goal is to obtain a material tuned according to the specific requirements of the desired application/route of administration, without losing the original properties such as biocompatibility, biodegradability, ability to interact with cells and living tissues. Modified hyaluronan derivatives normally exhibit major hydrophobicity and higher resistance to biodegradation, thus they are normally used for augmentation of soft tissues,[97] viscosupplementation,[98] as scaffolds for cell culture or matrices for controlled drug release.[99] Also, as previously mentioned, conjugation of HA with drugs is an interesting approach for targeted

delivery. Significant attention has been given to the preparation of hyaluronic acid derivatives that are able to undergo crosslinking reaction under mild physiological condition. Such materials are suitable for the encapsulation of living cells into hydrogel matrices or are suitable to form a 3D, in situ hydrogel network.[83, 86, 100] For all these reasons, HA has been proposed as medical product for over three decades: as targeting ligand in platforms designed as delivery systems for cancer, [101] as healing component in tissue engineering [85] and for the sustained release of antiviral drugs,[102] nevertheless has been recognized as an important building block for the creation of new biomaterials with utility in tissue engineering and regenerative medicine applications.[103]

1.5.1 Applications of HA-based biomaterials

HA based drug research has been of great interest lately, due to some advantageous properties like mucoadhesion, biocompatibility and ease of chemical modification. Such properties made this versatile polymer very useful in applications ranging from tissue regeneration to anti-aging and anti-inflammatory medications (Figure 13). Moreover, thanks to a wide range of molecular weights, HA and its derivatives can be utilized in different formulations like fillers, creams, gels and drops. As aforementioned, HA can be conjugated, functionalized or used as nanocarrier to provide sustained release of payloads, thus most of researchers have been focused on the creation of covalently modified systems, nanoparticle-based systems and hydrogel systems. Being a hydrophilic polymer, HA is particularly indicated to carry and improve the solubility of small hydrophobic drugs. Additionally, this kind of covalent systems are able to self-assemble or complexing with other components, which could further shield the drug from being degraded by the external environment. Below are reported some examples of HA-based systems proposed for the treatment of various diseases:

- *Tissue engineering*: HA-based hydrogel scaffolds have been developed to exploit their mucoadhesive properties, able to modify the three-dimensional and natural ECM-like

structure of tissues, together with the possibility to deliver growth factors. Hydrogels are typically used in two different forms: i) bulk or conventional hydrogels and ii) injectable hydrogels or gels. Bulk hydrogels are typically implanted at the intended site and are generally preformed ex-situ as semi-solid formulations. On the other hand, injectable ones are hydrophilic materials that undergo sol-gel transition after injection in response to a change in physiological stimuli such as temperature or pH.[104]

- *Wound repair*: skin acts like a mechanical barrier for the body, protecting from the ingress of infectious agents and traumas. For this reason, a prompt and fast healing of the skin layers is fundamental. The healing process includes several phases originated from homeostasis of platelet-derived factors that lead to the typical manifestations such as inflammation, granulation formation, re-epithelization. HA plays a multifaceted and strategic role in the mediation of these processes, as it is the principal component of natural ECM. HA based scaffolds have been created by attaching proteins like fibronectin onto its backbone, to facilitate cell migration into the wound. In a recent study HA was used in combination with adipose stem-cell derived exosomes to help increase the re-ephitelialization and vascularization of acute cutaneous wounds. Specifically, HA role was to immobilize the exosomes in its matrix and thus prolong their residence time within the tissue vasculature.[105]
- *Inflammation*: HA has some contradictory functions during the inflammation process. In fact, it has been demonstrated that during the early stages of inflammation, an increase in the synthesis of HA occurs in response to the production of inflammatory cytokines. In this case HA plays a moderator and scavenging role because it contributes to the stabilization of connective tissue matrix, balancing the diffusion and injury caused by inflammatory cells byproducts such as reactive oxygen metabolites. Recently, HA has been approved for the treatment of degenerative knee arthritis via intra articular injection directly into the joint,[106] contemporary acting as lubricant and shock absorber in the joint, thereby lessening the pain.

- *Respiratory diseases*: asthma is a chronic disease of the airways and the lungs, characterized by some histopathological tissue transformations such as ECM degeneration. As a significant part of the ECM, HA has been known to play a part in inflammatory illnesses, acting as a shield for the organ scleroprotein. Therefore, HA may be utilized to vehicle drugs and prolong their retention time by providing sustained release within the airways. Targeted gene silencing is currently gaining a lot of attention. In a novel study, PEG and HA modified lipoplexes were used for local delivery of siRNA to the lungs. With the mucopenetration ability of PEG along with selective targeting provided by HA, the modified lipoplexes were used to deliver siRNA to the CD44 overexpressed lung tumor cells.[107]
- *Cancer*: it is well documented that for an efficient cancer treatment, a targeted delivery is of utmost importance as most anticancer drugs distribute throughout the body causing toxicity to normal healthy cells. Cancer cells overexpressing CD44 on their surface can be exploited as targets for HA based formulations. HA and its derivatives may be used as carriers for proteins, peptides, nucleic acids and various anti-tumoral agents. Moreover, in some kind of cancers, mucopolysaccharide levels correlate with malignancy and poor prognosis, thus HA can also be used as tumor marker to monitor disease progression. As an example, HA was conjugated with folic acid for a tumor targeted delivery of the anticancer agent Doxorubicin in a micellar formulation, showing reduced cytotoxicity and CD44 mediated cellular uptake.[108] Additionally, PEG-conjugated hyaluronic acid nanoparticles were investigated as carriers for anticancer drugs including Doxorubicin and Camptothecin.[109] Other functional motifs could also be introduced into HA based DDS for the diagnosis or combined therapy. Zheng and coworkers[110] introduced the superparamagnetic iron oxide nanoparticles (SPIONs) into HA-C_{16} copolymer system for the magnetic resonance imaging and photothermal therapy, while Docetaxel was encapsulated in the hydrophobic core. The photothermal effect was assisted and accelerated by the contemporary drug release. Fluorescent motifs could also be introduced for fluorescent imaging.

Figure 13 Hyaluronic Acid usages in the biomedical field [111]

1.5.2 Hyaluronic acid modification approaches

High hydrophilicity and enzymatic vulnerability of native HA makes it inferior relative to commercially available synthetic polymers.[112] This can be overcome through its mechanical enforcement employing covalent and non-covalent approaches, without affecting those properties that make this polymer of unarguable importance in the biomedical and pharmaceutical field. Each disaccharide unit of HA contains four hydroxyl, one amide and one carboxyl groups, resulting in strong inter- and intra-molecular hydrogen bonding associations. HA modification must be performed in aqueous solution to easily access the available functional groups, precluding synthetic procedures that require the use of organic solvents.[113] Interestingly, hydrophobic modification on the HA framework not only improves the solubility in common organic solvents, but also the compatibility with other hydrophobic biomaterials, obtaining amphiphilic structures able to self-assemble in physiological solutions under mild experimental conditions and thus allowing a more efficient exploitation of this material. Hydrophobicity in HA is achievable through the linkage of aliphatic/aromatic hydrophobic substituents.[114, 115] Carboxyl groups are useful for amidation and

esterification reactions while the hydroxyl groups give origin to ester or ether linkages. The aggregates formed may range from core-shell- or micelle-like structures to bilayer vesicles,[116] depending on the grade of hydrophobicity acquired (Figure 14). It is also possible to confer certain desirable properties to these assemblies, such as stimuli responsiveness, by using "smart" hydrophobic moieties.

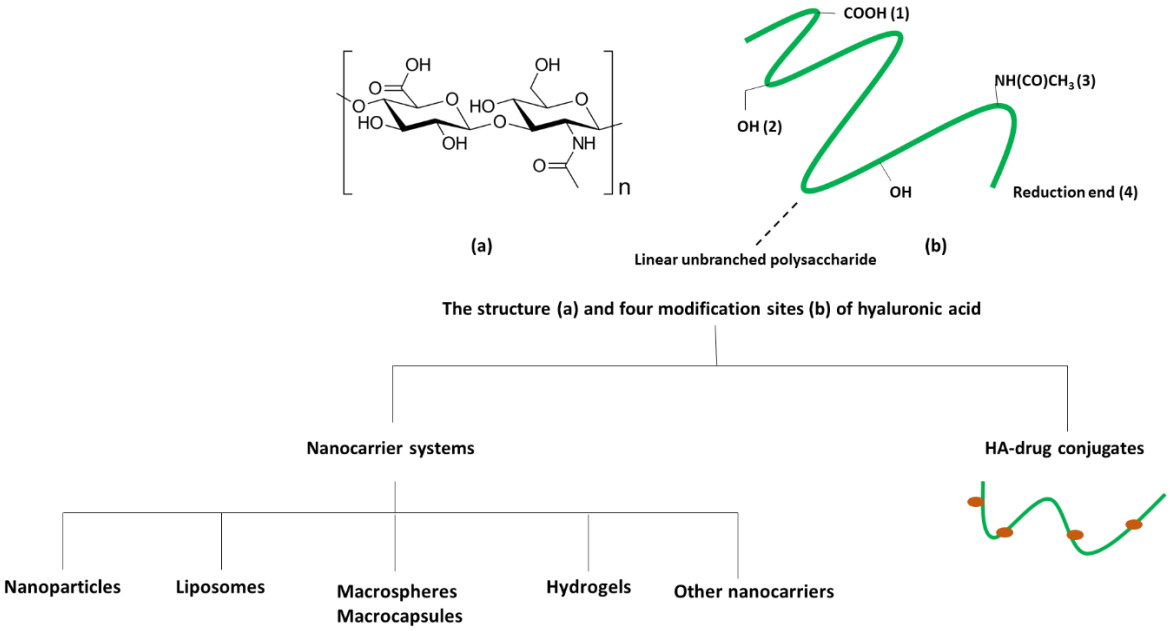

Figure 14 (a) Hyaluronic acid molecular formula and (b) evidence of functional groups suitable for chemical modification for the generation of superior structured systems

The most widely exploited strategies to derivatize hyaluronic acid can be classified in covalent and non-covalent approaches. Covalent approaches involve the carboxyl and hydroxyl groups but as aforementioned they are not promptly available owing to strong hydrogen interactions among polymer chains[117] and insolubility of HA in organic solvents, hence preparatory step to activate the reactive groups are necessary (i.e. chemical cross-linking via carbodiimide reaction). On the other hand, non-covalent approaches require mild chemical conditions causing less structural damage on the polymer integrity and basically consist in adsorbing species on HA backbone. An example of this

is the development of hybrid hydrogels obtained by combining HA with synthetic or natural polymers or by electrostatic interaction with oppositely charged species forming polyion complexes.[118, 119] Finally, another widely explored strategy, especially in drug-delivery applications, is the direct conjugation of a drug to improve its solubility in aqueous media, stability and circulation half-life.[120] Cleavable HA-drug conjugates have shown dramatic improvement in both the absorption and efficacy profile;[121] nevertheless HA may also act as targeting moiety,[122] selectively releasing the drug in desired district of the organism by exhibiting changes in response to certain physiological stimuli (pH, reductive potential, enzymes). However, direct HA-drug reaction is generally difficult due to steric hindrance and limited nucleophilicity of reactive centers.[123] Therefore it is necessary a conversion into more reactive derivatives prior to conjugation, by utilizing activating agents or specific coupling reagents, often associated with the use of linear spatiators (e.g. short hydrophilic aliphatic chains). Figure 15 schematizes some common derivatizations of HA and corresponding destinations of use.

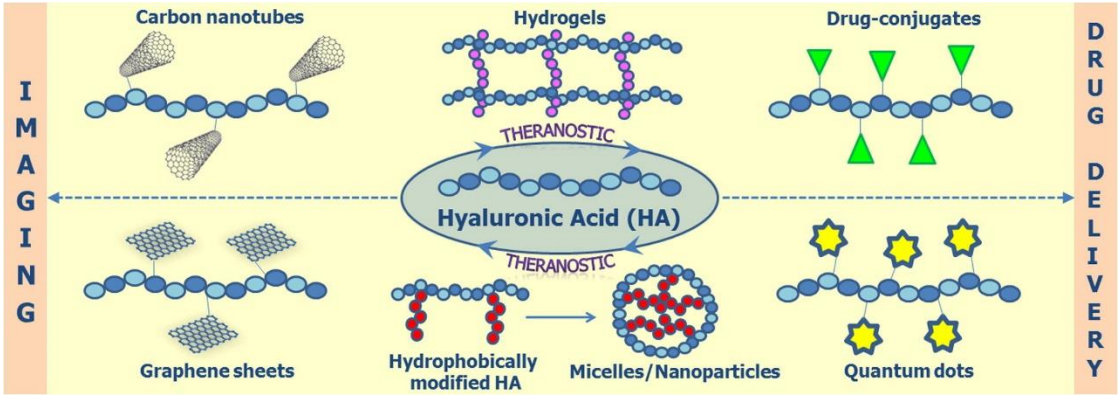

Figure 15 Some examples of HA most common derivatizations [124]

1.6 Hydrogels

Since the first example of synthetic hydrogels, reported by Wichterle and Lim in 1960,[125] synthetic hydrogels based on both natural and synthetic polymers have been of great interest for a wide range of biomedical applications including drug delivery and tissue engineering. Applications of hydrogels in biomedical fields include sensors,[126, 127] actuators,[128] device coatings,[129, 130] wound dressings and

adhesives,[131] liquid-absorbing hygiene products,[132] delivery vehicles for active compounds or cells,[133-135] soft contact lenses,[136] and matrices and implants in tissue engineering and regenerative medicine.[137-139] Figure 16 depicts some of the applications and constituents, both of natural and synthetic origin, of such nanocomposite biomaterials.

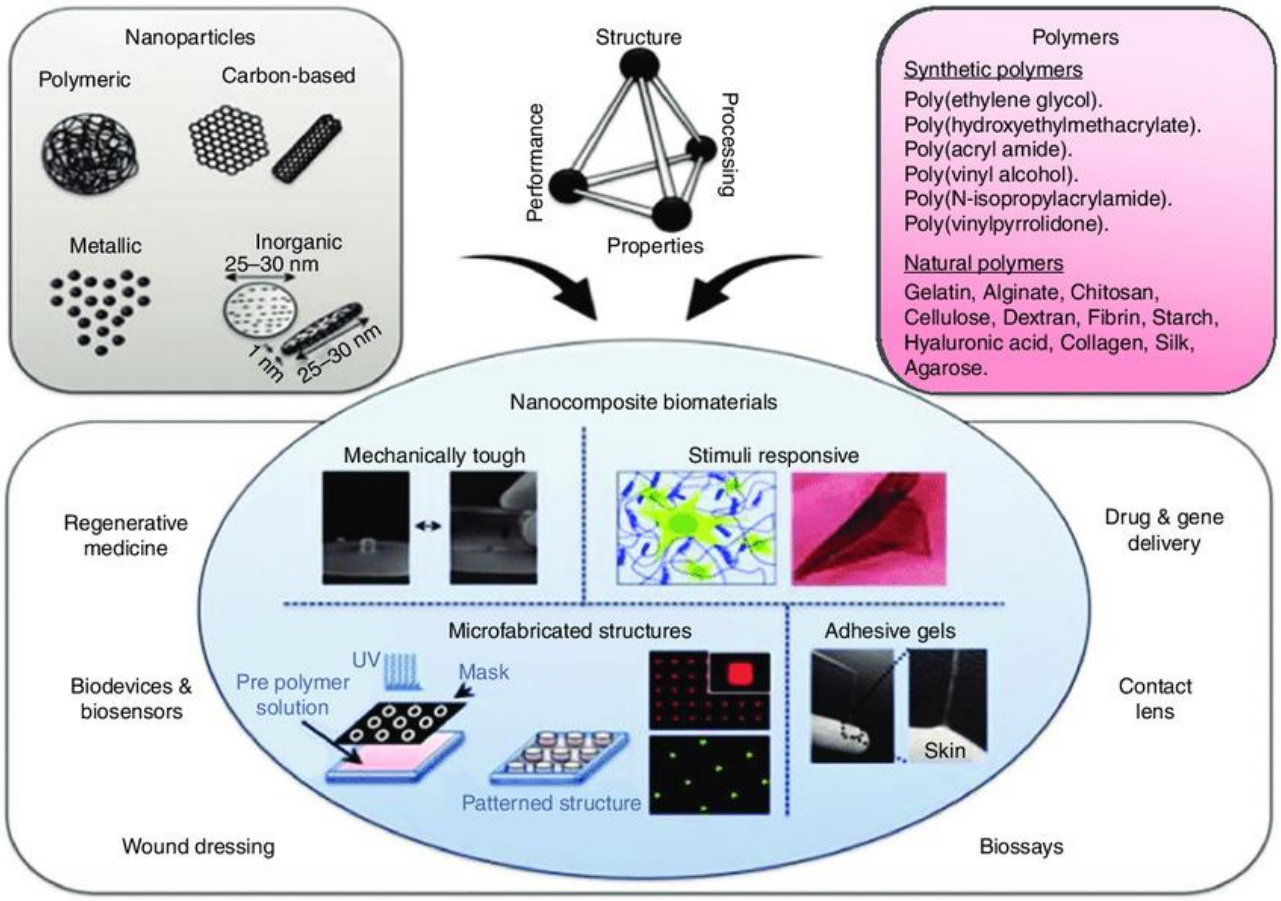

Figure 16 Nanocomposite hydrogels for biomedical applications[140]

Hydrogel formation can occur through covalent or non-covalent mechanisms (Figure 17) and they can be classified as:[141]

- *Physical hydrogels*: thermosensitive hydrogels which respond to changes in temperature and usually undergo a sol-gel phase transition when the temperature changes from room to physiological temperature. This makes them particularly useful, as temperature is generally an easy stimulus to control. Thermosensitive hydrogels are usually triblock polymers made

up from poly(ethylene glycol) (PEG) linked to hydrophobic polymer blocks. PEG is well-established for its use in hydrogel formulations as it possesses high water solubility, biocompatibility and low immunogenicity,[142] whereas other blocks increase the hydrophobicity and drug loading capacity of hydrophobic drugs by micellization. Problems during administration using a syringe/needle[143] were detected for thermosensitive hydrogels having a gelation transition temperature of 37 °C: the patient's body temperature caused the rapid gelation of the hydrogel and thus blocked the needle. The addition of pH-sensitive moieties was proposed to overcome this drawback. Thus, the gelation of thermosensitive copolymers occurred when two conditions have been achieved. For example, a formulation in the sol-state at room temperature and at pH 8.0 will have the transition to the gel-state when the temperature rise to 37° C and the pH value is of 7.4.[144]

- *Covalent hydrogels*: creation of a co-network by cross-linking hydrophobic chains/monomers with hydrophilic ones. A similar effect can be obtained by using hydrophobic crosslinkers. These hydrogels are also called amphiphilic hydrogels. This strategy has the advantage of a wide range of polymer choices, because basically exploits the reactivity between specific chemical groups such as alcohol or anhydrides, avoiding the use of initiators, coupling agents and other additives that can present toxicity problems, limiting the biomedical applications.[145]
- *Nanoparticle-containing hydrogels*: this approach is often used to include hydrophobic depots in the hydrogel structure. The nanoparticles can be covalently linked to the hydrogel structure or just simply absorbed inside the material. For the first approach, nanoparticles can be prepared containing polymerizable groups in their surface that can be copolymerized with hydrophilic momomers. Additionally, if the particles are multifunctionalised they can act as crosslinkers for the hydrogels. Using this approach, the diffusion of the particles during the swelling process can be prevented. The more common approach is to incorporate the nanoparticles before the crosslinking process (physical or chemical). For this purpose, the particles should be prepared previously and added to the reaction mixture. In this way the

particles can be easily incorporated into the hydrogel structure. However, they are not covalently attached to the structure and, consequently, they can diffuse out from the hydrogel during the swelling process.[146]

- *Supramolecular hydrogels*: novel class of non-covalently cross linked polymer materials. The supramolecular cross-linking, obtained by various noncovalent interactions such as hydrogen bonding, metal–ligand coordination, host–guest recognition, and electrostatic interaction, remarkably reduces the structural flexibility and alters the macroscopic performance, resulting in the formation of 3D cross-linked networks. In sharp contrast, such noncovalent hydrogels show not only the moderate mechanical properties gained from polymeric building blocks, but also show reversible gel–sol transition behavior in response to a wide variety of bio-related stimuli (e.g., pH, redox agents, enzymes, bioactive molecules). In particular, CDs based host-guest couples are non-toxic and biocompatible, and are primarily useful in water, thereby providing a powerful platform to build smart supramolecular hydrogels for numerous biological applications. In addition, multivalent electrostatic interactions between two oppositely charged polyelectrolytes usually promote the formation of extremely strong and opaque materials.[147]

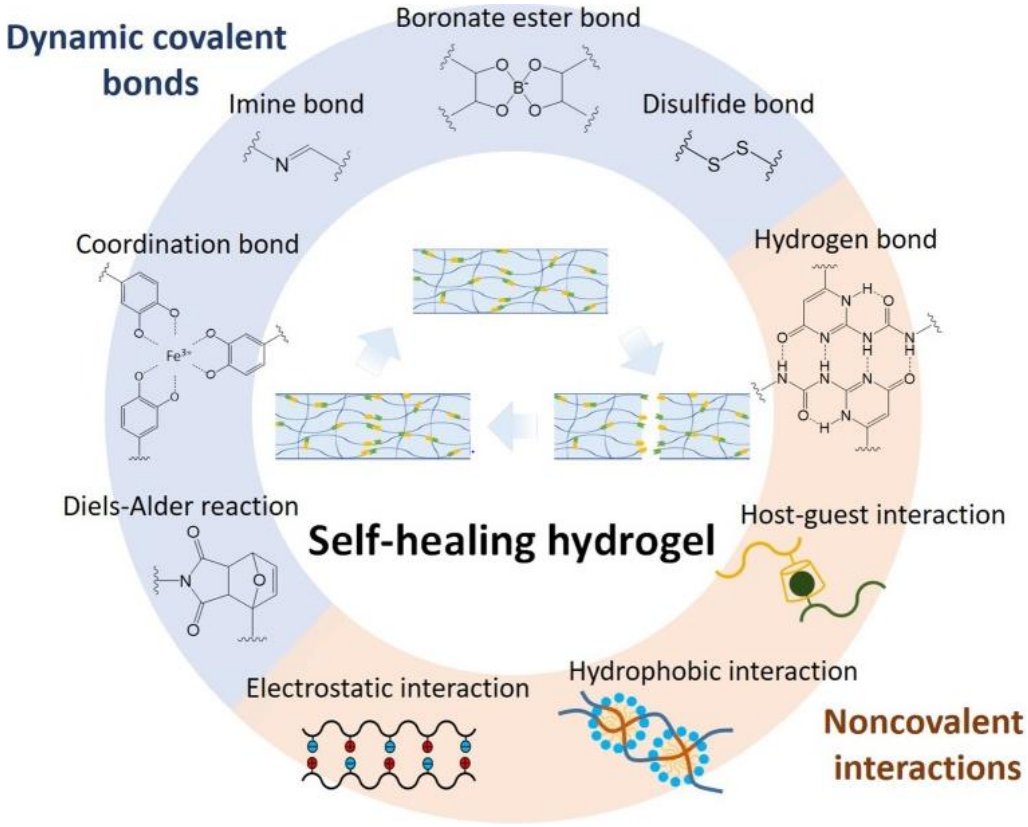

Figure 17 Common chemical motifs that drive covalent and non-covalent interactions for hydrogel formation[148]

1.6.1 Supramolecular hydrogels in drug delivery

Hydrogels based on inclusion complexes have been extensively investigated as injectable drug delivery systems for a broad spectrum of bioactive agents including small molecular drugs, proteins, vaccines or DNA.[48] The physicochemical properties, biocompatibility, biodegradability, and sensitivity of supramolecular hydrogels can be elegantly tailored by carefully selection of appropriate guest polymers for assembling. Through this approach, hydrogels with various functions, such as temperature-, photon-, chemical-, redox-, or pH-sensitivity, have been prepared for drug delivery applications.[149] Since these hydrogels are formed by supramolecular self-assembly in an aqueous solution without the use of chemical crosslinkers, the loading of drug payload can be achieved at room temperature and under mild conditions, which is especially beneficial to biomacromolecular drugs.[150] Depending on the characteristics of guest polymer, the entrapped drugs may be released in

a rapid, sustained, triggered, or a combined manner. Under certain circumstances, drugs can be incorporated into hydrogels by covalent conjugation to modulate their release kinetics.

Co-assembly of cyclodextrins (CDs) or their derivatives with hydrophobic modified polymers is another widely explored strategy to self-assemble hydrogels. Complexation between CD units and hydrophobic groups drives their formation.[151-153] Hydrogels can be instantaneously formed at room temperature by mixing β-CD polymers or β-CD conjugated polymers with hydrophobic modified hydrophilic polymers such as PEG, dextran, chitosan, and hyaluronic acid, which can sustain the release of proteins or hydrophobic drugs. Pharmacologically active cargos varying from small molecules to proteins are generally loaded into these hydrogels by physical entrapment during the self-assembling process.

The conventional polymer hydrogels having covalent cross-linkages are often brittle, have poor transparency, and lack the ability to self-heal. In contrast, the 3D noncovalent crosslinked networks of supramolecular hydrogels show unique mechanical properties, including both stiffness/toughness and elasticity/flexibility to retain the hydrogel structure. The macroscopic mechanical properties of hydrogels are highly correlated with the cross-linking density. Increasing the crosslinking density of the network results in an increase in the storage and loss moduli of the hydrogels.[154] In addition, thanks to the presence of these dynamic interactions between the constitutive building blocks, supramolecular hydrogels can be spontaneously degraded or metabolized in the variable physiological environment of the human body, resulting in a major biocompatibility both *in vitro* and *in vivo*. Moreover, external stimuli from the surrounding environment, including physical (e.g., temperature, light, voltage, magnetic field) and chemical (e.g., pH, ionic strength, redox agent, glucose, enzyme, competitive host/guest) have a remarkable impact on the cross linkages, leading to the swelling or dissociation of the cross-linked hydrogel networks.[155-157] In conclusion, with proper design, the swelling degree and gel–sol transition behavior of these hydrogel can be effectively controlled.

HA-based hydrogels show numerous advantages, such as high water content for the diffusion of entrapped molecules, unique mechanical properties similar to that of human tissues, ease of degradation in vivo, in-situ forming capacity in contact with tissues and facile incorporation of functional components. They have been proposed as carriers for improving the water-solubility and bioavailability, prolonging the circulation time, inducing preferential accumulation at tumor sites through the enhanced permeability and retention effect (EPR), and reducing the systemic side effects of therapeutic agents.[147]

One of the most interesting applications of HA-hydrogels is the delivery of encapsulated molecules or proteins for the stimulation of natural healing processes, being HA actively produced during tissue injuries and involved in the physiological regulation of tissue repair.[102] Tissue engineering aims at achieving local regeneration of lost or malfunctioning tissues and organs by culturing a patient's own cells on a polymer matrix.[158] The biological environment and cell–biomaterial interaction play important roles in the functioning of the implanted biomaterials.

In conclusion, supramolecular hydrogels not only effectively combine tunable mechanical properties with regulation of degradability, but also afford excellent biological environments for encapsulating bioactive moieties such as growth factors and cells. They show great potential as biocompatible scaffolds in tissue engineering for supporting, guiding, and stimulating the sustainable growth of tissues.

So far, this chapter provided a brief *excursus* about bio-compatible naturally-derived polymers used as building blocks for the formulation of novel bio-mimetic systems and the recent advances about their applications. All these types of gels can be differentially classified based on their formulation technology or their intended use, both from the biomedical and technological viewpoints (Figure 18). In conclusion, hybrid polymer gels have the potentiality to become the most important area of material science, promising their use as soft materials in both biomedical and technological sciences.

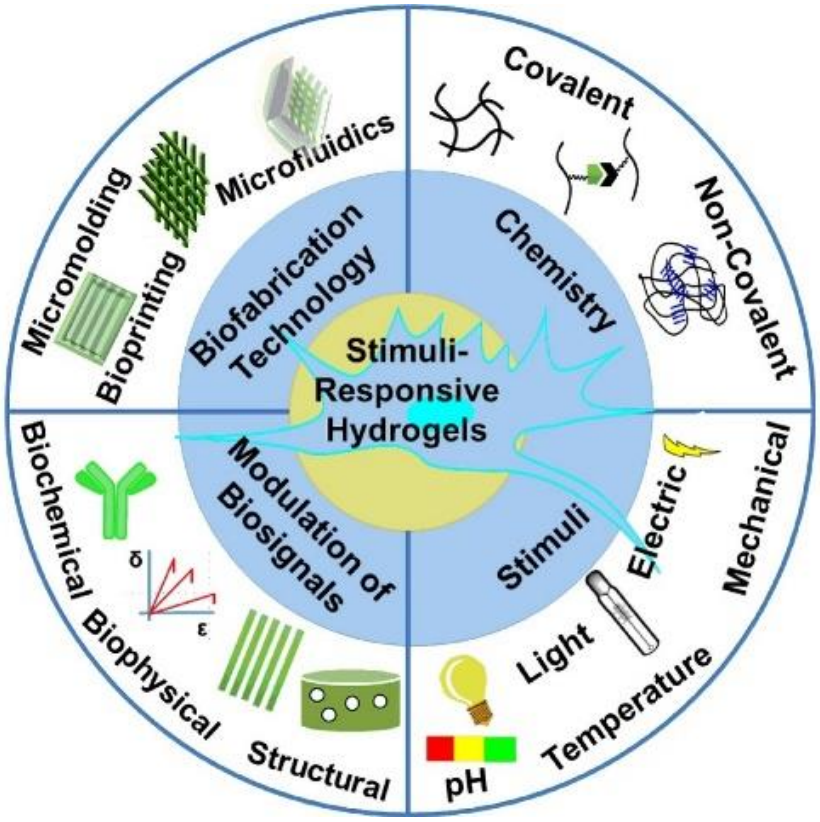

Figure 18 Classification of stimuli-responsive hydrogels based on biofabrication technology, chemistry, type of perceived external stimulus and effect produced [159]

References

1. Park, J. B.; Lakes, R. S., *Biomaterials*. Springer: New York, 2007.
2. Hanks, C. T.; Wataha, J. C.; Sun, Z., In vitro models of biocompatibility: A review. *Dental Materials* **1996,** *12* (3), 186-193.
3. Williams, D., Chapter 9 - Biocompatibility. In *Tissue Engineering*, Blitterswijk, C. v.; Thomsen, P.; Lindahl, A.; Hubbell, J.; Williams, D. F.; Cancedda, R.; Bruijn, J. D. d.; Sohier, J., Eds. Academic Press: Burlington, 2008; pp 255-278.
4. Murray, P. E.; Garcia Godoy, C.; Garcia Godoy, F., How is the biocompatibilty of dental biomaterials evaluated? *Medicina oral, patologia oral y cirugia bucal* **2007,** *12* (3), E258-66.
5. Imai, Y.; Watanabe, A.; Chang, P. I.; Masuhara, E., Evaluation of the Biologic Effects of Dental Materials Using a New Cell Culture Technique. *Journal of Dental Research* **1982,** *61* (8), 1024-1027.

6. Mitragotri, S.; Burke, P. A.; Langer, R., Overcoming the challenges in administering biopharmaceuticals: formulation and delivery strategies. *Nature Reviews Drug Discovery* **2014,** *13* (9), 655-672.

7. Griffith, M.; Islam, M. M.; Edin, J.; Papapavlou, G.; Buznyk, O.; Patra, H. K., The Quest for Anti-inflammatory and Anti-infective Biomaterials in Clinical Translation. *Front Bioeng Biotechnol* **2016,** *4* (71).

8. Fenton, O. S.; Olafson, K. N.; Pillai, P. S.; Mitchell, M. J.; Langer, R., Advances in Biomaterials for Drug Delivery. *Advanced materials (Deerfield Beach, Fla.)* **2018,** *30* (29), e1705328.

9. Langer, R., Drug delivery and targeting. *Nature* **1998,** *392* (6679 Suppl), 5-10.

10. Lowman, A. M., Biomaterials in Drug Delivery. **2004**, 1-31.

11. Cheng, Y.; Ramos, D.; Lee, P.; Liang, D.; Yu, X.; Kumbar, S. G., Collagen Functionalized Bioactive Nanofiber Matrices for Osteogenic Differentiation of Mesenchymal Stem Cells: Bone Tissue Engineering. *Journal of Biomedical Nanotechnology* **2014,** *10* (2), 287-298.

12. Thanou, M.; Heinze, T.; Vercruysse, K.; Holt, I.; Draget, K. I.; Williams, P.; Abd-El-Aziz, A. S., *Renewable Resources for Functional Polymers and Biomaterials : Polysaccharides, Proteins and Polyesters*. Royal Society of Chemistry: Cambridge, 2015.

13. Shelke, N. B.; James, R.; Laurencin, C. T.; Kumbar, S. G., Polysaccharide biomaterials for drug delivery and regenerative engineering. **2014,** *25* (5), 448-460.

14. Alvarez-Lorenzo, C.; Blanco-Fernandez, B.; Puga, A. M.; Concheiro, A., Crosslinked ionic polysaccharides for stimuli-sensitive drug delivery. *Advanced drug delivery reviews* **2013,** *65* (9), 1148-71.

15. Wasupalli, G. K.; Verma, D., 3 - Polysaccharides as biomaterials. In *Fundamental Biomaterials: Polymers*, Thomas, S.; Balakrishnan, P.; Sreekala, M. S., Eds. Woodhead Publishing: 2018; pp 37-70.

16. van de Manakker, F.; Vermonden, T.; van Nostrum, C. F.; Hennink, W. E., Cyclodextrin-Based Polymeric Materials: Synthesis, Properties, and Pharmaceutical/Biomedical Applications. *Biomacromolecules* **2009,** *10* (12), 3157-3175.

17. Mura, P., Analytical techniques for characterization of cyclodextrin complexes in aqueous solution: A review. *Journal of Pharmaceutical and Biomedical Analysis* **2014,** *101*, 238-250.

18. Crini, G., Review: A History of Cyclodextrins. *Chemical Reviews* **2014,** *114* (21), 10940-10975.

19. Del Valle, E. M. M., Cyclodextrins and their uses: a review. *Process Biochemistry* **2004,** *39* (9), 1033-1046.

20. Abarca, R. L.; Rodríguez, F. J.; Guarda, A.; Galotto, M. J.; Bruna, J. E., Characterization of beta-cyclodextrin inclusion complexes containing an essential oil component. *Food Chemistry* **2016,** *196*, 968-975.

21. Crini, G.; Fourmentin, S.; Fenyvesi, É.; Torri, G.; Fourmentin, M.; Morin-Crini, N., Fundamentals and Applications of Cyclodextrins. In *Cyclodextrin Fundamentals, Reactivity and Analysis*, Fourmentin, S.; Crini, G.; Lichtfouse, E., Eds. Springer International Publishing: Cham, 2018; pp 1-55.

22. Marques, H. M. C., A review on cyclodextrin encapsulation of essential oils and volatiles. *Flavour and Fragrance Journal* **2010,** *25* (5), 313-326.

23. Nanoencapsulation of Food Ingredients in Cyclodextrins: Effect of Water Interactions and Ligand Structure. In *Functional Food Product Development*, pp 24-38.

24. Zhang, Q.-F.; Jiang, Z.-T.; Li, R., Complexation of allyl isothiocyanate with β-cyclodextrin and its derivatives and molecular microcapsule of allyl isothiocyanate in β-cyclodextrin. *Eur Food Res Technol* **2007,** *225* (3-4), 407-413.

25. Badr-Eldin, S. M.; Elkheshen, S. A.; Ghorab, M. M., Inclusion complexes of tadalafil with natural and chemically modified beta-cyclodextrins. I: preparation and in-vitro evaluation. *European journal of pharmaceutics and biopharmaceutics : official journal of Arbeitsgemeinschaft fur Pharmazeutische Verfahrenstechnik e.V* **2008,** *70* (3), 819-27.

26. Wang, J.; Fan, H.; Zhang, M., General Methods for the Preparation of Cyclodextrin Inclusion Complexes. In *Cyclodextrins*, pp 25-50.

27. Shan-Yang, L.; Yuh-Horng, K., Solid particulates of drug-β-cyclodextrin inclusion complexes directly prepared by a spray-drying technique. *International Journal of Pharmaceutics* **1989,** *56* (3), 249-259.

28. Ventura, C. A.; Giannone, I.; Paolino, D.; Pistarà, V.; Corsaro, A.; Puglisi, G., Preparation of celecoxib-dimethyl-β-cyclodextrin inclusion complex: characterization and in vitro permeation study. *European Journal of Medicinal Chemistry* **2005,** *40* (7), 624-631.

29. Yang, J. S.; Yang, L., Preparation and application of cyclodextrin immobilized polysaccharides. *Journal of Materials Chemistry B* **2013,** *1* (7), 909-918.

30. Scala, A.; Piperno, A.; Grassi, G.; Scolaro, L. M.; Mazzaglia, A., Chapter 12 - Nanoconstructs Based on Cyclodextrins for Antimicrobial Applications. In *Nano- and Microscale Drug Delivery Systems*, Grumezescu, A. M., Ed. Elsevier: 2017; pp 229-244.

31. Gidwani, B.; Vyas, A., A Comprehensive Review on Cyclodextrin-Based Carriers for Delivery of Chemotherapeutic Cytotoxic Anticancer Drugs. *Biomed Res Int* **2015,** *2015*, 198268-198268.

32. Williams, R. O., 3rd; Mahaguna, V.; Sriwongjanya, M., Characterization of an inclusion complex of cholesterol and hydroxypropyl-beta-cyclodextrin. *European journal of pharmaceutics and biopharmaceutics : official journal of Arbeitsgemeinschaft fur Pharmazeutische Verfahrenstechnik e.V* **1998,** *46* (3), 355-60.

33. Brewster, M. E.; Loftsson, T., Cyclodextrins as pharmaceutical solubilizers. *Advanced drug delivery reviews* **2007,** *59* (7), 645-66.

34. Szejtli, J., Introduction and General Overview of Cyclodextrin Chemistry. *Chemical Reviews* **1998,** *98* (5), 1743-1754.

35. Jicsinszky, L.; Caporaso, M.; Martina, K.; Calcio Gaudino, E.; Cravotto, G., Efficient mechanochemical synthesis of regioselective persubstituted cyclodextrins. *Beilstein J Org Chem* **2016,** *12*, 2364-2371.

36. Loftsson, T.; Duchene, D., Cyclodextrins and their pharmaceutical applications. *Int J Pharm* **2007,** *329* (1-2), 1-11.

37. Uekama, K.; Hirayama, F.; Irie, T., Cyclodextrin Drug Carrier Systems. *Chem Rev* **1998,** *98* (5), 2045-2076.

38. Loftsson, T.; Brewster, M. E., Pharmaceutical applications of cyclodextrins: effects on drug permeation through biological membranes. *The Journal of pharmacy and pharmacology* **2011,** *63* (9), 1119-35.

39. Szente, L.; Szejtli, J., Highly soluble cyclodextrin derivatives: chemistry, properties, and trends in development. *Advanced drug delivery reviews* **1999,** *36* (1), 17-28.

40. Sallas, F.; Darcy, R., Amphiphilic Cyclodextrins – Advances in Synthesis and Supramolecular Chemistry. *European Journal of Organic Chemistry* **2008,** *2008* (6), 957-969.

41. Ravoo, B. J.; Darcy, R., Cyclodextrin Bilayer Vesicles. *Angew Chem Int Ed Engl* **2000,** *39* (23), 4324-4326.

42. Mazzaglia, A.; Donohue, R.; Ravoo, Bart J.; Darcy, R., Novel Amphiphilic Cyclodextrins: Graft-Synthesis of Heptakis(6-alkylthio-6-deoxy)-β-cyclodextrin 2-Oligo(ethylene glycol) Conjugates and Their ω-Halo Derivatives. *European Journal of Organic Chemistry* **2001,** *2001* (9), 1715-1721.

43. Zagami, R.; Romeo, A.; Mazzaglia, A., Bio-soft cyclodextrin nanomaterials. *Riv. Nuovo Cim. La Rivista del Nuovo Cimento* **2019,** *42* (9), 407-441.

44. Mazzaglia, A., Photodynamic Tumor Therapy with Cyclodextrin Nanoassemblies. In *Cyclodextrins in Pharmaceutics, Cosmetics, and Biomedicine*, Bilensoy, E., Ed. 2011; pp 343-361.

45. Mazzaglia, A.; Micali, N.; Scolaro, L. M.; Sciortino, M. T.; Sortino, S.; Villari, V., Design of photosensitizer/cyclodextrin nanoassemblies: spectroscopy, intracellular delivery and photodamage. *Journal of Porphyrins and Phthalocyanines* **2010,** *14* (08), 661-677.

46. Simoes, S.; Rey-Rico, A.; Concheiro, A.; alvarez-lorenzo, C., Supramolecular cyclodextrin-based drug nanocarriers. *Chemical communications (Cambridge, England)* **2015,** *51*.

47. Harada, A.; Takashima, Y.; Yamaguchi, H., Cyclodextrin-based supramolecular polymers. *Chemical Society Reviews* **2009,** *38* (4), 875-882.

48. Li, J., Self-assembled supramolecular hydrogels based on polymer–cyclodextrin inclusion complexes for drug delivery. *NPG Asia Materials* **2010,** *2* (3), 112-118.

49. Zhang, J.; Ma, P. X., Host-guest interactions mediated nano-assemblies using cyclodextrin-containing hydrophilic polymers and their biomedical applications. *Nano Today* **2010,** *5* (4), 337-350.

50. Zhou, J.; Ritter, H., Cyclodextrin functionalized polymers as drug delivery systems. *Polymer Chemistry* **2010,** *1* (10), 1552-1559.

51. Zhang, J.; Ma, P. X., Cyclodextrin-based supramolecular systems for drug delivery: recent progress and future perspective. *Advanced drug delivery reviews* **2013,** *65* (9), 1215-1233.

52. Ortiz Mellet, C.; Garcia Fernandez, J. M.; Benito, J. M., Cyclodextrin-based gene delivery systems. *Chem Soc Rev* **2011,** *40* (3), 1586-608.

53. Wang, X., *Azo Polymers: Synthesis, Functions and Applications*. Springer: 2016.

54. Szeman, J.; Fenyvesi, E.; Szejtli, J.; Ueda, H.; Machida, Y.; Nagai, T., Water soluble cyclodextrin polymers: Their interaction with drugs. *Journal of inclusion phenomena* **1987,** *5* (4), 427-431.

55. Li, J.; Xiao, H.; Li, J.; Zhong, Y., Drug carrier systems based on water-soluble cationic beta-cyclodextrin polymers. *International journal of pharmaceutics* **2004,** *278* (2), 329-342.

56. Smith, R. C.; Riollano, M.; Leung, A.; Hammond, P. T., Layer-by-layer platform technology for small-molecule delivery. *Angew Chem Int Ed Engl* **2009,** *48* (47), 8974-7.

57. Rodriguez-Tenreiro, C.; Alvarez-Lorenzo, C.; Rodriguez-Perez, A.; Concheiro, A.; Torres-Labandeira, J. J., Estradiol sustained release from high affinity cyclodextrin hydrogels. *European journal of pharmaceutics and biopharmaceutics : official journal of Arbeitsgemeinschaft fur Pharmazeutische Verfahrenstechnik e.V* **2007,** *66* (1), 55-62.

58. Rodriguez-Tenreiro, C.; Alvarez-Lorenzo, C.; Rodriguez-Perez, A.; Concheiro, A.; Torres-Labandeira, J. J., New cyclodextrin hydrogels cross-linked with diglycidylethers with a high drug loading and controlled release ability. *Pharmaceutical research* **2006,** *23* (1), 121-30.

59. Binello, A.; Robaldo, B.; Barge, A.; Cavalli, R.; Cravotto, G., Synthesis of cyclodextrin-based polymers and their use as debittering agents. **2008,** *107* (4), 2549-2557.

60. Fan, Z.; Guo, M.; Dong, B.; Diao, C.; Jing, Z.; Chen, X., Different self-assembly behaviors of mono-modified β-cyclodextrin substituted by benzoic acid derivatives. *Science China Chemistry* **2010,** *53* (5), 1089-1094.

61. Trotta, F.; Zanetti, M.; Cavalli, R., Cyclodextrin-based nanosponges as drug carriers. *Beilstein J Org Chem* **2012,** *8*, 2091-2099.

62. Schmidt, B.; Barner-Kowollik, C., Dynamic Macromolecular Material Design-The Versatility of Cyclodextrin-Based Host-Guest Chemistry. *Angew Chem Int Ed Engl* **2017,** *56* (29), 8350-8369.

63. Kost, B.; Brzeziński, M.; Socka, M.; Baśko, M.; Biela, T., Biocompatible Polymers Combined with Cyclodextrins: Fascinating Materials for Drug Delivery Applications. *Molecules* **2020,** *25*, 3404.

64. Rey-Rico, A.; Cucchiarini, M., polymers Supramolecular Cyclodextrin-Based Hydrogels for Controlled Gene Delivery. *Polymers* **2019,** *11*.

65. Timothy, T.; Siu-choon, N.; Yong, W.; Yin, X., Synthesis of mono-6-tosyl-β-cyclodextrin, a key intermediate for the functional cyclodextrin derivatives. *Protocol Exchange* **2020**.

66. Tang, W.; Ng, S.-C., Facile synthesis of mono-6-amino-6-deoxy-α-, β-, γ-cyclodextrin hydrochlorides for molecular recognition, chiral separation and drug delivery. *Nature Protocols* **2008,** *3* (4), 691-697.

67. Donohue, R.; Mazzaglia, A.; Ravoo, B. J.; Darcy, R., Cationic β-cyclodextrin bilayer vesicles. *Chemical Communications* **2002,** (23), 2864-2865.

68. Trotta, F.; Caldera, F.; Cavalli, R.; Mele, A.; Punta, C.; Melone, L.; Castiglione, F.; Rossi, B.; Ferro, M.; Crupi, V.; Majolino, D.; Venuti, V.; Scalarone, D., Synthesis and characterization of a hyper-branched water-soluble β-cyclodextrin polymer. *Beilstein J Org Chem* **2014,** *10*, 2586-2593.

69. Liu, Y.-Y.; Fan, X.-D.; Gao, L., Synthesis and Characterization ofβ-Cyclodextrin Based Functional Monomers and its Copolymers withN-isopropylacrylamide. *Macromolecular bioscience* **2003,** *3* (12), 715-719.

70. Auzély-Velty, R.; Rinaudo, M., Chitosan Derivatives Bearing Pendant Cyclodextrin Cavities: Synthesis and Inclusion Performance. *Macromolecules* **2001,** *34* (11), 3574-3580.

71. Renard, E.; Volet, G.; Amiel, C., Synthesis of a novel linear water-soluble β-cyclodextrin polymer. *Polymer International* **2005,** *54* (3), 594-599.

72. Renard, E.; Sebille, B.; Barnathan, G.; Deratani, A., Polycondensation of cyclodextrins with epichlorohydrin. Influence of reaction conditions on the polymer structure. *Macromolecular Symposia* **1997,** *122* (1), 229-234.

73. Crini, G.; Morcellet, M., Synthesis and applications of adsorbents containing cyclodextrins. *Journal of Separation Science* **2002,** *25* (13), 789-813.

74. Pellicer, J. A.; Rodríguez-López, M. I.; Fortea, M. I.; Lucas-Abellán, C.; Mercader-Ros, M. T.; López-Miranda, S.; Gómez-López, V. M.; Semeraro, P.; Cosma, P.; Fini, P.; Franco, E.; Ferrándiz, M.; Pérez, E.; Ferrándiz, M.; Núñez-Delicado, E.; Gabaldón, J. A., Adsorption Properties of β- and Hydroxypropyl-β-Cyclodextrins Cross-Linked with Epichlorohydrin in Aqueous Solution. A Sustainable Recycling Strategy in Textile Dyeing Process. *Polymers* **2019,** *11* (2), 252.

75. Gidwani, B.; Vyas, A., Synthesis, characterization and application of Epichlorohydrin-β-cyclodextrin polymer. *Colloids and Surfaces B: Biointerfaces* **2014,** *114*, 130-137.

76. Malanga, M.; Bálint, M.; Puskás, I.; Tuza, K.; Sohajda, T.; Jicsinszky, L.; Szente, L.; Fenyvesi, É., Synthetic strategies for the fluorescent labeling of epichlorohydrin-branched cyclodextrin polymers. *Beilstein J Org Chem* **2014,** *10*, 3007-3018.

77. Yang, S. Y.; Hoonor, R.; Jin, H.-S.; Kim, J., Synthesis and Characterization of Cationic and Anionic Cyclodextrin Oligomers and Their Use in Layer-by-Layer Film Formation. *Bulletin of the Korean Chemical Society* **2013,** *34* (7), 2016-2022.

78. Morin-Crini, N.; Crini, G., Environmental applications of water-insoluble β-cyclodextrin–epichlorohydrin polymers. *Progress in Polymer Science* **2013,** *38* (2), 344-368.

79. Wankar, J.; Kotla, N. G.; Gera, S.; Rasala, S.; Pandit, A.; Rochev, Y. A., Recent Advances in Host–Guest Self-Assembled Cyclodextrin Carriers: Implications for Responsive Drug Delivery and Biomedical Engineering. *Advanced Functional Materials* **2020,** *n/a* (n/a), 1909049.

80. Marreto, R. N.; Cardoso, G.; dos Santos Souza, B.; Martin-Pastor, M.; Cunha-Filho, M.; Taveira, S. F.; Concheiro, A.; Alvarez-Lorenzo, C., Hot melt-extrusion improves the properties of cyclodextrin-based poly(pseudo)rotaxanes for transdermal formulation. *International Journal of Pharmaceutics* **2020,** *586*, 119510.

81. Gil, E. S.; Hudson, S. M., Stimuli-reponsive polymers and their bioconjugates. *Progress in Polymer Science* **2004,** *29* (12), 1173-1222.

82. Ganta, S.; Devalapally, H.; Shahiwala, A.; Amiji, M., A review of stimuli-responsive nanocarriers for drug and gene delivery. *Journal of Controlled Release* **2008,** *126* (3), 187-204.

83. Xu, X.; Jha, A. K.; Harrington, D. A.; Farach-Carson, M. C.; Jia, X., Hyaluronic acid-based hydrogels: from a natural polysaccharide to complex networks. *Soft Matter* **2012,** *8* (12), 3280-3294.

84. Kogan, G.; Šoltés, L.; Stern, R.; Gemeiner, P., Hyaluronic acid: a natural biopolymer with a broad range of biomedical and industrial applications. *Biotechnology Letters* **2007,** *29* (1), 17-25.

85. Knopf-Marques, H.; Pravda, M.; Wolfova, L.; Velebny, V.; Schaaf, P.; Vrana, N. E.; Lavalle, P., Hyaluronic Acid and Its Derivatives in Coating and Delivery Systems: Applications in Tissue Engineering, Regenerative Medicine and Immunomodulation. *Advanced healthcare materials* **2016,** *5* (22), 2841-2855.

86. Burdick, J. A.; Prestwich, G. D., Hyaluronic acid hydrogels for biomedical applications. *Advanced materials (Deerfield Beach, Fla.)* **2011,** *23* (12), H41-56.

87. Schiller, J.; Fuchs, B.; Arnhold, J.; Arnold, K., Contribution of reactive oxygen species to cartilage degradation in rheumatic diseases: molecular pathways, diagnosis and potential therapeutic strategies. *Current medicinal chemistry* **2003,** *10* (20), 2123-45.

88. Turley, E. A.; Noble, P. W.; Bourguignon, L. Y., Signaling properties of hyaluronan receptors. *The Journal of biological chemistry* **2002,** *277* (7), 4589-92.

89. Naor, D.; Nedvetzki, S.; Golan, I.; Melnik, L.; Faitelson, Y., CD44 in cancer. *Critical reviews in clinical laboratory sciences* **2002,** *39* (6), 527-79.

90. Tzircotis, G.; Thorne, R. F.; Isacke, C. M., Chemotaxis towards hyaluronan is dependent on CD44 expression and modulated by cell type variation in CD44-hyaluronan binding. *Journal of Cell Science* **2005,** *118* (21), 5119.

91. Takada, M.; Yamamoto, M.; Saitoh, Y., The significance of CD44 in human pancreatic cancer: I. High expression of CD44 in human pancreatic adenocarcinoma. *Pancreas* **1994,** *9* (6), 748-52.

92. Chen, C.; Zhao, S.; Karnad, A.; Freeman, J. W., The biology and role of CD44 in cancer progression: therapeutic implications. *Journal of Hematology & Oncology* **2018,** *11* (1), 64.

93. Yan, Y.; Zuo, X.; Wei, D., Concise Review: Emerging Role of CD44 in Cancer Stem Cells: A Promising Biomarker and Therapeutic Target. **2015,** *4* (9), 1033-1043.

94. Mattheolabakis, G.; Milane, L.; Singh, A.; Amiji, M. M., Hyaluronic acid targeting of CD44 for cancer therapy: from receptor biology to nanomedicine. *Journal of drug targeting* **2015,** *23* (7-8), 605-18.

95. Cyphert, J. M.; Trempus, C. S.; Garantziotis, S., Size Matters: Molecular Weight Specificity of Hyaluronan Effects in Cell Biology. *International journal of cell biology* **2015,** *2015*, 563818.

96. Campo, G. M.; Avenoso, A.; D'Ascola, A.; Prestipino, V.; Scuruchi, M.; Nastasi, G.; Calatroni, A.; Campo, S., Hyaluronan differently modulates TLR-4 and the inflammatory response in mouse chondrocytes. *BioFactors (Oxford, England)* **2012,** *38* (1), 69-76.

97. Duranti, F.; Salti, G.; Bovani, B.; Calandra, M.; Rosati, M. L., Injectable hyaluronic acid gel for soft tissue augmentation. A clinical and histological study. *Dermatologic surgery : official publication for American Society for Dermatologic Surgery [et al.]* **1998,** *24* (12), 1317-25.

98. Arrich, J.; Piribauer, F.; Mad, P.; Schmid, D.; Klaushofer, K.; Müllner, M., Intra-articular hyaluronic acid for the treatment of osteoarthritis of the knee: systematic review and meta-analysis. *Canadian Medical Association Journal* **2005,** *172* (8), 1039.

99. Kurisawa, M.; Chung, J. E.; Yang, Y. Y.; Gao, S. J.; Uyama, H., Injectable biodegradable hydrogels composed of hyaluronic acid–tyramine conjugates for drug delivery and tissue engineering. *Chemical Communications* **2005,** (34), 4312-4314.

100. Highley, C. B.; Prestwich, G. D.; Burdick, J. A., Recent advances in hyaluronic acid hydrogels for biomedical applications. *Current Opinion in Biotechnology* **2016,** *40*, 35-40.

101. Dosio, F.; Arpicco, S.; Stella, B.; Fattal, E., Hyaluronic acid for anticancer drug and nucleic acid delivery. *Advanced drug delivery reviews* **2016,** *97*, 204-36.

102. Piperno, A.; Zagami, R.; Cordaro, A.; Pennisi, R.; Musarra-Pizzo, M.; Scala, A.; Sciortino, M. T.; Mazzaglia, A., Exploring the entrapment of antiviral agents in hyaluronic acid-cyclodextrin conjugates. *Journal of Inclusion Phenomena and Macrocyclic Chemistry* **2019,** *93* (1), 33-40.

103. Prestwich, G. D., Hyaluronic acid-based clinical biomaterials derived for cell and molecule delivery in regenerative medicine. *J Control Release* **2011,** *155* (2), 193-199.

104. Saludas, L.; Pascual-Gil, S.; Prósper, F.; Garbayo, E.; Blanco-Prieto, M., Hydrogel based approaches for cardiac tissue engineering. *International Journal of Pharmaceutics* **2017,** *523* (2), 454-475.

105. Liu, K.; Chen, C.; Zhang, H.; Chen, Y.; Zhou, S., Adipose stem cell-derived exosomes in combination with hyaluronic acid accelerate wound healing through enhancing re-epithelialization and vascularization. *Br J Dermatol* **2019,** *181* (4), 854-856.

106. Altman, R.; Bedi, A.; Manjoo, A.; Niazi, F.; Shaw, P.; Mease, P., Anti-Inflammatory Effects of Intra-Articular Hyaluronic Acid: A Systematic Review. *CARTILAGE* **2018,** *10* (1), 43-52.

107. Almeida, A. P. B.; Damaceno, G. B. R.; Carneiro, A. F.; Bohr, A.; Goncalves, H. R.; Valadares, M. C.; Nascimento, T. L.; Lima, E. M., Mucopenetrating lipoplexes modified with PEG and hyaluronic acid for CD44-targeted local siRNA delivery to the lungs. *J Biomater Appl* **2019,** *34* (5), 617-630.

108. Yang, Y.; Zhao, Y.; Lan, J.; Kang, Y.; Zhang, T.; Ding, Y.; Zhang, X.; Lu, L., Reduction-sensitive CD44 receptor-targeted hyaluronic acid derivative micelles for doxorubicin delivery. *International journal of nanomedicine* **2018,** *13*, 4361-4378.

109. Choi, K. Y.; Yoon, H. Y.; Kim, J.-H.; Bae, S. M.; Park, R.-W.; Kang, Y. M.; Kim, I.-S.; Kwon, I. C.; Choi, K.; Jeong, S. Y.; Kim, K.; Park, J. H., Smart Nanocarrier Based on PEGylated Hyaluronic Acid for Cancer Therapy. *ACS Nano* **2011,** *5* (11), 8591-8599.

110. Zheng, S.; Han, J.; Jin, Z.; Kim, C.-S.; Park, S.; Kim, K.-p.; Park, J.-O.; Choi, E., Dual tumor-targeted multifunctional magnetic hyaluronic acid micelles for enhanced MR imaging and combined photothermal-chemotherapy. *Colloids and Surfaces B: Biointerfaces* **2018,** *164*, 424-435.

111. Oliveira, J.; Carvalho, L.; Gomes, A.; Queiroz, L.; Magalhães, B.; Skorupa Parachin, N., Genetic basis for hyper production of hyaluronic acid in natural and engineered microorganisms. *Microbial cell factories* **2016,** *15*, 119.

112. Stern, R.; Asari, A. A.; Sugahara, K. N., Hyaluronan fragments: An information-rich system. *European Journal of Cell Biology* **2006,** *85* (8), 699-715.

113. Collins, M. N.; Birkinshaw, C., Hyaluronic acid solutions-A processing method for efficient chemical modification. *Journal of Applied Polymer Science* **2013,** *130* (1), 145-152.

114. Wang, X.; Gu, X.; Wang, H.; Sun, Y.; Wu, H.; Mao, S., Synthesis, characterization and liver targeting evaluation of self-assembled hyaluronic acid nanoparticles functionalized with glycyrrhetinic acid. *European Journal of Pharmaceutical Sciences* **2017,** *96*, 255-262.

115. Tiwari, S.; Bahadur, P., Modified hyaluronic acid based materials for biomedical applications. *International Journal of Biological Macromolecules* **2019,** *121*, 556-571.

116. Hill, T. K.; Abdulahad, A.; Kelkar, S. S.; Marini, F. C.; Long, T. E.; Provenzale, J. M.; Mohs, A. M., Indocyanine Green-Loaded Nanoparticles for Image-Guided Tumor Surgery. *Bioconjugate Chemistry* **2015,** *26* (2), 294-303.

117. Michalicová, P.; Mravec, F.; Pekař, M., Fluorescence study of freeze-drying as a method for support the interactions between hyaluronan and hydrophobic species. *PLOS ONE* **2017,** *12* (9), e0184558.

118. Shabafrooz, V.; Mozafari, M.; Kohler, G. A.; Assefa, S.; Vashaee, D.; Tayebi, L., The effect of hyaluronic acid on biofunctionality of gelatin-collagen intestine tissue engineering scaffolds. *Journal of biomedical materials research. Part A* **2014,** *102* (9), 3130-9.

119. Ma, X.; Xu, T.; Chen, W.; Qin, H.; Chi, B.; Ye, Z., Injectable hydrogels based on the hyaluronic acid and poly (γ-glutamic acid) for controlled protein delivery. *Carbohydrate Polymers* **2018,** *179*, 100-109.

120. Tripodo, G.; Trapani, A.; Torre, M. L.; Giammona, G.; Trapani, G.; Mandracchia, D., Hyaluronic acid and its derivatives in drug delivery and imaging: Recent advances and challenges. *European Journal of Pharmaceutics and Biopharmaceutics* **2015,** *97*, 400-416.

121. Yang, X.; Dogan, I.; Pannala, V. R.; Kootala, S.; Hilborn, J.; Ossipov, D., A hyaluronic acid–camptothecin nanoprodrug with cytosolic mode of activation for targeting cancer. *Polymer Chemistry* **2013,** *4* (17), 4621-4630.

122. Song, L.; Pan, Z.; Zhang, H.; Li, Y.; Zhang, Y.; Lin, J.; Su, G.; Ye, S.; Xie, L.; Li, Y.; Hou, Z., Dually folate/CD44 receptor-targeted self-assembled hyaluronic acid nanoparticles for dual-drug delivery and combination cancer therapy. *Journal of Materials Chemistry B* **2017,** *5* (33), 6835-6846.

123. Buffa, R.; Odstrčilová, L.; Šedová, P.; Basarabová, I.; Novotný, J.; Velebný, V., Conjugates of modified hyaluronic acid with amino compounds for biomedical applications. *Carbohydrate Polymers* **2018,** *189*, 273-279.

124. Hangzhou Singclean Medical Products CO., L. http://it.hzxhe.org/info/hyaluronic-acid-and-its-derivatives-in-drug-de-23833773.html (accessed 22 Oct).

125. Wichterle, O.; LÍM, D., Hydrophilic Gels for Biological Use. *Nature* **1960,** *185* (4706), 117-118.

126. Richter, A.; Paschew, G.; Klatt, S.; Lienig, J.; Arndt, K. F.; Adler, H. P., Review on Hydrogel-based pH Sensors and Microsensors. *Sensors (Basel, Switzerland)* **2008,** *8* (1), 561-581.

127. Buenger, D.; Topuz, F.; Groll, J., Hydrogels in sensing applications. *Progress in Polymer Science* **2012,** *37* (12), 1678-1719.

128. Ionov, L., Hydrogel-based actuators: possibilities and limitations. *Materials Today* **2014,** *17* (10), 494-503.

129. Morais, J. M.; Papadimitrakopoulos, F.; Burgess, D. J., Biomaterials/tissue interactions: possible solutions to overcome foreign body response. *The AAPS journal* **2010,** *12* (2), 188-96.

130. Campoccia, D.; Montanaro, L.; Arciola, C. R., A review of the biomaterials technologies for infection-resistant surfaces. *Biomaterials* **2013,** *34* (34), 8533-54.

131. Ghobril, C.; Grinstaff, M. W., The chemistry and engineering of polymeric hydrogel adhesives for wound closure: a tutorial. *Chem Soc Rev* **2015,** *44* (7), 1820-35.

132. Kabiri, K.; Omidian, H.; Zohuriaan-Mehr, M. J.; Doroudiani, S., Superabsorbent hydrogel composites and nanocomposites: A review. *Polymer Composites* **2011,** *32* (2), 277-289.

133. Wan, J., Microfluidic-Based Synthesis of Hydrogel Particles for Cell Microencapsulation and Cell-Based Drug Delivery. *Polymers* **2012,** *4* (2), 1084-1108.

134. Olabisi, R. M., Cell microencapsulation with synthetic polymers. *Journal of biomedical materials research. Part A* **2015,** *103* (2), 846-59.

135. Kearney, C. J.; Mooney, D. J., Macroscale delivery systems for molecular and cellular payloads. *Nature materials* **2013,** *12* (11), 1004-17.

136. Xinming, L.; Yingde, C.; Lloyd, A. W.; Mikhalovsky, S. V.; Sandeman, S. R.; Howel, C. A.; Liewen, L., Polymeric hydrogels for novel contact lens-based ophthalmic drug delivery systems: a review. *Contact lens & anterior eye : the journal of the British Contact Lens Association* **2008,** *31* (2), 57-64.

137. Kharkar, P. M.; Kiick, K. L.; Kloxin, A. M., Designing degradable hydrogels for orthogonal control of cell microenvironments. *Chem Soc Rev* **2013,** *42* (17), 7335-72.

138. Gibbs, D. M.; Black, C. R.; Dawson, J. I.; Oreffo, R. O., A review of hydrogel use in fracture healing and bone regeneration. *Journal of tissue engineering and regenerative medicine* **2016,** *10* (3), 187-98.

139. Hastings, C. L.; Roche, E. T.; Ruiz-Hernandez, E.; Schenke-Layland, K.; Walsh, C. J.; Duffy, G. P., Drug and cell delivery for cardiac regeneration. *Advanced drug delivery reviews* **2015,** *84*, 85-106.

140. Rafieian, S.; Mirzadeh, H.; Mahdavi, H.; Masoumi, M., A review on nanocomposite hydrogels and their biomedical applications. *Science and Engineering of Composite Materials* **2018,** *26*.

141. Larraneta, E.; Stewart, S.; Ervine, M.; Al-Kasasbeh, R.; Donnelly, R. F., Hydrogels for Hydrophobic Drug Delivery. Classification, Synthesis and Applications. *Journal of functional biomaterials* **2018,** *9* (1).

142. Zhang, M.; Li, X. H.; Gong, Y. D.; Zhao, N. M.; Zhang, X. F., Properties and biocompatibility of chitosan films modified by blending with PEG. *Biomaterials* **2002,** *23* (13), 2641-2648.

143. Shim, W. S.; Yoo, J. S.; Bae, Y. H.; Lee, D. S., Novel injectable pH and temperature sensitive block copolymer hydrogel. *Biomacromolecules* **2005,** *6* (6), 2930-4.

144. Nguyen, M. K.; Lee, D. S., Injectable biodegradable hydrogels. *Macromolecular bioscience* **2010,** *10* (6), 563-79.

145. Rikkou-Kalourkoti, M.; Kitiri, E. N.; Patrickios, C. S.; Leontidis, E.; Constantinou, M.; Constantinides, G.; Zhang, X.; Papadakis, C. M., Double Networks Based on Amphiphilic Cross-Linked Star Block Copolymer First Conetworks and Randomly Cross-Linked Hydrophilic Second Networks. *Macromolecules* **2016,** *49* (5), 1731-1742.

146. Dannert, C.; Stokke, B. T.; Dias, R. S., Nanoparticle-Hydrogel Composites: From Molecular Interactions to Macroscopic Behavior. *Polymers* **2019,** *11* (2), 275.

147. Dong, R.; Pang, Y.; Su, Y.; Zhu, X., Supramolecular hydrogels: synthesis, properties and their biomedical applications. *Biomaterials Science* **2015,** *3* (7), 937-954.

148. Liu, Y.; Hsu, S.-H., Synthesis and Biomedical Applications of Self-healing Hydrogels. *Frontiers in chemistry* **2018,** *6*, 449.

149. Yu, J.; Fan, H.; Huang, J.; Chen, J., Fabrication and evaluation of reduction-sensitive supramolecular hydrogel based on cyclodextrin/polymer inclusion for injectable drug-carrier application. *Soft Matter* **2011,** *7* (16), 7386-7394.

150. Li, J.; Ni, X.; Leong, K. W., Injectable drug-delivery systems based on supramolecular hydrogels formed by poly(ethylene oxide)s and alpha-cyclodextrin. *Journal of biomedical materials research. Part A* **2003,** *65* (2), 196-202.

151. Zhang, Y. M.; Liu, Y. H.; Liu, Y., Cyclodextrin-Based Multistimuli-Responsive Supramolecular Assemblies and Their Biological Functions. *Advanced materials (Deerfield Beach, Fla.)* **2020,** *32* (3), e1806158.

152. Pottanam Chali, S.; Ravoo, B. J., Adamantane-Terminated Polypeptides: Synthesis by N-Carboxyanhydride Polymerization and Template-Based Self-Assembly of Responsive Nanocontainers via Host-Guest Complexation with beta-Cyclodextrin. *Macromol Rapid Commun* **2020,** *41* (18), e2000049.

153. Mazzaglia, A.; Ravoo, B. J.; Darcy, R.; Gambadauro, P.; Mallamace, F., Aggregation in Water of Nonionic Amphiphilic Cyclodextrins with Short Hydrophobic Substituents. *Langmuir* **2002,** *18* (5), 1945-1948.

154. Koenigs, M. M. E.; Pal, A.; Mortazavi, H.; Pawar, G. M.; Storm, C.; Sijbesma, R. P., Tuning Cross-Link Density in a Physical Hydrogel by Supramolecular Self-Sorting. *Macromolecules* **2014,** *47* (8), 2712-2717.

155. Tran, N. Q.; Joung, Y. K.; Lih, E.; Park, K. M.; Park, K. D., Supramolecular hydrogels exhibiting fast in situ gel forming and adjustable degradation properties. *Biomacromolecules* **2010,** *11* (3), 617-25.

156. Alvarez-Lorenzo, C.; Concheiro, A., 15 Review of Smart Materials for Controlled Drug Release. In *Fundamentals of Smart Materials*, Royal Society of Chemistry: 2020; p 170.

157. Davidson-Rozenfeld, G.; Stricker, L.; Simke, J.; Fadeev, M.; Vázquez-González, M.; Ravoo, B. J.; Willner, I., Light-responsive arylazopyrazole-based hydrogels: their applications as shape-memory materials, self-healing matrices and controlled drug release systems. *Polymer Chemistry* **2019,** *10* (30), 4106-4115.

158. Griffith, L. G.; Naughton, G., Tissue engineering--current challenges and expanding opportunities. *Science* **2002,** *295* (5557), 1009-14.

159. Chatterjee, S.; Hui, P. C.-l., Stimuli-Responsive Hydrogels: An Interdisciplinary Overview. In *Hydrogels-Smart Materials for Biomedical Applications*, IntechOpen: 2018.

Chapter 2

The chapter reports the studies about cyclodextrin cationic polymer as cartilage-penetrating nanomedicine for intra-articular administration of therapeutic and diagnostic agents and for the monitoring and mitigation of inflammatory diseases. Specifically, nanoassemblies based on poly-β-amino cyclodextrin (PolyCD) loaded with diclofenac (DCF) and linked by supramolecular interactions with a fluorescent probe (adamantanyl-Rhodamine conjugate, Ada-Rhod) have been studied (Figure 1). Finally, the biological profile of PolyCD@Ada-Rhod/DCF (*i.e.* cytotoxitocity, cellular uptake and ability to suppress IL-1β production) in human bone marrow-derived mesenchymal stromal cells (hMSCs) was investigated.

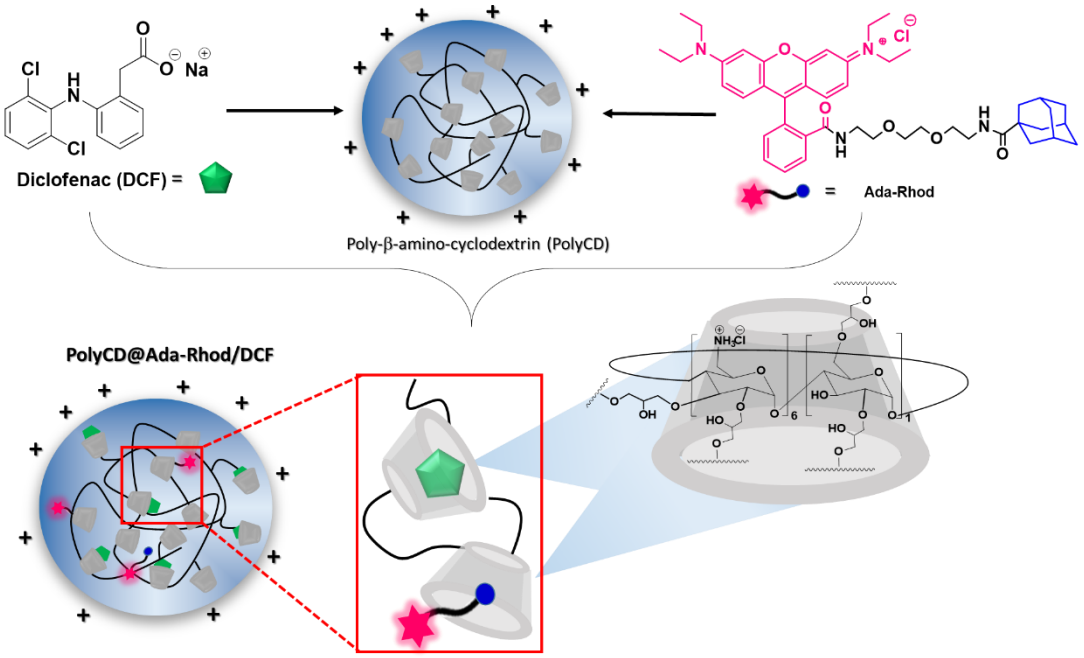

Figure 1 Sketched view of PolyCD@Ada-Rhod/DCF nanoassemblies

2.1 *Nanoassemblies* of drug-loaded poly-β-cyclodextrin for intra-articular treatment of osteoarthritis

Introduction

Osteoarthritis (OA) is a lifelong degenerative joint disease characterized by the progressive loss and damage of the articular cartilage, osteophyte formation and reduction of the synovial fluid viscosity, which leads to reduced joint lubrication with typical symptoms like pain, rigidity and anatomical deformations. At cellular level, the main cause is an abnormal alteration of tissue metabolism, leading to a continuous, more less localized, inflammatory state.[1] Current pharmacological therapies for OA mainly include analgesics or non-steroidal anti-inflammatory drugs (NSAIDs) alongside antirheumatic drugs, steroid hormones and biologic drugs that could help suppressing the symptoms. Unfortunately, they may lead to severe unavoidable side effects after systemic distribution, such as gastrointestinal and renal toxicity, cardiovascular risk and anaphylaxis.[2] Hence, direct injection of drugs at the intra-articular level represents a valuable option to improve the therapeutic efficiency by achieving appropriate drug concentration at the site of action (with a lower dosage compared to systemic administration). This clinical approach is limited by the rapid clearance of the drug administered in its free form, resulting in a very low rate of cartilage penetration. Consequently, frequent injections are often necessary to enable pharmacologically relevant amount of drug to enter the cartilage, with increased risk of infections and obvious patient's uncompliance.[1] To overcome these drawbacks, different innovative drug delivery systems (*i.e*, 3D scaffolds and nanoassemblies) able to enhance drug retention time inside the joint region by releasing the drugs in a controlled manner for a longer period of time were proposed. The basic principle of 3D scaffolds involves the use of drug-loaded polymeric matrices either surgically implanted in solid form into cartilage or delivered to the injured site in liquid form after injection, with subsequent polymerization *in situ*, triggered by external or internal stimuli. The other approach consists in the delivery of designed nano-formulations in the cartilage sub-compartments.[3] To be effective, these therapeutic systems must

satisfy a series of requirements in terms of biocompatibility and biodegradability and their physical and chemical properties need to be accurately tuned. Among NSAIDs, Diclofenac sodium [(2-(2,6-dichloroanilino) phenyl acetic acid, DCF] is the most popular prescribed non-steroidal compound, with pronounced anti-inflammatory, analgesic and antipyretic properties. Mechanism of action of DCF consists in the unselective inhibition of the cyclooxygenase enzymes (COX I and COX II) which catalyze the conversion of arachidonic acid to prostaglandins (PGH_2), involved in many inflammatory processes and in the regulation of homeostasis in various tissues such as kidneys and vascular system (Figure 2).[4] Hence, besides its well-known anti-inflammatory effects, it is also useful in delaying the cartilage degradation and promoting regeneration processes. Similarly, to other NSAIDs, diclofenac use is associated with some gastrointestinal side effects, including ulceration and hemorrhage. In fact, because of its very low solubility in gastric juice (~15 μg/ml at pH =2)[5] DCF causes undesirable effects on the gastric mucosa when it is orally administered. To improve the absorption and increase the gastrointestinal tolerability, DCF was encapsulated inside β-CD and its derivatives and the resulting inclusion complexes have been widely studied both in solution and in the solid state.[6-8]

Regarding its use in OA treatments, studies have shown that DCF has an intra-articular mean elimination half-life of ~5.2 h in human patients affected by knee rheumatoid arthritis.[2, 9]

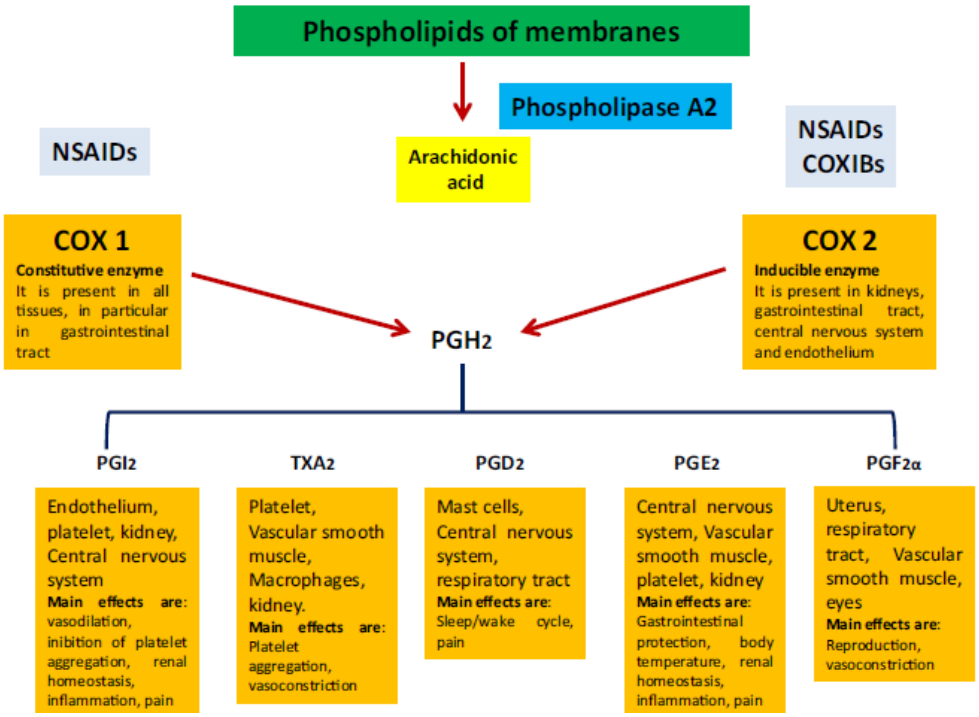

Figure 2 Schematic mechanism of action of COX-I and COX-II and effects mediated by prostaglandines[4]

Along my research activity, I focused on the development of a newly injectable *nanoassembly* based on a cationic poly-amino-β-cyclodextrin polymer (**PolyCD**), able to contemporary entrap in a water-soluble interconnected scaffold both **DCF** as anti-inflammatory agent and the synthetic diagnostic *probe* obtained by conjugation between Rhodamine B and adamantane carboxylic acid (**Ada-Rhod**). The conjugation of Rhodamine with adamantane allows to obtain a derivative which strongly interacts with the CD cavity and has frequently been exploited as strategy to design self-assembled systems, due to their well-known high values of binding equilibrium constants (K_b = ~ 5 x 10^4 M^{-1}).[10]

Results and Discussion

Preparation and characterization of PolyCD@Ada-Rhod and PolyCD@Ada-Rhod/DCF nanoassemblies

All the nanoassemblies were prepared according to the the solvent-evaporation technique at r.t. (≅ 25°C),[11] i.e. hydration of organic film followed by slight sonication.

For the ternary complex, Ada-Rhod film was first hydrated with an aqueous dispersion of PolyCD and the obtained PolyCD@Ada-Rhod aqueous dispersion was then used for rehydration of DCF film. The interactions of PolyCD with Ada-Rhod within PolyCD@Ada-Rhod, with Diclofenac in PolyCD@DCF and with both within PolyCD@Ada-Rhod/DCF were investigated by UV/Vis, steady-state and time-resolved fluorescence emission, DLS and ζ-potential measurements. All nanoassemblies were obtained with high Ada-Rhod and DCF entrapment efficiencies (~ 92 and 100%, respectively). Ada-Rhod residual film was used to determine Ada-Rhod actual loading into the system. No residual of DCF was found in the dispersions of PolyCD@Ada-Rhod/DCF, confirming its complete entrapment. Moreover, it was observed that the recovery yield for all systems is 80%, probably due to the presence of a little water percentage in the starting cyclodextrin polymer powder, because of its highly hygroscopic nature. Table 1 summarizes the main technological features of the nanoassemblies, as well as calculated loadings and entrapment efficiencies for each payload (see experimental section for details).

Table 1 Overall properties of PolyCD-based nanoassemblies: mean D_H, polidispersity index (PDI) and ζ-potential values (ζ), loading and EE% in ultrapure water.

sample	medium	Mean D_H (nm ± SD)[a](%)[b]	PDI	ζ (mV ± SD)	Theoretical loading (%)	[c]Actual Loading (%)	[d]EE (%)
PolyCD	H_2O	268 ± 10 (97)	0.07	19 ± 6	--	--	--
PolyCD@Ada-Rhod	H_2O	498 ± 54 (85)	0.2	25 ± 5	1.28(1)	1.18 ± 0.04(1)	92.0 ± 3.3(1)
PolyCD@ AdaRhod/DCF	H_2O	229 ± 35 (85) 29 ± 13 (12)	≤0.3	22 ± 4	1.18(1)	1.09 ± 0.05(1)	92.0 ± 3.9(1)

			15.5[2]	15.0 ± 0.4[2]	96.7 ± 2.3[2]
PBS pH 7.4	230 ± 24 (83) 25 ± 13 (11)	≤0.2			
NaCl (0.9 wt %)	228 ± 21 (89) 18 ± 13 (12)	≤0.2			

[a]SD was calculated on three different batches. [b] Mean size with corresponding intensity % distribution (only main populations). [c]Actual loading is expressed as the amount of drug (mg) encapsulated per 100 mg of nanoassembly. [d]Ratio between actual and theoretical loading × 100. [1] Values are referred to Ada-Rhod; [2] Values are referred to Diclofenac.; PolyCD (0.5 mg/ml) and PolyCD@Ada-Rhod/DCF (0.5 mg/ml, [Ada-Rhod] = 8 μM, [DCF] = 236 μM).

DLS analysis of PolyCD and PolyCD@Ada-Rhod/DCF nanoassemblies (Figure 3) pointed out a size distribution centered around 250 nm (D_H) for the main population and a ζ-potential of about +20 mV, due to the positive charges confered by the amino groups in the polymer backbone. Unexpectedly, PolyCD@Ada-Rhod shows a size distribution that is two-fold higher respect to the analogue complex with DCF, suggesting a different rearrangment in the colloidal environment.

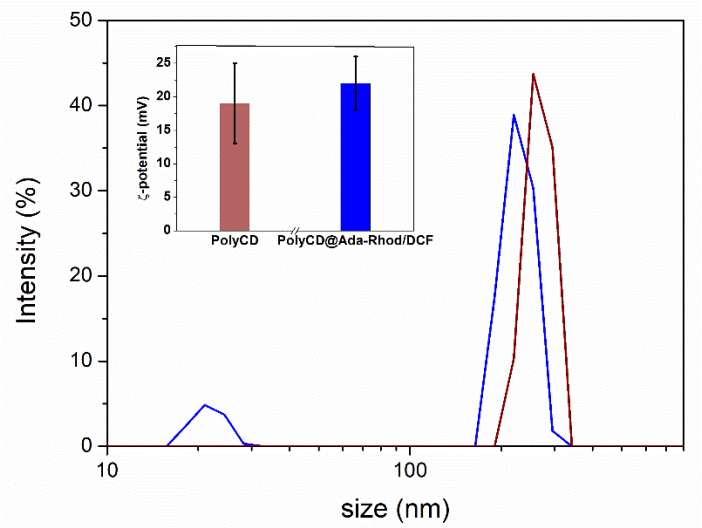

Figure 3 Size (or D_H) distribution of PolyCD (wine trace) and PolyCD@Ada-Rhod/DCF (blue trace) in ultrapure water. In the inset ζ potential ± SD of PolyCD (wine bar) and PolyCD@Ada-Rhod/DCF (blue bar). Experimental conditions: PolyCD and PolyCD@Ada-Rhod/DCF 0.5 mg/mL [DCF] = 236 μM; [Ada-Rhod] = 8 μM, in ultrapure water at r.t.

Synthesis of Ada-Rhod

The fluorescent probe Ada-Rhod has been prepared according to the synthetic procedures reported in Scheme 1. The conjugation of adamantane carboxylic acid and linker (**2**), in presence of CDI/HOBt as coupling reagents, followed by deprotection with trifluoroacetic acid (TFA), yielded compound (**3**). The conjugation of derivative (**3**) with Rhodamine B in presence of EDCI/HOBt afforded the

fluorescent probe Ada-Rhod (**5**). The chemical structure of (**5**) has been confirmed with ^{1}H, ^{13}C NMR and MALDI-TOF analysis. Ada-Rhod (**5**) has been revealed as cationic species with *m/z* 735.5 (M^{+} without Cl^{-}).

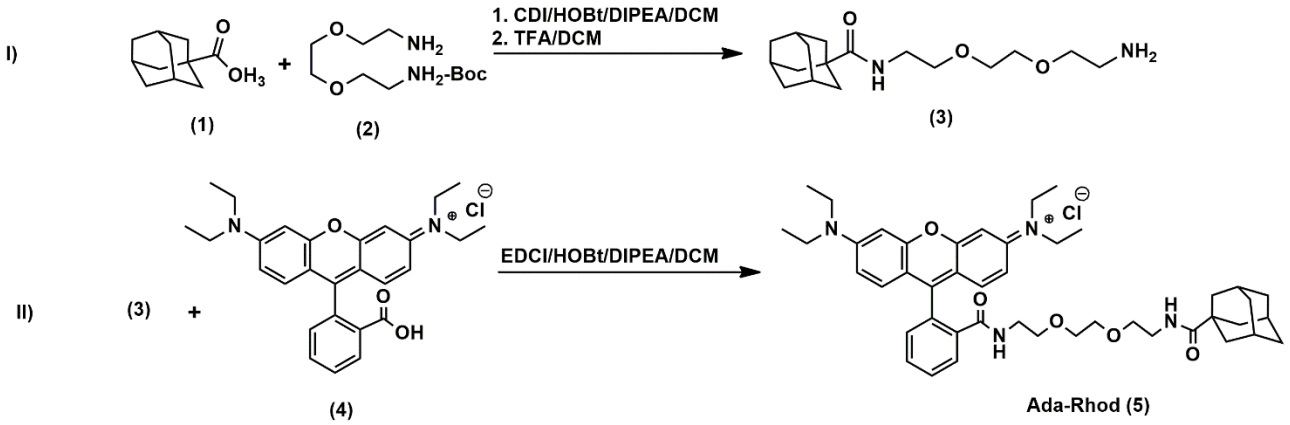

Scheme 1 Synthetic procedure for the preparation of Ada-Rhod

Interaction and complexation studies

The non-covalent interactions between PolyCD and either Ada-Rhod and DCF were investigated by spectroscopic analysis. Ada-Rhod's absorption profile shows a major band centered at 558 nm in DCM. A calibration curve for Ada-Rhod in DCM was plotted in the concentration range 25 – 200 μM (Figure 4).

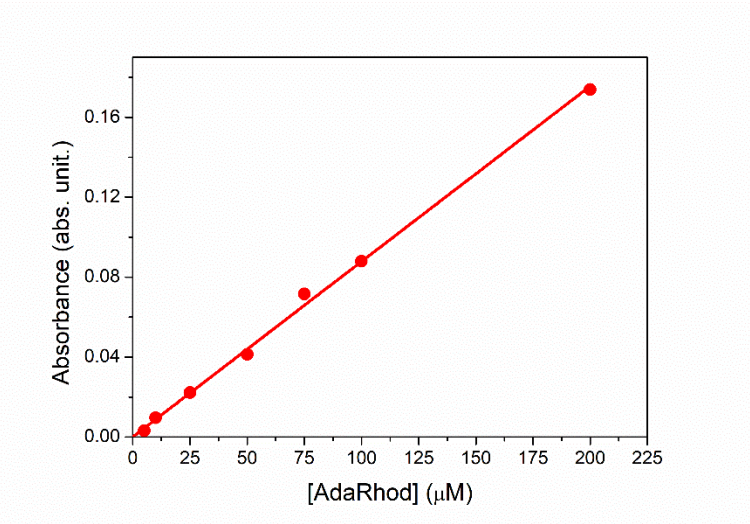

Figure 4 Determination of molar extinction coefficient by Lambert-Beer law of free Ada-Rhod in DCM at r.t.: $\varepsilon_{\text{Ada-Rhod } (\lambda max=558 \text{ nm})}$ = 877.8 ± 10 M^{-1} cm^{-1}, (R^2 = 0.99).

The entrapment of Ada-Rhod within the CD cavities onto the polymer framework has been achieved by exploiting the solvent-evaporation technique, as well as for DCF; i.e. the fluorophore was first dissolved in DCM, then evaporated in order to obtain a thin organic film, re-hydrated with an aqueous solution of PolyCD and sonicated. The chosen molar ratio for the complexation was ≅ 33:1 [CD]:[Ada-Rhod].

The complexation of Ada-Rhod within CD cavity was confirmed by UV/Vis and fluorescence emission measurements. Figure 5 displays the spectra of free Ada-Rhod in DCM vs. PolyCD@Ada-Rhod complex in ultrapure water. Ada-Rhod showed a major absorption band centered at 558 nm in DCM, which was red-shifted at 561 nm in PolyCD@Ada-Rhod, which is unambiguous evidence for Ada-Rhod complexation, since the free fluorophore is not soluble in water (Figure 5-A). Steady state emission fluorescence (Figure 5-B) of Ada-Rhod in DCM showed a band centered at 575 nm, whereas after the interaction with PolyCD in aqueous medium the fluorescence emission profile split into two bands, centered at 542 and 584 nm respectively. This double band profile is typical of Rhodamine derivatives because of the tautomeric equilibrium that occurs in water, and is strictly influenced even by slight pH changes.[12, 13]

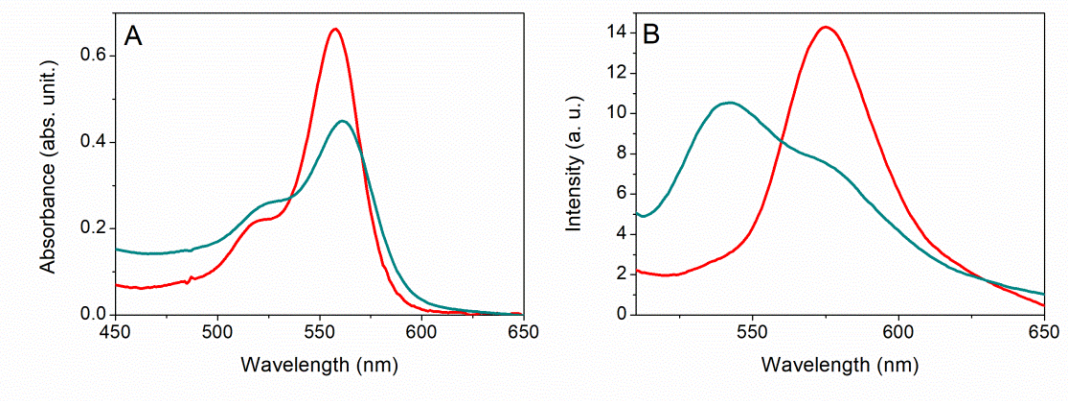

Figure 5 UV/Vis spectra (A) and steady steady state emission spectra(B) of free Ada-Rhod in DCM (red trace) and PolyCD@Ada-Rhod (blue cyan trace) in ultrapure water, pH = 4. A): PolyCD@Ada-Rhod is 44 mg/ml, [Ada-Rhod] = 713 µM, pH = 4, d = 1 cm and scattering subtracted in the spectrum of the complex. B): PolyCD@Ada-Rhod is 0.5 mg/mL, [Ada-Rhod] = 8 µM, λ_{exc} = 480 nm. [Ada-Rhod] entrapped inside the nanoassembly was obtained from EE% (Table 2) and calculated as reported in the Experimental Section.

By these findings, it is so possible to assume that the fluorophore interaction with PolyCD actually occurred, likely driven by the high affinity of adamantane moiety for CD cavity . However, it is not possible to esclude a non-specific interaction of Ada-Rhod with the polymer chains, led by weaker interactions (van der Waals or π–π bonds).

Molar extinction coefficient (ε) of DCF was spectroscopically determined by interpolation according to Lambert-Beer law, at T = 25°C. DCF solutions at different concentrations were prepared in the same conditions by evaporation of an acetone film and subsequent re-hydration, and analyzed by UV/Vis. Calibration curves of DCF either in water and in PBS (pH = 7.4) were performed and the corresponding calculated values of ε were 8130 ± 225 M^{-1} cm^{-1} and 9700 ± 767 M^{-1} cm^{-1}, respectively (Figure 6).

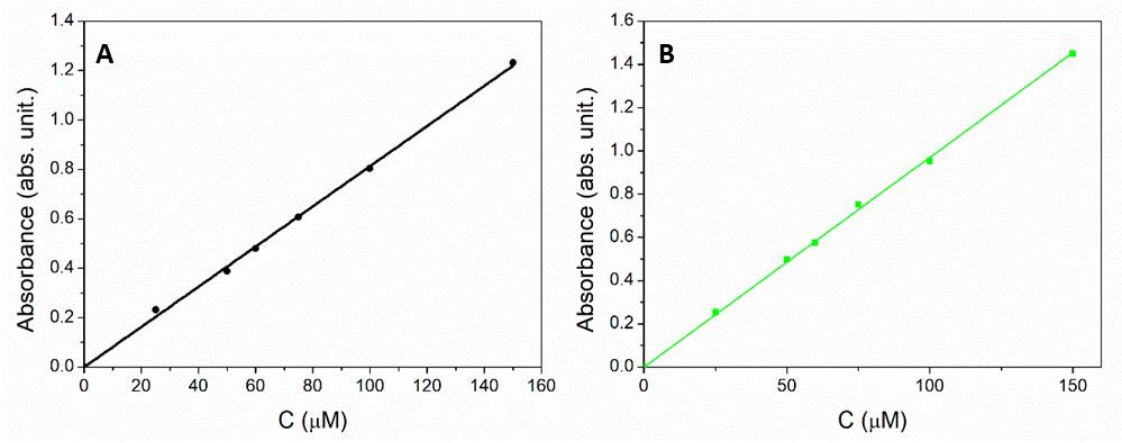

*Figure 6 Determination of molar extinction coefficients by Lambert-Beer law: **A**) in ultrapure water (free DCF, black trace) at T= 25°C: $\varepsilon_{DCF\ (\lambda max=276\ nm)}$ = 8130 ±800 M^{-1} cm^{-1} (R^2 = 0.99); **B**) in PBS (free DCF, green trace) at T = 25°C: $\varepsilon_{DCF(PBS)\ (\lambda max=276\ nm)}$ = 9700 ±767 M^{-1} cm^{-1} (R^2=0.99).*

The interaction of PolyCD with DCF was firstly studied by UV/Vis spectroscopy. As shown in Figure 7-A, free DCF displays a single absorption band centered at 276 nm, in agreement with literature data.[14] After simple mixing of the two aqueous solutions of DCF and PolyCD in equimolar amount, a slight hypercromic red shift at 278 nm was observed. For comparison, a spectrum was registered for the same complex obtained by solvent evaporation technique (i.e. hydration of organic film and sonication) and a similar shift was observed, thus confirming the interaction (data not shown).

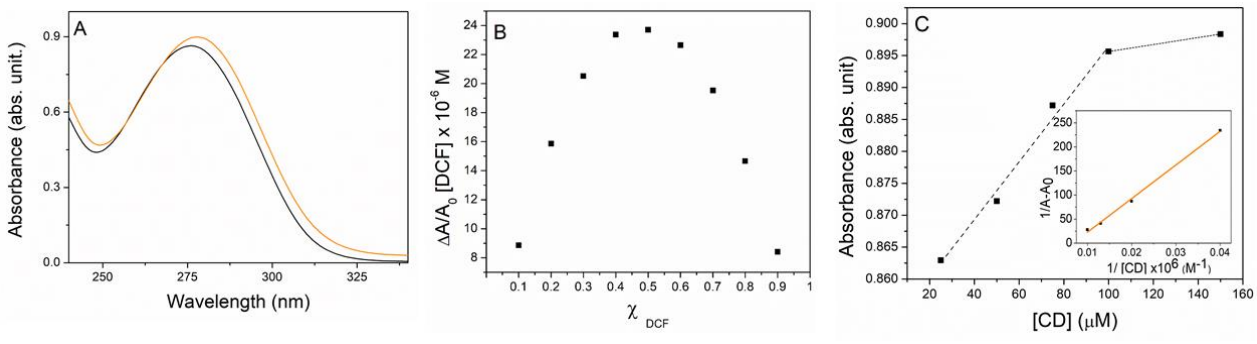

*Figure 7 (**A**) UV/Vis of free DCF (black trace) and PolyCD/DCF (orange trace), [CD] = [DCF] = 100 μM; (**B**) Job's plot for the complexation of DCF with PolyCD from UV/Vis measurements in ultrapure water (see Experimental section); (**C**) UV/Vis spectral changes of DCF vs CD concentration (dashed black traces) and plot of (1/ΔA) vs 1/[CD] (inset, orange trace, R^2 = 0.997) in ultrapure water, [DCF] = 100 μM, [CD] = 25-150 μM; d = 1 cm; T = 25 °C.*

Further interaction studies in solution have been carried out to determine the stoichiometry of the complex between the drug and the cyclodextrin's cavity by the continuous variations method.[15] The method involves preparing a series of solutions containing both the host and the guest in varying proportions so that a complete range of molar ratios is sampled, where the sum of total concentration and volume of the binding species is maintained constant for each solution, while molar fractions (χ) are varied.[16-18] Hence, the absorption values ($\Delta A/A_0$), observed at the fixed wavelength of 278 nm, were plotted against the mole fraction of the *guest*. The shape of Job's plot ($\Delta A/A_0$ × [DCF] vs. χ DCF) was highly symmetrical, showing a maximum value at χ DCF = 0.5 pointing out a formation of complex with prevalent 1:1 stoichiometry (Figure 7-B). A titration of the *guest* (at constant concentration of DCF) towards the *host* (increasing concentration of PolyCD by considering the number of CD cavities) at T= 25°C was carried out, measuring the absorbance increase vs. CD concentration in the range 0 – 150 μM. The plot reveals a bimodal behavior, with a linear increase up to 100 μM and afterwards a pseudo plateau (Figure 7-C). In the first linear portion a A_L type diagram with a slope less of a unit ($4.521 \cdot 10^{-4}$) was observed. At higher host concentrations complexes with a higher order and undefined stoichiometry could occur. The apparent binding constant for the 1:1 complex can be evaluated by using the Benesi–Hildebrand Equation:[19]

$$\frac{1}{A - A_0} = \frac{1}{K_b \times (A_{max} - A_0) \times [CD]} + \frac{1}{A_{max} - A_0} \quad (1)$$

where A is the absorbance at maximum of the PolyCD/DCF complex, A_0 is the absorbance of DCF in the absence of PolyCD, [CD] is the PolyCD concentration in CD units, A_{max} is the absorbance at $[CD]_{max}$ (100 μM) and K_b is the apparent equilibrium binding constant. The apparent binding constant was estimated from the slope $/A_{max} - A_0$ (plot of $1/(A - A_0)$ vs. 1/[CD]) and is found to be 4.1×10^3 M^{-1} (log $K_b \cong 3.60$; inset of Figure 7-C). This value agrees with data found for complexation of DCF in cationic CD cross-linked oligomers (log $K_b \cong 3.47$).[17]

Fluorescence time-decays (at λ_{exc} = 390 nm) of Ada-Rhod free and within nanoassemblies were fitted by one and three exponential profiles respectively, estimating three different fluorescence lifetimes when the probe is embedded into the polymeric structure (Figure 8).

Table 2 Fluorescence lifetimes (τ) measured at λ_{exc} = 390 nm and rotational correlation time (θ_R) of PolyCD@Ada-Rhod/DCF vs Ada-Rhod (r.t.)

Sample	λ_{em} (nm)	medium	$\tau_1 \pm 0.1$, ns	$\tau_2 \pm 0.1$, ns	$\tau_3 \pm 0.1$, ns	A_1, %	A_2, %	A_3, %	$\theta_R \pm 0.2$, ns
Ada-Rhod	576	DCM	3.6	--	--	100	--	--	0.8
PolyCD@Ada-Rhod	540	H_2O	0.9	3.2	10	35	59	6	--
PolyCD@ Ada-Rhod/DCF	540	H_2O	0.4	2.4	5.8	23	34	43	2.2

The values of fluorescence lifetimes (τ) found by fitting of the correspondent time fluorescence decay (Table 2) pointed out that free Ada-Rhod in DCM is present mostly as a monomer (τ_1 = 3.6 ns). When analyzing the ternary complex, three lifetimes were observed and one of these (τ_2 = 2.4 ns) was ascribable to Ada-Rhod that is entrapped within the polymer chains in the monomeric form.[20, 21] This might explain also the time resolved fluorescence anisotropy after interaction of Ada-Rhod within PolyCD after addition of DCF (0.8 ns in free Ada-Rhod *vs* 2.2 ns in the ternary complex), suggesting that the probe is effectively incorporated into the structure, but still has a certain freedom to rotate upon itself.[22] This is compatible with a growing complexity of the system, so it reflects effective

changes in the colloidal microenvironment surrounding the fluorophore. For what concerns the shorter times (0.9 and 0.4 ns in the complexes with and without DCF, respectively) they could be supposedly due to Ada-Rhod self-oligomers formation and other aggregation phenomena, likely generated by self π–π stacking, that led to fluorescence quenching. Finally, the longer ones ($\tau_3 \cong$ 10 and 5.8 ns) are tentatively ascribable to species of Ada-Rhod interacting differently with CD cavities (i.e., inclusion of Ada portion) both in PolyCD@Ada-Rhod and PolyCD@Ada-Rhod/DCF, respectively.

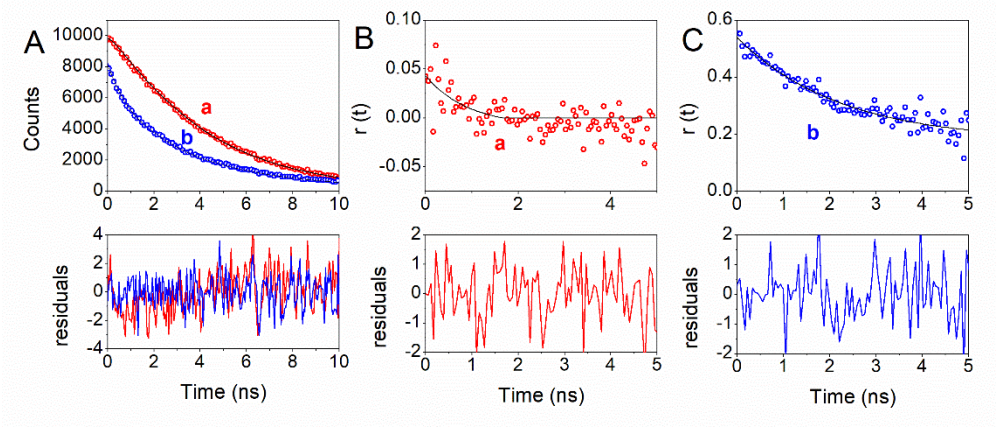

Figure 8 Fluorescence time decay (A) and time-resolved fluorescence anisotropy (B,C) of a) Ada-Rhod 100 μM in DCM; b) PolyCD@Ada-Rhod/DCF (0.5 mg/mL, [Ada-Rhod] = 8 μM, [DCF] = 236 μM) in ultrapure water at r.t.

Overall, it is possible to affirm that both DCF and Ada-Rhod certainly interact with CD cavities. Host-guest complexation of Ada-Rhod is driven by the high affinity of adamantane portion towards CD cavities ($K_b = 5 \times 10^4\ M^{-1}$),[10] and this interaction is stronger with respect to DCF with a CD cavity: indeed no Ada-Rhod displacement was observed even if DCF was used in excess *vs* Ada-Rhod. It is highly probable that upon inclusion of the adamantane unit into the CD cavity, the rhodamine residue of Ada-Rhod is located in a more hydrophilic environment, likely outside the cavity and in proximity of the CD rims. This might explain the formation of larger aggregates in PolyCD@Ada-Rhod rather than PolyCD@Ada-Rhod/DCF, observed in other nanoassemblies based on polymeric systems functionalized with rhodamine.[23] Moreover, the formation of supramolecular self-oligomers of Ada-Rhod with shorter fluorescence lifetimes (0.4 ns with amplitude 23%) could

occur, leading to an average increase of D_H in PolyCD@Ada-Rhod. On the other hand, the decrease of D_H and ζ-potential values in PolyCD@Ada-Rhod/DCF could be tentatively ascribed to the formation of more compacted and smaller nanoassemblies due to an increased colloidal stability originated from the significant interactions of DCF with both CD cavity and cationic external CD rims.

Stability studies in ultrapure water and other relevant biological media

In order to investigate if the aggregation properties of the nanoassemblies are influenced by a dispersing medium, we carried out stability studies *vs* time in water and in biologically relevant media by DLS and UV/Vis. For freshly prepared solutions at t = 0, all the absorption spectra showed a single band centered at 278 nm. Figures 9 - 11 show the changes of absorption spectra, D_H and ζ-potential *vs* time for PolyCD@Ada-Rhod/DCF nanoassemblies. In ultrapure water (Figure 9-A), within two weeks, the absorbance of the band at 278 nm decreased of about 30% with respect to the freshly prepared dispersion. Size of the nanoassemblies were monitored for up to 2 weeks. At t = 0, all the samples exhibited a size distribution with a mean diameter roughly of 250 nm, which remained approximatively costant for the first 7 days. After 2 weeks, the size significantly increased for all the dispersions in all media.

For what it concerns the other biological media (PBS and NaCl 0.9% wt), an immediate increase in size is observable after the first day (Figure 10 – 11), suggesting that the ionic strength can influence the aggregation tendency of the nanoassemblies.

In conclusion, it is possible to affirm that PolyCD@Ada-Rhod/DCF nanoassemblies are stable in aqueous solution at 25°C up to 7 days, though it is advisable to administer the saline injectable formulation within the first day after reconstitution in order to maintain a higher concentration of DCF at joint level. The ζ-potential values *vs* time were measured in ultrapure water at r.t. With a starting value at t = 0 around +20 mV, a significant increase was observed from the 7th day on. However, the sharply positive surface charge is advantageous for a rapid cellular uptake of the

nanoassemblies from the target cells, that should be completed far before one week since the local administration.

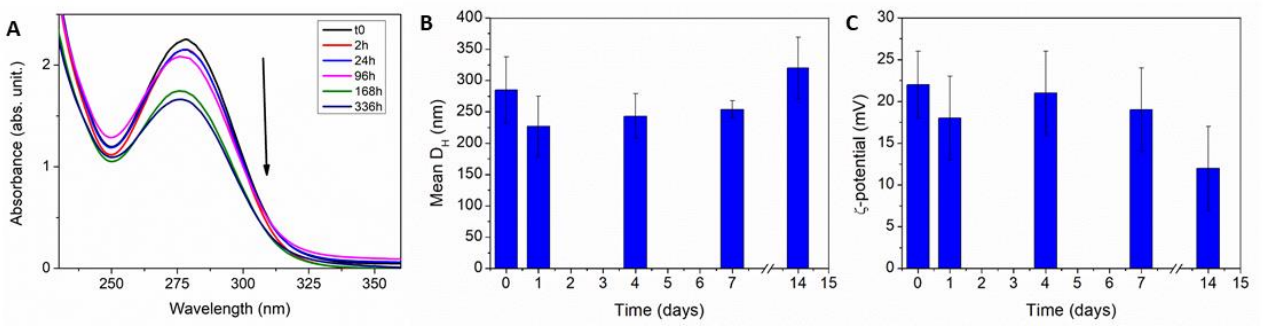

Figure 9 UV/Vis spectra (A), mean $_{DH}$ (main populations only) (B) and ξ-potential (C) vs. time of PolyCD@Ada-Rhod/DCF nanoassemblies in ultrapure water (0.5 mg/mL, [Ada-Rhod] = 8 μM, [DCF] = 236 μM). Data were acquired at t = 0, 1, 4, 7 and 14 days. Nanoassemblies dispersions were stored at 25 °C under stirring along the experimental time.

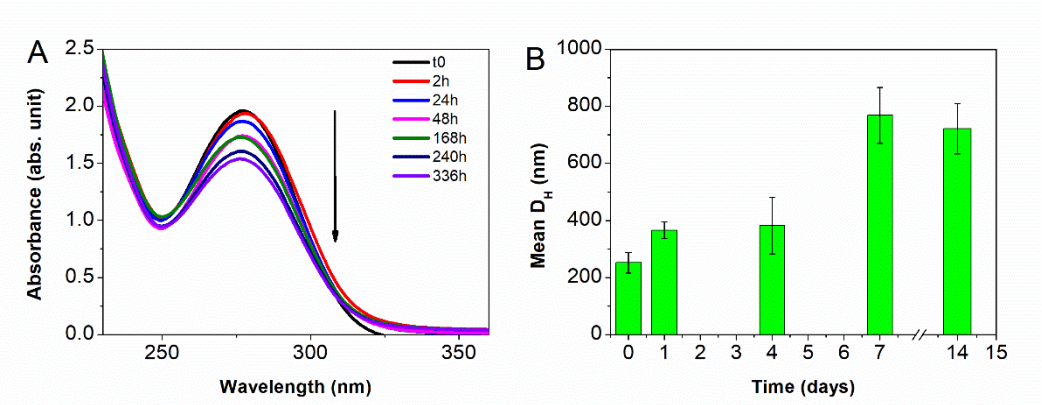

Figure 10 UV spectra (A) and mean D_H (main populations only) (B) vs time of PolyCD@Ada-Rhod/DCF nanoassemblies in NaCl wt. 0.9% (0.5 mg/mL, [Ada-Rhod] = 8 μM, [DCF] = 235 μM). Data were acquired at t = 0, 1, 4, 7 and 14 days. Nanoassembly dispersions were stored at 25 °C along the experimental time.

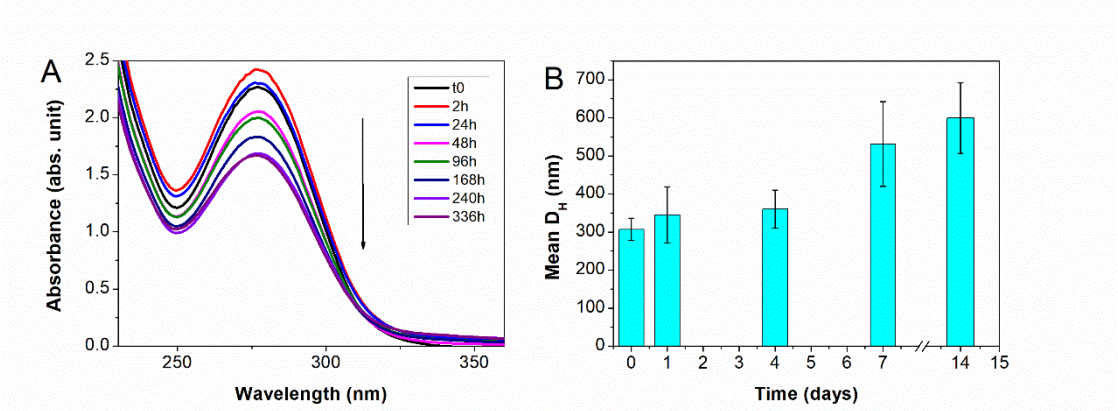

Figure 11 UV spectra (A) and mean D_H (main populations only) (B) vs time of PolyCD@Ada-Rhod/DCF nanoassemblies in PBS at pH=7.4 (0.5 mg/mL, [Ada-Rhod] = 8 μM, [DCF] = 235 μM). Data were acquired at t = 0, 1, 4, 7 and 14 days. Nanoassembly dispersions were kept at 25 °C along the experimental time.

Kinetic release of DCF from PolyCD@Ada-Rhod/DCF nanoassembly

Finally, kinetic release profiles of DCF from PolyCD@Ada-Rhod/DCF were evaluated in PBS at 37°C up to 10 days (Figure 12). Released DCF was determined exploiting the calibration curve by UV/Vis of DCF in PBS. No initial burst release was observed from the nanoassembly, with a slow and controlled release in time, leading to a final 35% of DCF in the external medium. the corresponding unreleased amount of drug in the donor compartment (55%) was determined by UV/Vis.

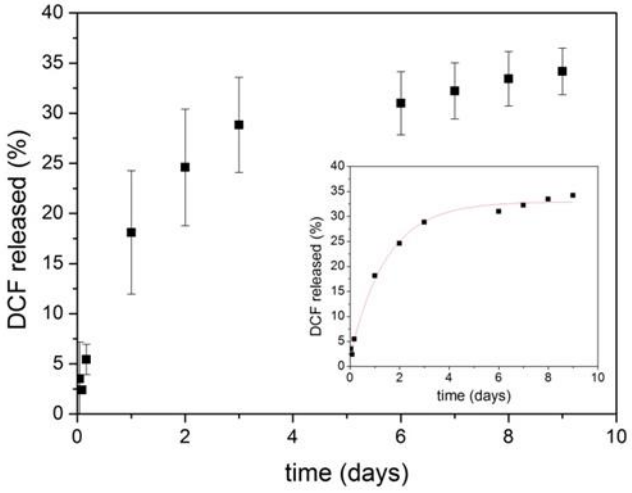

Figure 12 Release profile of DCF from PolyCD@Ada-Rhod/DCF nanoassemblies in PBS at pH = 7.4 and 37 °C (Spectra/Por® dialysis bags, MWCO 3.5 kDa). Data are reported as the mean three independent experiments ± SD. In the inset experimental data are best-fitted first order kinetic model.

The kinetic measurements were carried out according to three different models reported in the literature by Higuchi, Baker–Lonsdale and a simple first order process for different pharmaceutical dosage forms (i.e., semisolid and solid; see Table 3)[24, 25] and potentially applicable to nanoparticulate dispersions.[26, 27]

Table 3 Regression coefficient (R^2) and rate constants (k_H and k) of DCF release data from PolyCD@Ada-Rhod /DCF fitted according to different kinetic models.

Higuchi		Baker-Lonsdale		First order	
R^2	k_H ($h^{-1/2}$)	R^2	$k(h^{-1})$	R^2	$k(h^{-1})$
0.9047	12.8057 ± 0.6679	0.9241	$3.3 \times 10^{-3} \pm 3 \times 10^{-4}$	0.9952	0.6828 ± 0.0552

By best-fit of data (Figure 12, inset) it was possible to evaluate the regression coefficient (R^2) and release parameters (k/h^{-1}). By considering a first order process, as commonly known for molecular permeation across a membrane from a stirred donor into a stirred receiving phase under quasi-stationary and sink conditions,[28] the model can be represented by the following equation:

$$C_t = C_\infty(1 - e^{-kt}) \quad (2)$$

where C_t and C_∞ are the amount of drug released (in percentage) in the receiving phase at time t and at t_∞, at the end of release process, and k is the rate constant of the process. Altogether, kinetic analysis agrees with a simple mono-exponential decay that the release of DCF from the nanoassembly is a dependent first order process, showing a plateau of drug released (≅ 36%) after about 10 days.

Biological Evaluation

Biological profile of PolyCD@Ada-Rhod/DCF nanoassemblies was evaluated in collaboration with Prof Magali Cucchiarini (Center of Experimental Orthopaedics, Saarland University Medical Center, Homburg/Saar, Germany). Specifically, cellular uptake, cytotoxicity and anti-inflammatory effect were evaluated using bone-marrow derived human mesenchymal stem cells (hMSCs). The tests were performed comparing the full loaded system with PolyCD@Ada-Rhod, DCF alone and DMEM as positive controls. Figure 13 shows the strong fluorescence intensity detected in the treated cell lines, just after 2 h of incubation, that persists for at least 24 h, meaning that the doped assembly is effectively uptaken by the cells.

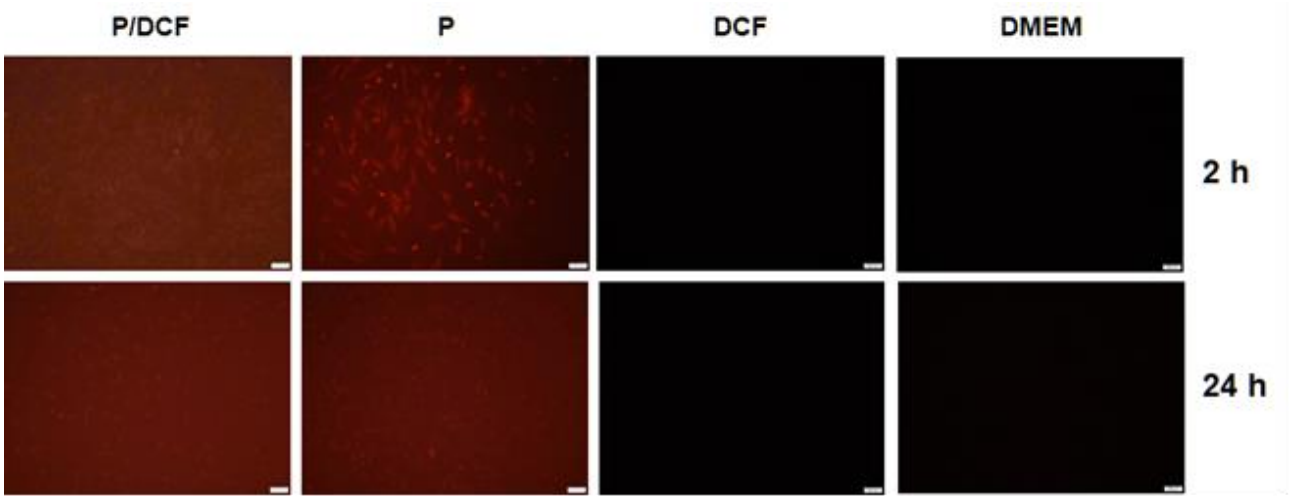

Figure 13 Detection of live fluorescence in hMSCs treated with PolyCD@Ada-Rhod/DCF (2 mg/ml). hMSCs (2 x 10^4 cells/well in 24-well plates) were directly incubated with the compounds and live fluorescence was monitored after 2 and 24 h by fluorescent microscopy as described in the Materials and Methods (scale bars: 200 μm). Abbreviations: P/DCF: PolyCD@Ada-Rhod/DCF; P: PolyCD@Ada-Rhod; DCF: diclofenac; DMEM: Dulbecco's modified Eagle's medium; P: PolyCD@Ada-Rhod.

PolyCD@Ada-Rhod showed no deleterious effects on the levels of cell proliferation and viability after 48 h, compared to the controls, highlighting the cytocompatibility of the system and its suitability as drug vehicle for biomedical application (Figure 14).

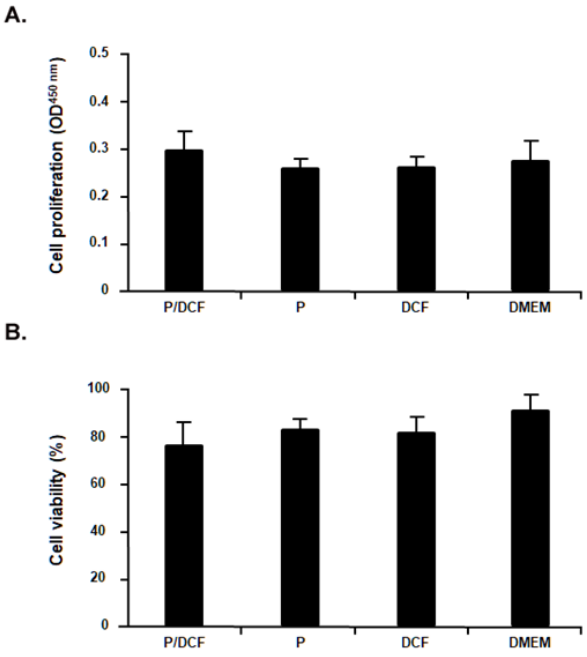

Figure 14 Analysis of cell proliferation and viability of hMSCs treated with the PolyCD-based nanoassemblies (2 mg/mL). hMSCs (2 × 10^4 cells/well in 24-well plates) were directly incubated with the compounds. Cell proliferation (A) and cell viability (B) were evaluated after 48 h. Abbreviations: P/DCF: PolyCD@Ada-Rhod/DCF; DMEM: Dulbecco's modified Eagle's medium; P: PolyCD@Ada-Rhod.

As previously stated [29] DCF has a pronounced anti-inflammatory effect due to the inibition of COX enzymes. This translates into a reduction of prostaglandine (PGE_2, PGH_2) concentrations together with other known pro-inflammatory biomarkers such as tumor necrosis factor alpha (TNF-α) and interleukines (IL-1, IL-6, IL-8). In our analysis, PolyCD@Ada-Rhod/DCF was tested to evidence its protective activity agains pro-inflammatory responses. Inflammatory responses (A: IL-1β; B: TNF-α) were detected using IL-1β and TNF-α ELISAs, respectively, after 48 h. Remarkably, the intrinsic levels of IL-1β production in hMSCs were significantly reduced after 48 h in the presence of PolyCD@Ada-Rhod/DCF *versus* all other conditions (PolyCD@Ada-Rhod in absence of DCF, DCF alone, DMEM) (up to 1.6-fold decrease, $P \leq 0.002$) (Figure 15-A).

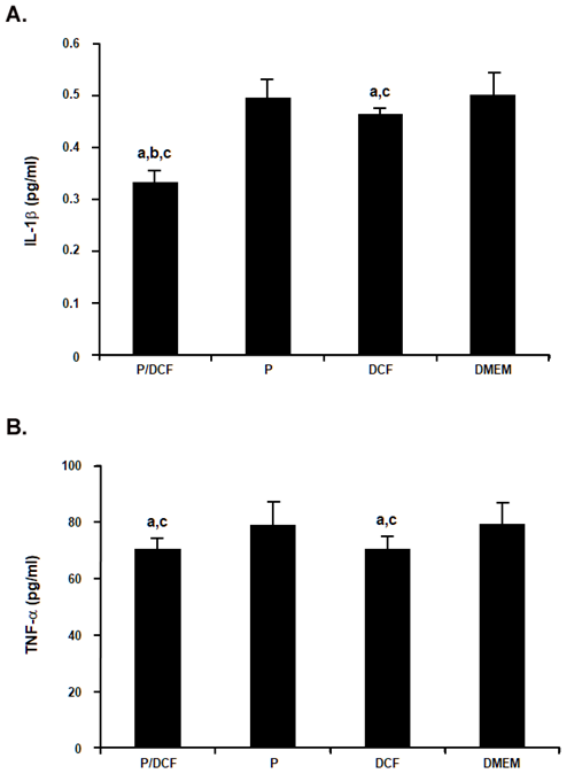

Figure 15 Analysis of inflammatory responses in hMSCs treated with PolyCD-based nanoassemblies (2 mg/mL). hMSCs (2 × 10^4 cells/well in 24-well plates) were directly incubated with the compounds. Inflammatory responses (A: IL-1β; B: TNFα) were detected using IL-1β and TNF-α ELISAs, respectively, after 48 h as described in the Materials and Methods. Statistically significant compared with DMEM (a), DCF (b), and P (c). Abbreviations: P/DCF: PolyCD@Ada-Rhod/DCF; DMEM: Dulbecco's modified Eagle's medium; P: PolyCD@Ada-Rhod.

The intrinsic levels of TNF-α production in hMSCs were also slighitly reduced after 48 h in the presence of PolyCD@Ada-Rhod/DCF *versus* PolyCD@Ada-Rhod (without DCF) and DMEM (up

to 1.2-fold decrease, $P \leq 0.003$), but without significant difference relative to DCF alone ($P = 0.188$) (Figure 15-B). This could be ascribable to the necessity of a higher dosage of DCF to effectively inhibit TNF-α production at cellular level. Anyway, it is important to remember that TNF-α and, in general, interleukins production is not only dependent by PGH deriving stimuli, but could be affected by other signaling pathways that can occur through the cell to guarantee an optimal and balanced response to inflammation.

CONCLUSIONS

In this study, the ability of poly-amino β-cyclodextrin polymer cross-linked with epichlorohydrin (PolyCD) to act as theranostic platform for the simultaneous loading of the therapeutic agent DCF and of the fluorescent probe Ada-Rhod was investigated. PolyCD was selected to take advantage of its intrinsic capability to encapsulate a wide variety of active agents and to regulate the release mechanisms by exploiting the affinity constant of the polymer towards complexed guests and their hydrophilic/lipophilic features. Physico-chemical properties of PolyCD@Ada-Rhod/DCF were elucidated by complementary spectroscopic techniques including UV/Vis, steady-state and time-resolved fluorescence, DLS and ζ-potential measurements. The nanoassembly appears as a promising candidate to manage inflammation in osteoarticular diseases. PolyCD@Ada-Rhod/DCF is suitable to develop a syringeable formulation that could sustainably release the anti-inflammatory drug for several weeks at the site of injection, allowing for a localized treatment.

Release experiments evidenced a different aptitude to deliver the payloads: a retarded release without burst effect was found for DCF, whereas no trace of florescent probe (Ada-Rhod) was detected in the aqueous medium. Biological evaluations revealed no detrimental effects on cell proliferation and viability in hMSCs. Cellular uptake is fast, within 2 h, and the cells remained fluorescent until 24 h. Finally, PolyCD@Ada-Rhod/DCF significantly suppressed IL-1β production in hMSCs, revealing the anti-inflammatory properties of these nanoassemblies.

Experimental Section

Matherials

Soluble Amino β-cyclodextrin polymer cross-linked with epichlorohydrin (NH_2-BCD)PS (PolyCD, Average MW = 25kDa, CD content ~70%) was synthesized in Cyclolab (Budapest, Hungary) as previously reported.[30] Diclofenac sodium salt (2-[2-(2,6-dichloroanilino)phenyl]acetic acid, MW = 318.13 g/mol), Rhodamine B (MW = 479.01 g/mol), adamantane carboxylic acid (MW = 180.24 g/mol), carbonyldiimidazole (CDI, MW = 162.15 g/mol), N-Boc- 2,2′-(ethylenedioxy)diethylamine (MW = 248.32 g/mol), N,N-Diisopropylethylamine (DIPEA, MW = 129.24 g/mol) and all the solvents (analytical grade) were purchased from Sigma-Aldrich (Milano, Italy). All the dispersions used for nanoassemblies preparation and spectroscopic characterizations were prepared in ultrapure water (Fresenius Kabi Italia) or in 10 mM phosphate buffer containing NaCl (137 mM) and KCl (2.7 mM) at pH 7.4 (PBS) at room temperature (r.t ≅ 25 °C). pH measurements were obtained using a 827 pH Lab pHmeter – Metrohm. N, N'-carbonyldiimidazole (CDI), N-(3-dimethylaminopropyl)-N′-ethylcarbodiimide hydrochloride (EDC), N,N-diisopropylethylamine (DIPEA), Hydroxybenzotriazole (HOBt) and all the reagents and solvents (analytical grade) were purchased from Sigma-Aldrich (Milano, Italy).

For the biological tests: all reagents were from Sigma (Munich, Germany) unless otherwise indicated. Recombinant FGF-2 (rFGF-2) was purchased at R&D Systems (Wiesbaden-Nordenstadt, Germany). The Cell Proliferation Reagent WST-1 and the Cytotoxicity Detection KitPLUS (LDH) were obtained at Roche Applied Science (Mannheim, Germany). The Human IL-1β and TNF-α enzyme-linked immunosorbent assays (ELISAs) (Human IL-1β Quantikine ELISA, TNF-α Quantikine ELISA) were from R&D Systems.

Characterization techniques

NMR spectra were recorded on a Varian 500 and 300 MHz spectrometer at room temperature (25°C). The chemical shifts are expressed in ppm downfield from tetramethylsilane (TMS).

MALDI-TOF mass spectra were collected by a Voyager DE (PerSeptive Biosystem) using a delay extraction procedure (25 kV applied after 2600 ns with a potential gradient of 454 V mm^{-1} and a wire voltage of 25 V) and detecting the ions in linear mode. The analyses were performed by loading on the sample plate 0.005 mmol of sample and 0.4 mmol of *trans*-2-[3-(4-*tert*-butylphenyl)-2- methyl-2 propenylidene]-malononitrile (DCTB) as a matrix, using $CHCl_3$ or DMF as solvents. 5,10-di(p-dodecanoxyphenyl)-15,20-di(p-hydroxyphenyl) porphyrin ($C_{68}H_{78}N_4O_4$, 1014 Da), tetrakis(p-dodecanoxyphenyl)porphyrin ($C_{92}H_{126}N_4O_4$, 1350 Da) and a PEG sample of known molecular structure were used as external standards for *m*/*z* calibration. Mass spectra were elaborated with *Grams* software (ver. 3.04), by *Perseptive Biosystems.*

Size and ζ-potential measurements

The mean diameter, width of distribution (polidispersity index, PDI) and ζ-potential of the PolyCD based nanoassemblies were measured through photon correlation spectroscopy (PCS) by a Zetasizer Nano ZS (Malvern Instrument, Malvern, U.K.) at r.t. (T≅ 25°C) in ultrapure water. The measurements were performed at a 173° angle with respect to the incident beam for each dispersion. The deconvolution of the measured correlation curve to an intensity size distribution was achieved by using a non-negative least-squares algorithm. The ζ-potential values were determined using a Zetasizer Nano ZS Malvern Instrument equipped with a He−Ne laser at a power P = 4.0 mW and λ = 633 nm. The results are reported as the mean of three separate measurements on three different batches ± the standard deviation (SD).

UV/Vis Spectroscopy

UV/Vis spectra were obtained on an Agilent model 8453 diode array spectrophotometer, using 1 cm and 0.5 cm path length quartz cells at r.t. (T≅ 25 °C) or, where it is specified, at T= 25°C by using a thermostatic bath.

Steady state and time-resolved fluorescence spectroscopy

Steady-state fluorescence measurements were performed on a Jasco model FP-750 spectrofluorimeter equipped with a 150W Xenon lamp with right angle detection geometry, by using a 1 cm path length quartz cell. Time-resolved measurements were registered with a Jobin Yvon-Spex Fluoromax 4 spectrofluorimeter and elaborated according to the *Time-Correlated Single-Photon Counting* (TCSPC) technique. A NanoLed (λ = 390 nm) was used as excitation source. All spectra were recorded at r.t. (T≅ 25 °C).

Aminoβ-cyclodextrin polymer cross-linked with epichlorohydrin (NH_2-BCD)PS (PolyCD)

PolyCD samples (synthesized at CycloLab, Budapest) were prepared via classical polycondensation strategy with epichlorohydrine in alkaline medium.[30] The average polymer molecular weight (average MW) is 25 kDa with a CD content of ~70%. We estimated that average number of CD cavities on polymer network is 15 and the molecular weight for the PolyCD repetitive unit is 1666,67 g/mol. PolyCD possesses amino groups in chlorohydrate form, a colorimetric Kaiser Test[31] to estimate the amount of amino groups, according to the following equation:

$$\mathrm{NH_2\ loading\ (mmol/g)^a} = \frac{[\mathrm{Abs_{sample}} - \mathrm{Abs_{blank}}]\ \mathrm{x\ dilution\ (mL)\ x\ 10^3}}{\varepsilon\ (\mathrm{M^{-1}cm^{-1}})\ \mathrm{x\ sample\ weight\ (mg)x\ optical\ path\ (cm)}} \qquad (3)$$

where Abs_{sample} is the absorbance at absorption maximum due to the amino groups of the PolyCD sample (λ_{max} = 574 nm), Abs_{blank} was measured at the same conditions but without PolyCD. Dilution was fixed to 5 mL and extinction coefficient (ε) at 574 nm was 15,000 M^{-1} cm^{-1}. Optical path was 0.5

cm. By applying the reported equation, the amount of amino group determined by UV/Vis was 0.21 mmol/g, with a maximum absorption at 574 nm, corresponding to what reported in literature.[32]

Fluorescent probe **Ada-Rhod** has been prepared according to literature methods.[20, 33]

Synthesis of N-(2-(2-(2-aminoethoxy)ethoxy)ethyl)adamantane-1-carboxamide (**3**)

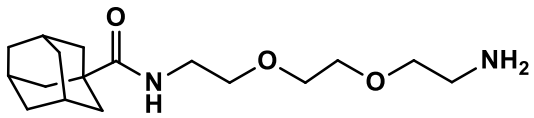

Adamantyl carboxylic acid (**1)**, (180 mg, 1 mmol) was added to a round-bottom flask containing dry toluene (20 mL) and fitted with a reflux condenser, a dry Argon inlet, and a magnetic stirrer. The solution was heated up to 60 °C and stirred. CDI (169 mg, 1 mmol) was added to the solution and stirred until the CO_2 evolution had ceased. The solution was heated for a further 30 min and purged with argon. N-Boc- 2,2′-(ethylenedioxy)diethylamine (**2**) (250 mg 1.0 mmol) was added to the solution and allowed to stir at 60 °C for a further 2 h and then cooled to room temperature. The reaction mixture was concentrated in vacuo, and the remaining clear liquid was dissolved in dichloromethane (DCM) and washed three times with water (3 x 10 mL). The washed DCM solution was dried with anhydrous Na_2SO_4, filtered, and concentrated to give 408 mg of Ada-LinkerNHBoc as a clear oil. Ada-LinkerNHBoc ($C_{22}H_{38}N_2O_5$) was obtained in nearly quantitative yield (98%) and was used without further purification. **^{1}H NMR** (500 MHz, $CDCl_3$): δ = 1.36 (s, 9H), 1.61-66 (m, 6H, 1,7,9-H), 1.76 (m,6H, 3,5,10-H), 1.96 (s, 3H, 2,6,8-H), 3.25 (m, 2H, 17-H), 3.35 (m, 2H, 12-H), 3.50 (m, 4H, 14,15-H), 3.55 (m, 4H, 13,16-H), 4.95 (s, 1H, NH), 6.15 (s, 1H, NH). Finally, to a solution of Ada-LinkerNHBoc (380 mg, 1 mmol) in DCM (2 mL), 3 mL of trifluoroacetic acid (TFA) was added dropwise and the reaction mixture was stirred at room temperature for 2 h. The reaction mixture was washed with a solution of KOH (10 %) and the organic phases were dried, filtered, and concentrated. The crude product was purified by column chromatography using DCM/ethanol in 2:1 mixture; (silica gel, 1% NH_3, Rf = 0.25). N-(2-(2-(2-

aminoethoxy)ethoxy)ethyl)adamantane-1-carboxamide (**3**) was obtained as sticky white solid (235 mg, 0.75 mmol, 75 % yield). NMR spectra matched those reported in the literature.[34, 35] MALDI-TOF (m/z): 311.23 [MH+] and [MNa+] 333.23 cld for $C_{17}H_{30}N_2O_3$ 310.23.

Synthesis of Ada-Rhod **(5)**

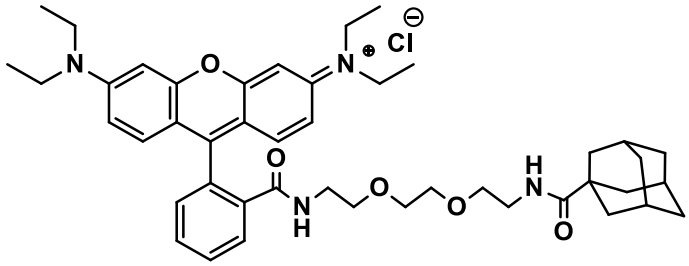

Rhodamine B (308 mg, 60.44 mmol) and EDCI (186 mg, 96 mmol) were solubilized in 10 mL of dry DCM in a 100 mL round-bottomed flask. The mixture was stirred for 30 minutes and then HOBt (130 mg, 96 mmol) dissolved in 5 mL of dry DCM, **(3)** (200 mg, 60.44 mmol) and DIPEA (134 µL, 77 mmol) were added. The purple solution was left over stirring in dark at r.t. for 24 h. Finally, the solvent was removed under reduced pressure and the obtained oil was washed twice with citric acid (10% w/w) and a saturated solution of $NaHCO_3$; the organic phase was dried with Na_2SO_4, filtered and evaporated. The residue was purified by column chromatography using $CHCl_3$/MeOH 95/5 eluent mixture to obtain Ada-Rhod **(5)** (yield = 140 mg, 60%).

^{1}H NMR (300 MHz, $CDCl_3$,) δ: 1.11 (t, 12H, J=6 Hz), 1.61-1.66 (m, 6H), 1.77 (d, 6 H, J= 3Hz), 1.79 (m, 1H), 1.83 (m, 1H), 1.86 (m, 1H), 3.10-3.15 (t, 4H, J= 6Hz), 3.30 (q, 8H, J= 6Hz), 3.38-3.58 (m, 8H), 6.20-6.38 (m, 6H), 6.97-7.03 (m, 1H), 7.34-7.39 (m, 2H), 7.81-7.86 (m, 1 H).

^{13}C NMR (300 MHz, $CDCl_3$) δ: 12.39, 27.64, 27.70, 27.84, 36.23, 36.28, 38.57, 38.59, 38.69, 38.83, 39.02, 44.16, 69.6, 69.81, 67.55, 64.66, 97.19, 105.19, 107.41, 122.41, 123.44, 127.19, 128.52, 130.57, 132.35, 148.29, 152.85, 153.43, 168.12, 177.95.

MALDI-TOF (m/z): 735.5 $[M\text{-}Cl^-]^+$

Preparation of Nanoassemblies (PolyCD@Ada-Rhod, PolyCD/DCF, PolyCD@Ada-Rhod/DCF)

PolyCD@Ada-Rhod. The complex was prepared at [CD]:[Ada-Rhod] ≅ 33:1 molar ratio (0.017 μmol of Ada-Rhod / mg of PolyCD). Briefly, Poly CD was dissolved in ultrapure water (44 mg/ 4.4 ml) and sonicated in ultrasonic bath (10 min). A thin Ada-Rhod organic film (0.6 mg) was prepared by slow evaporation of a dichloromethane (DCM) solution and this latter was hydrated with the previously prepared polymer solution (heated at 50°C), followed by sonication in ultrasonic bath (1h 30 min). The pink aqueous phase was collected and analyzed, whereas the residual Ada-Rhod film was separed by slight centrifugation and used to determine Ada-Rhod actual loading into the complex by difference with the starting weighed amount.

PolyCD/DCF. An aqueous solution of PolyCD was prepared by solubilizing PolyCD in ultrapure water (MW of repetitive unit = 1666.67 g mol^{-1}; 2.5 mg/3 mL) and by using a probe sonicator for 10 minutes. Such solution was used to re-hydrate a DCF organic thin film ([CD]:[DCF] ≅ 1:1), previously obtained by evaporation from acetone.

PolyCD@Ada-Rhod/DCF. An organic film of DCF (17 mg at [CD]:[DCF] 1:1 molar ratio), previously prepared by slow evaporation of an acetone solution, was hydrated with an aqueous solution of PolyCD@Ada-Rhod (92.3 mg/10 mL). All the samples were freeze-dried and then reconstituted in aqueous medium. After freezedrying, recovery yield was calculated considering the final recovered amount of product (mg) vs. the initial weighed amount of each component.

Loading and Entrapment Efficiency

Both Ada-Rhod or DCF actual loading (AL%) and entrapment efficiency percentages (EE%) were evaluated by UV/Vis spectroscopy using the following equations:

$$AL\ (\%) = \frac{amount\ of\ Ada-Rhod\ or\ DCF\ into\ the\ nanoassembly}{weight\ of\ nanoassembly} \times 100 \qquad (4)$$

$$TL\ (\%) = \frac{amount\ of Ada-Rhod\ or\ DCF\ initially\ added\ to\ formulation}{weight\ of\ nanoassembly} \times 100 \qquad (5)$$

$$EE\ (\%) = \frac{amount\ of\ Ada-Rhod\ or\ DCF\ in\ nanoassembly}{amount\ of\ Ada-Rhod\ or\ DCF\ initially\ added\ to\ formulation} \times 100 \qquad (6)$$

The amount of Ada-Rhod loaded into the system was calculated by re-dissolving the residual film from the complexation reaction in DCM and measuring its absorption intensity. Molar extinction coefficient for Ada-Rhod (ε = 877.8 M^{-1} cm^{-1}) was determined by performing a Lambert-Beer calibration curve in DCM, in the concentration range 25 – 200 μM.

DCF actual loading inside PolyCD@Ada-Rhod system and EE% were evaluated by dissolving a weighed amount of freeze-dried nanoassembly (0.5 mg/mL) in ultrapure water under magnetic stirring at r.t. and analyzing it by UV/Vis. Calibration curves both for free DCF and for the 1:1 complex were performed either in water and PBS and the calculated molar extinction coefficients were respectively 8310 $\pm$ 200 M^{-1} cm^{-1} and 9700 $\pm$ 767 M^{-1} cm^{-1}.

Stability studies

Stability studies were carried out by dissolving PolyCD@Ada-Rhod/DCF in different biological media: (i) ultrapure water, (ii) 0.9 wt % NaCl aqueous solution, (iii) PBS at pH 7.4. All the solutions were kept under stirring (T = 25°C) along 14 days and analyzed by UV/Vis and DLS at r.t. in triplicate. ζ-Potential was measured along 2 weeks on the dispersions prepared in ultrapure water and stored at 25 °C.

Release study

Release profile of DCF from PolyCD@Ada-Rhod/DCF nanoassembly was evaluated in PBS at pH 7.4 by a dialysis method. PolyCD@Ada-Rhod/DCF (10 mg) in PBS (1 ml) were put into a dialysis tube (Spectra/Por® dialysis bags, MWCO 3500 kDa) and immersed into 10 ml of PBS (sink condition) under continuous stirring (250 rpm) at 37 ± 0.5 °C. At fixed times, 1 ml of release medium was withdrawn and replaced with an equal volume of fresh aqueous solution of PBS. The amount of

DCF released was evaluated by UV-Vis spectroscopy (at λ= 276 nm) and was expressed as percentage ratio between the weight of released DCF and the total amount of entrapped drug. The kinetic analysis was carried by three models proposed in the literature such as Higuchi, Baker–Lonsdale and the first order process[24, 26].

Kinetic analysis of release

The kinetic analysis (Table 4) was performed using three different models proposed in the literature by Higuchi, Baker-Lonsdale and a simple first order process. The first model describes drug release from the matrix as a square root of a time dependent process based on Fickian diffusion. It is possible to resume the Higuchi model with the following expression (generally known as the simplified Higuchi model):

$$C_t = k_H t^{\frac{1}{2}} \quad (7)$$

where C_t is the amount of the drug released (in percentage) as function of time t and k_H is the Higuchi dissolution constant.

The Baker-Lonsdale model describes the drug controlled release from a spherical matrix, as follows:

$$\frac{3}{2}\left[1-\left(1-\frac{C_t}{C_\infty}\right)^{2/3}\right]-\frac{C_t}{C_\infty}=kt \quad (8)$$

where C_t and C_∞ are the amounts of drug released in the receiving phase (in percentage) at time t and t_∞, respectively.

BIOLOGICAL ASSAYS

Cell Culture

Bone marrow aspirates (~ 15 ml) were obtained from distal femurs of patients undergoing total knee arthroplasty (n = 8, age 68-74 years). The study was approved by the Ethics Committee of the Saarland Physicians Council. All procedures were in accordance with the Helsinki Declaration and all patients provided informed consent before inclusion in the study. Bone marrow-derived human mesenchymal stromal cells (hMSCs) were isolated according to standard protocols [36, 37] by washing and centrifuging the aspirates in Dulbecco's modified Eagle's Medium (DMEM). The cell pellet was resuspended in red blood cell lysing buffer (Sigma) and DMEM (1:1). The mixture was washed, pelleted, and resuspended in DMEM with 10% fetal bovine serum, 100 U/ml penicillin, and 100 µl/ml streptomycin (growth medium). The cells were plated in T75 flasks and kept at 37°C under 5% CO_2 overnight. The medium was then removed and replaced by growth medium with recombinant FGF-2 (1 ng/ml), with medium exchanged every 2-3 days. Proliferating cells were replated when reaching a 85% density and hMSCs were further used at no more than passage 1-2.

Detection of live fluorescence

hMSCs were seeded in 24-well plates (2 x 104 cells/well) with growth medium for 12 h at 37°C under 5% CO_2. The PolyCD based compounds were then directly added to the cultures and live fluorescence was monitored in the samples by fluorescent microscopy using a rhodamine filter set (568 nm) (Olympus CKX41; Hamburg, Germany).[36, 38]

Cell proliferation and viability

hMSCs were seeded in 24-well plates (2 x 104 cells/well) with growth medium for 12 h at 37°C under 5% CO_2 prior to direct addition of the PolyCD based compounds to the cultures. Cell proliferation was evaluated using the Cell Proliferation Reagent WST-1 according to the manufacturer's recommendations.[36-38] Cell viability was determined with the Cytotoxicity Detection KitPLUS (LDH) in the supernatants of culture by assessing the absorbance at 450 nm on a GENios spectrophotometer/fluorometer (Tecan, Crailsheim, Germany). Cytotoxicity was calculated as follows:[38]

*cell viability (%) = (experimental value - low control) / (high control - low control) * 100*

where low control are samples without assay treatment and high control are samples incubated in the lysis buffer of the kit.

Inflammatory responses

hMSCs were seeded in 24-well plates (2 x 10^4 cells/well) with growth medium for 12 h at 37°C under 5% CO_2 prior to direct addition of the PolyCD compounds to the cultures. Inflammatory responses were monitored by measuring the production levels of IL-1β and TNF-α in the supernatants of culture by respective ELISAs on a GENios spectrophotometer/fluorometer.

Statistical analysis

All tests were performed in triplicate in three independent experiments. Data are expressed as mean ± standard deviation (SD) of separate experiments. The t-test was employed where appropriate, with $P < 0.05$ considered statistically significant.

References

1. He, Z.; Wang, B.; Hu, C.; Zhao, J., An overview of hydrogel-based intra-articular drug delivery for the treatment of osteoarthritis. *Colloids and Surfaces B: Biointerfaces* **2017,** *154*, 33-39.
2. Qi, X.; Qin, X.; Yang, R.; Qin, J.; Li, W.; Luan, K.; Wu, Z.; Song, L., Intra-articular Administration of Chitosan Thermosensitive In Situ Hydrogels Combined With Diclofenac Sodium–Loaded Alginate Microspheres. *Journal of Pharmaceutical Sciences* **2016,** *105* (1), 122-130.
3. Bottini, M.; Bhattacharya, K.; Fadeel, B.; Magrini, A.; Bottini, N.; Rosato, N., Nanodrugs to target articular cartilage: An emerging platform for osteoarthritis therapy. *Nanomedicine: Nanotechnology, Biology and Medicine* **2016,** *12* (2), 255-268.
4. Scavone, C.; Bonagura, A. C.; Fiorentino, S.; Cimmaruta, D.; Cenami, R.; Torella, M.; Fossati, T.; Rossi, F., Efficacy and Safety Profile of Diclofenac/Cyclodextrin and Progesterone/Cyclodextrin Formulations: A Review of the Literature Data. *Drugs in R&D* **2016,** *16* (2), 129-40.
5. Bogdan, M.; Caira, M. R.; Bogdan, D.; Morari, C.; Fărcaş, S. I., Evidence of a Bimodal Binding between Diclofenac-Na and β-Cyclodextrin in Solution. *Journal of inclusion phenomena and macrocyclic chemistry* **2004,** *49* (3), 225-229.
6. Szente, L.; Szejtli, J., Highly soluble cyclodextrin derivatives: chemistry, properties, and trends in development. *Advanced drug delivery reviews* **1999,** *36* (1), 17-28.
7. Cwiertnia, B.; Hladon, T.; Stobiecki, M., Stability of diclofenac sodium in the inclusion complex with beta-cyclodextrin in the solid state. *The Journal of pharmacy and pharmacology* **1999,** *51* (11), 1213-8.
8. Caira, M.; Griffith, V.; Nassimbeni, L.; calorimetry, Desorption of water from CD/drug inclusion complexes. *Journal of thermal analysis and calorimetry* **1998,** *51* (3), 981-991.
9. Owen, S. G.; Francis, H. W.; Roberts, M. S., Disappearance kinetics of solutes from synovial fluid after intra-articular injection. *Br J Clin Pharmacol* **1994,** *38* (4), 349-55.
10. Granadero, D.; Bordello, J.; Pérez-Alvite, M. J.; Novo, M.; Al-Soufi, W. J., Host-guest complexation studied by fluorescence correlation spectroscopy: adamantane–cyclodextrin inclusion. *International journal of molecular sciences* **2010,** *11* (1), 173-188.
11. Mandal, A.; Bisht, R.; Rupenthal, I. D.; Mitra, A. K., Polymeric micelles for ocular drug delivery: From structural frameworks to recent preclinical studies. *Journal of Controlled Release* **2017,** *248*, 96-116.

12. Stephenson, C. J.; Shimizu, K. D., A fluorescent diastereoselective molecular sensor for 1,2-aminoalcohols based on the rhodamine B lactone–zwitterion equilibrium. *Organic & Biomolecular Chemistry* **2010,** *8* (5), 1027-1032.

13. Beija, M.; Afonso, C. A. M.; Martinho, J. M. G., Synthesis and applications of Rhodamine derivatives as fluorescent probes. *Chemical Society Reviews* **2009,** *38* (8), 2410-2433.

14. Mehta, S. K.; Bhasin, K. K.; Dham, S., Energetically favorable interactions between diclofenac sodium and cyclodextrin molecules in aqueous media. *Journal of colloid and interface science* **2008,** *326* (2), 374-81.

15. Renny, J. S.; Tomasevich, L. L.; Tallmadge, E. H.; Collum, D. B., Method of continuous variations: applications of job plots to the study of molecular associations in organometallic chemistry. *Angew Chem Int Ed Engl* **2013,** *52* (46), 11998-2013.

16. Upadhyay, S. K.; Kumar, G., NMR and molecular modelling studies on the interaction of fluconazole with beta-cyclodextrin. *Chem Cent J* **2009,** *3*, 9-9.

17. Giglio, V.; Sgarlata, C.; Vecchio, G., Novel amino-cyclodextrin cross-linked oligomer as efficient carrier for anionic drugs: a spectroscopic and nanocalorimetric investigation. *RSC Advances* **2015,** *5* (22), 16664-16671.

18. MacCarthy, P., Simplified experimental route for obtaining Job's curves. *Analytical Chemistry* **1978,** *50* (14), 2165-2165.

19. Benesi, H. A.; Hildebrand, J. H., A Spectrophotometric Investigation of the Interaction of Iodine with Aromatic Hydrocarbons. *Journal of the American Chemical Society* **1949,** *71* (8), 2703-2707.

20. Piperno, A.; Mazzaglia, A.; Scala, A.; Pennisi, R.; Zagami, R.; Neri, G.; Torcasio, S. M.; Rosmini, C.; Mineo, P. G.; Potara, M.; Focsan, M.; Astilean, S.; Zhou, G. G.; Sciortino, M. T., Casting Light on Intracellular Tracking of a New Functional Graphene-Based MicroRNA Delivery System by FLIM and Raman Imaging. *ACS Applied Materials & Interfaces* **2019,** *11* (49), 46101-46111.

21. Mercadé-Prieto, R.; Rodriguez-Rivera, L.; Chen, X. D., Fluorescence lifetime of Rhodamine B in aqueous solutions of polysaccharides and proteins as a function of viscosity and temperature. *Photochemical & Photobiological Sciences* **2017,** *16* (11), 1727-1734.

22. Maiti, N. C.; Krishna, M. M. G.; Britto, P. J.; Periasamy, N., Fluorescence Dynamics of Dye Probes in Micelles. *The Journal of Physical Chemistry B* **1997,** *101* (51), 11051-11060.

23. Liénard, R.; Montesi, M.; Panseri, S.; Dozio, S. M.; Vento, F.; Mineo, P. G.; Piperno, A.; De Winter, J.; Coulembier, O.; Scala, A., Design of naturally inspired jellyfish-shaped

cyclopolylactides to manage osteosarcoma cancer stem cells fate. *Materials Science and Engineering: C* **2020,** *117*, 111291.

24. Siepmann, J.; Peppas, N. A., Higuchi equation: derivation, applications, use and misuse. *Int J Pharm* **2011,** *418* (1), 6-12.

25. Costa, P.; Sousa Lobo, J. M., Evaluation of Mathematical Models Describing Drug Release from Estradiol Transdermal Systems. *Drug Development and Industrial Pharmacy* **2003,** *29* (1), 89-97.

26. Zagami, R.; Franco, D.; Pipkin, J. D.; Antle, V.; De Plano, L.; Patanè, S.; Guglielmino, S.; Monsù Scolaro, L.; Mazzaglia, A., Sulfobutylether-β-cyclodextrin/5,10,15,20-tetrakis(1-methylpyridinium-4-yl)porphine nanoassemblies with sustained antimicrobial phototherapeutic action. *Int J Pharm* **2020,** *585*, 119487.

27. Zambito, Y.; Pedreschi, E.; Di Colo, G., Is dialysis a reliable method for studying drug release from nanoparticulate systems?-A case study. *Int J Pharm* **2012,** *434* (1-2), 28-34.

28. Bottari, F.; Colo, G. D.; Nannipieri, E.; Saettone, M. F.; Serafini, M. F., Evaluation of a dynamic permeation technique for studying drug-macromolecule interactions. *J Pharm Sci* **1975,** *64* (6), 946-9.

29. Bariguian Revel, F.; Fayet, M.; Hagen, M., Topical Diclofenac, an Efficacious Treatment for Osteoarthritis: A Narrative Review. *Rheumatology and Therapy* **2020**.

30. Malanga, M.; Bálint, M.; Puskás, I.; Tuza, K.; Sohajda, T.; Jicsinszky, L.; Szente, L.; Fenyvesi, É., Synthetic strategies for the fluorescent labeling of epichlorohydrin-branched cyclodextrin polymers. *Beilstein J Org Chem* **2014,** *10*, 3007-3018.

31. Kaiser, E.; Colescott, R. L.; Bossinger, C. D.; Cook, P. I., Color test for detection of free terminal amino groups in the solid-phase synthesis of peptides. *Analytical biochemistry* **1970,** *34* (2), 595-8.

32. Tuci, G.; Vinattieri, C.; Luconi, L.; Ceppatelli, M.; Cicchi, S.; Brandi, A.; Filippi, J.; Melucci, M.; Giambastiani, G., "Click" on tubes: a versatile approach towards multimodal functionalization of SWCNTs. *Chemistry* **2012,** *18* (27), 8454-63.

33. Zagami, R.; Rapozzi, V.; Piperno, A.; Scala, A.; Triolo, C.; Trapani, M.; Xodo, L. E.; Monsù Scolaro, L.; Mazzaglia, A., Folate-Decorated Amphiphilic Cyclodextrins as Cell-Targeted Nanophototherapeutics. *Biomacromolecules* **2019,** *20* (7), 2530-2544.

34. Guaragna, A.; Chiaviello, A.; Paolella, C.; D'Alonzo, D.; Palumbo, G.; Palumbo, G., Synthesis and evaluation of folate-based chlorambucil delivery systems for tumor-targeted chemotherapy. *Bioconjug Chem* **2012,** *23* (1), 84-96.

35. Dhar, S.; Liu, Z.; Thomale, J.; Dai, H.; Lippard, S. J., Targeted Single-Wall Carbon Nanotube-Mediated Pt(IV) Prodrug Delivery Using Folate as a Homing Device. *Journal of the American Chemical Society* **2008,** *130* (34), 11467-11476.

36. Cucchiarini, M.; Ekici, M.; Schetting, S.; Kohn, D.; Madry, H., Metabolic activities and chondrogenic differentiation of human mesenchymal stem cells following recombinant adeno-associated virus-mediated gene transfer and overexpression of fibroblast growth factor 2. *Tissue Eng Part A* **2011,** *17* (15-16), 1921-1933.

37. Venkatesan, J. K.; Ekici, M.; Madry, H.; Schmitt, G.; Kohn, D.; Cucchiarini, M., SOX9 gene transfer via safe, stable, replication-defective recombinant adeno-associated virus vectors as a novel, powerful tool to enhance the chondrogenic potential of human mesenchymal stem cells. *Stem cell research & therapy* **2012,** *3* (3), 22.

38. Rey-Rico, A.; Venkatesan, J. K.; Schmitt, G.; Concheiro, A.; Madry, H.; Alvarez-Lorenzo, C.; Cucchiarini, M., rAAV-mediated overexpression of TGF-beta via vector delivery in polymeric micelles stimulates the biological and reparative activities of human articular chondrocytes in vitro and in a human osteochondral defect model. *International journal of nanomedicine* **2017,** *12*, 6985-6996.

Chapter 3

In this chapter different synthetic approaches for hyaluronic acid (HA) chemical modification have been explored and evaluated, evidencing how they may have a significant impact upon the physicochemical properties of this versatile polymer, whose applications in the biomedical field range from tissue engineering to drug delivery and bio-imaging, due to its biodegradable, non-toxic, biocompatible, non-immunogenic and non-inflammatory characteristics. Specifically, along my PhD research activity several modified HA derivatives (Figure 1) have been investigated as hydrogel components and as platforms for delivery of antiviral drugs. Part of this work (section 3.1) has been carried out during a research period abroad at the Institute of Soft Nanoscience of the Westfälische Universität in Münster (Germany), under the supervision of Prof. Bart Jan Ravoo.

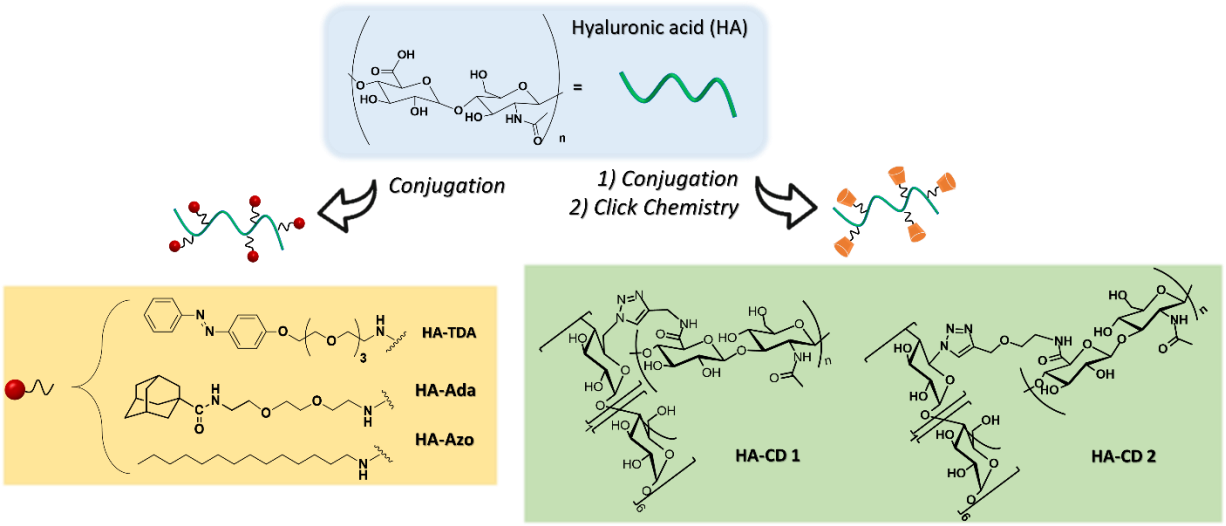

Figure 1 HA derivatives investigated as hydrogel components and/or as platforms for delivery of antiviral drugs

3.1 Photo-responsive supramolecular hydrogel based on HA with high molecular weight

Introduction

Hyaluronic acid is widely exploited for the design of hydrogels, due to its native biofunctionality and the numerous sites for modification. There are several examples of modified HA macromers used to form either covalent or physical hydrogels through crosslinking reactions (e.g., via click chemistry, Michael addition reaction etc.), or supramolecular assemblies of guest-host pairs.[1] Hydrophobic moieties can be conjugated to the HA backbone in order to render the derivative amphiphilic, thus enabling the nanoscale self-assembly of polymeric monomers in aqueous media. HA hydrogels range from relatively static matrices to those that exhibit spatio-temporally dynamic properties through external triggers like light. Photoresponsive molecules, able to change their structural and physicochemical properties upon light exposure, have attracted increasing interest in the recent decades.[2, 3] Among photo molecular switches, azobenzenes have been intensively investigated. Their grafting to HA enables the photo-reversible supramolecular crosslinks with β-CD, due to the cis-trans photoisomerization in response to different wavelengths.[4, 5] Azobenzenes (Azo) can isomerize from the stable *trans*- (E) form to the *cis*- (Z) form, after the exposure to UV light (~350 nm), and it is liable to reversely switch back under the action of visible light or slight heat.[6] Moreover, among all external stimuli, light offers non-invasivity and a precise spatio-temporal control. However, very low aqueous solubility and cytotoxicity have restricted so far azobenzenes applications in biomedicine-related fields. In order to solve this problem, water-soluble conjugates using biocompatible natural polysaccharides (*i.e*, hyaluronic acid, chitosan or chondroitin sulfate, etc) have been designed.[7]

Azobenzene also has an affinity for the hydrophobic cavity of cyclodextrins ($K_b = 5.8 \times 10^3\ M^{-1}$),[8] allowing the formation of non-covalent host-guest linkages that can be disrupted by conversion into

cis- isomer upon UV irradiation. The linear and apolar *trans*- isomer can be readily included into hydrophobic cavity of α-CD and β-CD, whereas host–guest complex formation is strongly disfavored for the sterically demanding and polar *cis*- isomer. This kind of interaction has been exploited to design supramolecular hydrogels that can perform *gel-sol* phase transition with light, enabling as well to eventually control the release kinetics of payloads. Literature papers[9, 10] exploited the supramolecular hydrogel obtained by non-covalent linkages between the host and guest fragments grafted on HA backbones; in figure 2 are reported the main examples of HA modified with Azobenzene. Here we describe the synthesis of a new azobenzene-hyaluronic acid derivative (HA-Azo) and the study of its self-assembly into a supramolecular hydrogel using as host β-CD conjugated polymers, Poly Acrylic Acid (PAA-βCD).

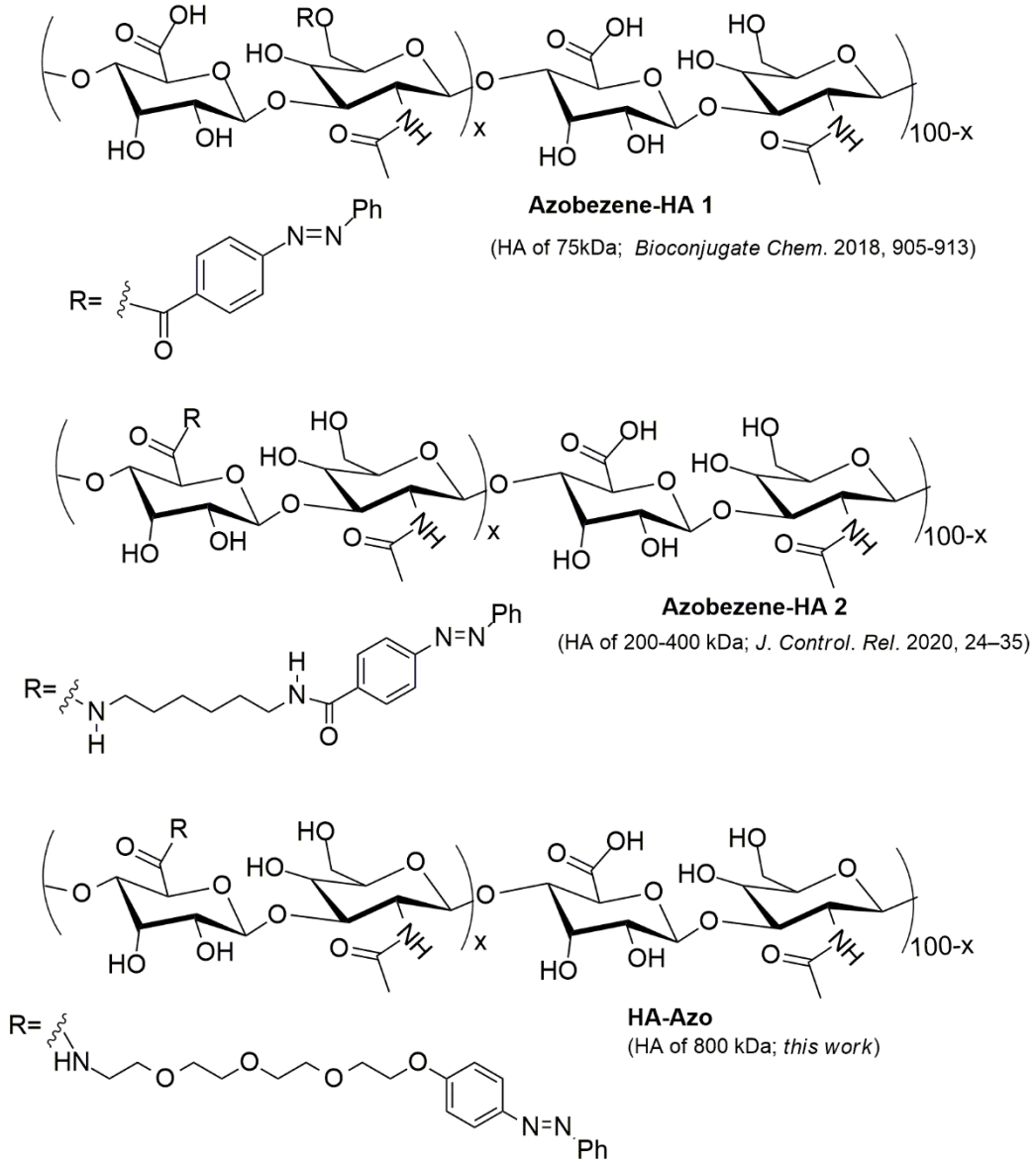

Figure 2 Literature examples of hyaluronic acid modified with azobenzene[9, 10] and chemical structure of HA-Azo developed in this thesis.

This investigation explores the structure–property relationship of HA-Azo based hydrogels using HA polymers with high molecular weight (800 kDa). Our experimental results point out that the chemical structure of the polymer backbones is the crucial requirement for supramolecular hydrogel formation. Specifically, we observed the formation of the supramolecular hydrogel (HA-Azo@PAA-βCD), at physiological conditions, only by mixing HA-Azo guest with the host cyclodextrins grafted on Poly Acrylic Acid (PAA-βCD). No hydrogels were obtained using PolyCD or HA-CD2 (Figure 1) as host.

Rheology measurements were conducted to investigate the viscoelastic behavior of different formulations for HA-Azo@PAA-βCD hydrogel. Finally, to investigate the changes in the mechanical properties induced through the photoisomerization of azobenzene, the HA-Azo@PAA-βCD hydrogel was observed by alternating the irradiation between ambient visible light (520 nm) and UV light (365 nm).

Results and Discussion

HA-Azo@PAA-βCD photo-responsive supramolecular hydrogel was fabricated through host-guest supramolecular interactions of two components, HA-Azo and PAA-βCD.

The grafting of amine-functionalized azobenzene (**5**) onto the HA backbone using the "triazine-activated amidation" method (Scheme 2) [11, 12] yielded the HA-Azo derivative (**7**). Compound (**5**) was synthetized starting from 4-phenylazophenol and tosylated tetraethylene glycol (**1**), followed by azidation reaction to compound (**4**) and final reduction with triphenylphosphine (Scheme 1).

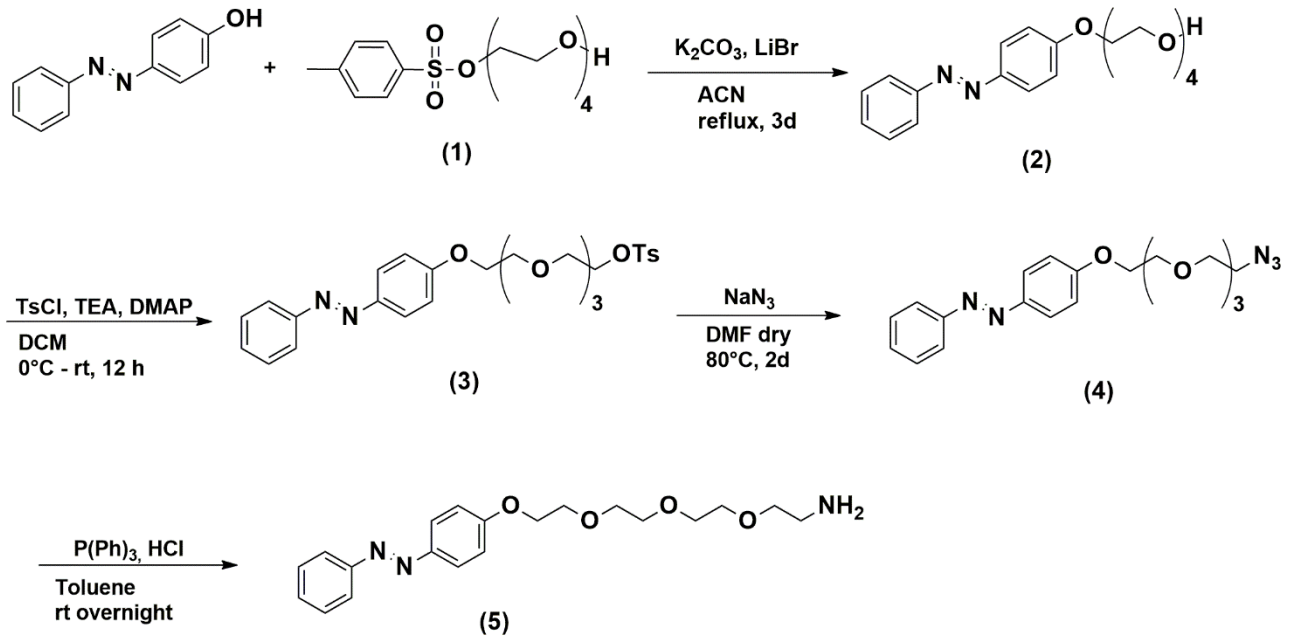

Scheme 2 Synthesis of amine-functionalized azobenzene moiety

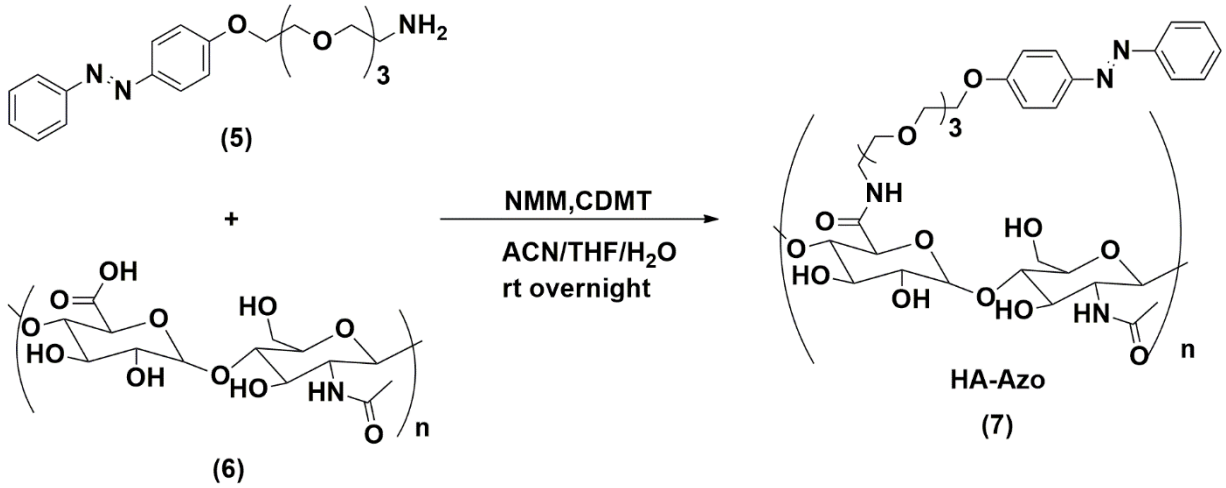

Scheme 3 Synthesis of the HA-Azo bioconjugate

The grafting of Azo group on HA induced an increment of the hydrophobic character with a resultant total or partial loss of water solubility. To avoid this drawback, the reaction was carried out using a molar ratio of 1:0.5 between carboxylic groups of HA-COOH and azobenzene-NH_2 (maximum substitution degree of ≃50%). The structure of HA–Azo was supported by spectral and analytical data. In particular, the detection of aromatic protons in ^{1}H NMR spectrum (Figure 3) clearly indicated the successful achievement of the coupling reaction; although their integral values cannot be used to evaluate the coupling efficiency. Probably, signals of hydrophobic component of macromolecule HA-Azo appear poorly detectable due to the amphiphilic feature and limited solubility of HA-Azo.

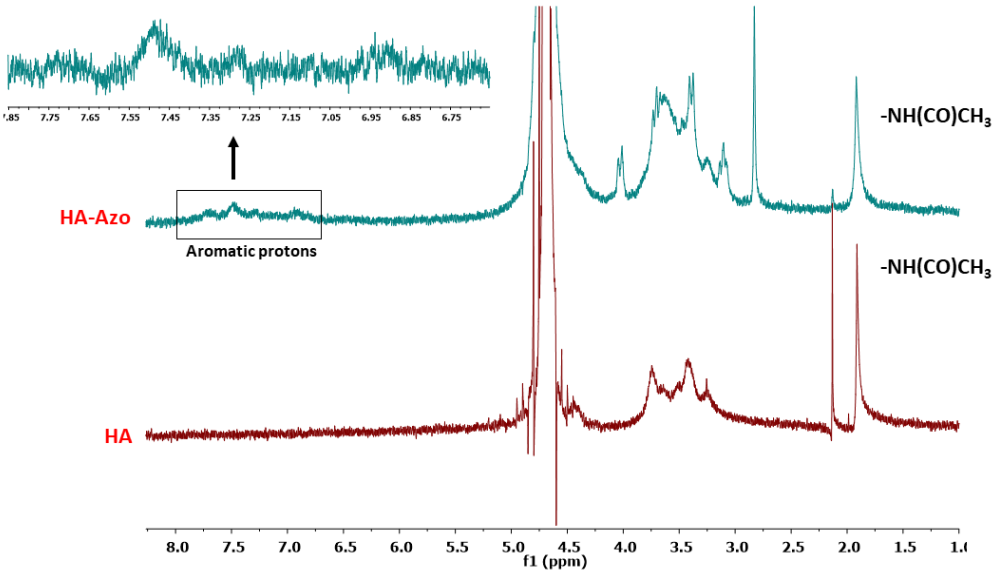

Figure 3 ^{1}H-NMR spectra of HA and HA-Azo recorded in D_2O.

Photophysical properties of HA-Azo were investigated by UV/Vis spectroscopy (Figure 4). Azobenzene is a light-responsive motif and undergoes isomerization upon UV (365 nm) and visible (520 nm) irradiation. According to literature data, it maintained its spectroscopic features after conjugation on the hyaluronic acid backbone, displaying a π-π* band at 341 nm and a n-π* band at 435 nm, as shown in Figure 4. Under UV irradiation (365 nm) for just 10 seconds, the π-π* appears decreased, whereas the n-π* band is increased, suggesting that the *cis*- isomerization is complete. After one hour of exposure to visible light, almost the original spectrum is restored, indicating near (Z) to (E) back isomerization. The photo-induced switching of HA-Azo is fully reversible for at least five cycles (Figure 5).

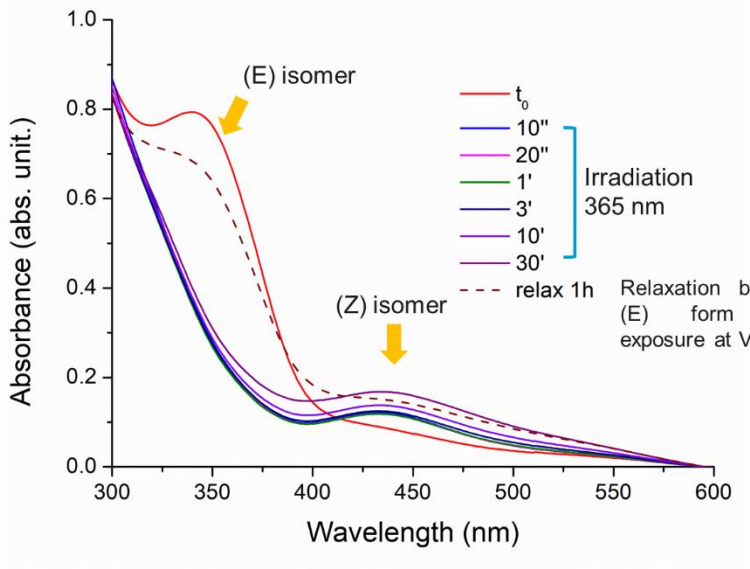

Figure 4 HA-Azo (2 wt%) spectroscopical behavior before and after irradiation for different time intervals

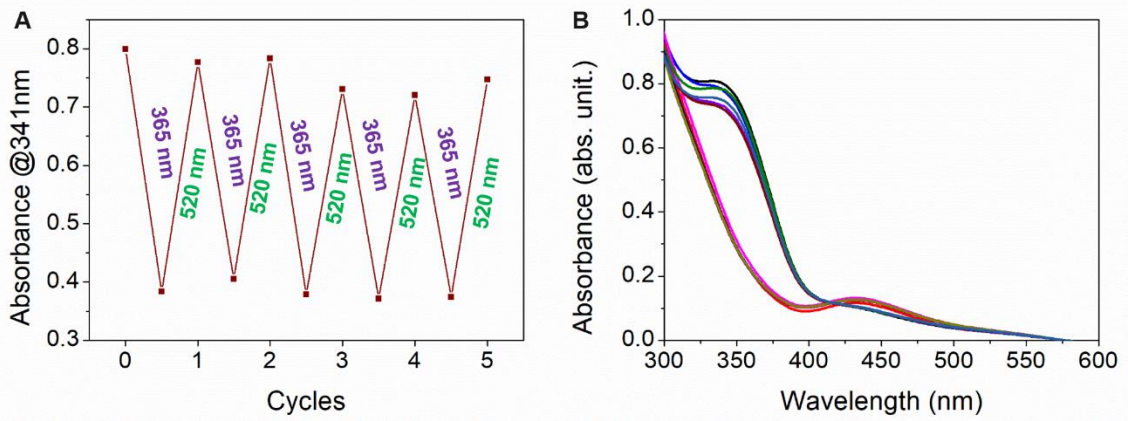

Figure 5 A) five cycles of fully reversible photo-isomerization of HA-Azo and B) UV7Vis spectra of E- and Z- isomers of HA-Azo (2wt%) in water after each cycle

Polyacrylic acid is a pH-sensitive and biocompatible polymer that is being used in many biomedical fields and has attracted considerable interest due to its ability to reversibly swell in response to pH changes. In general, acrylic derivatives possess an excellent water sorption capacity and are able to retain large amounts of water within their structure, which makes them ideal blocks for the preparation of biomedical scaffolds to be used in drug delivery or tissue engineering. However, single-network hydrogels only made of PAA often show weak mechanical properties because of rapid

dissolution rate and slow swelling/deswelling responses, thus they need reinforcements by combination with other polymers forming the so-called *interpenetrating polymer networks* (IPN).[13]

PAA-βCD was synthesized by Mehak Jain (PhD student, SoN, Münster) according to a method previously reported in literature [14] (Scheme 3), with a final CD content of ≃ 4%**.**

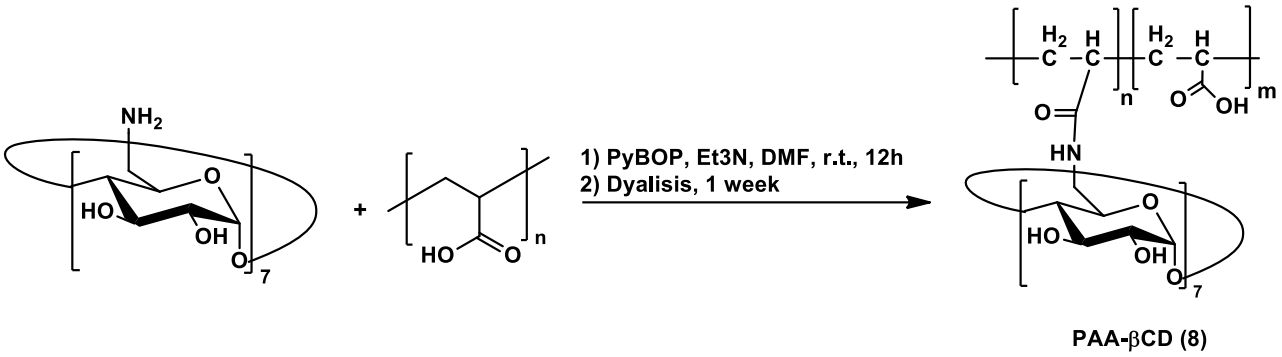

Scheme 4 Synthesis of PAA-βCD polymer

We exploited the preparation of the photo-responsive hydrogel network by the combination of β-cyclodextrin-modified Poly Acrylic Acid (**PAA-βCD**) and hyaluronic acid derivatized with azobenzene (**HA-Azo**). The precursors were self-assembled into gel upon mixing at room temperature according to two different procedures.

i. Stock solutions of PAA-βCD (fixed concentration 4 wt%; β-CD content ~4%) and HA-Azo (0.5, 1, 2, 3 wt%) were prepared by dissolving the polymers in MilliQ water and leaving them upon stirring overnight at room temperature. HA-Azo formed viscous, but clear, brownish solutions on the following day at all tested concentrations. 100 µL of both hydrogel components were mixed under gentle stirring at r.t. Strong gels were obtained within one night, for all tested concentrations, as confirmed visually with the "inverted vial" test (Figure 6a). The better performing sample in terms of elasticity and strength resulted to be the 2 wt%.

ii. The concentration of PAA-βCD was maintained constant and mixed with different volumes of HA-Azo 2 wt%. This formulation allowed to investigate the effect of the incrementing cross-linking density (i.e. supramolecular recognition between CD host and -Azo portion as guest molecule) in HA-Azo@PAA-βCD, induced by the gradual increase of the HA-Azo amount. Specifically, PAA-βCD 100 µL (fixed concentration 4 wt%; β-CD content ≃4%) were mixed with different volumes of HA-Azo (2 wt%), the final volume ratio were 1:0.1; 1:0.2; 1:05; 1:1. As a consequence, and coherently with expectations, with the increment of azobenzene motifs and cross-linking density the gel became mechanically stronger (Figure 6b).

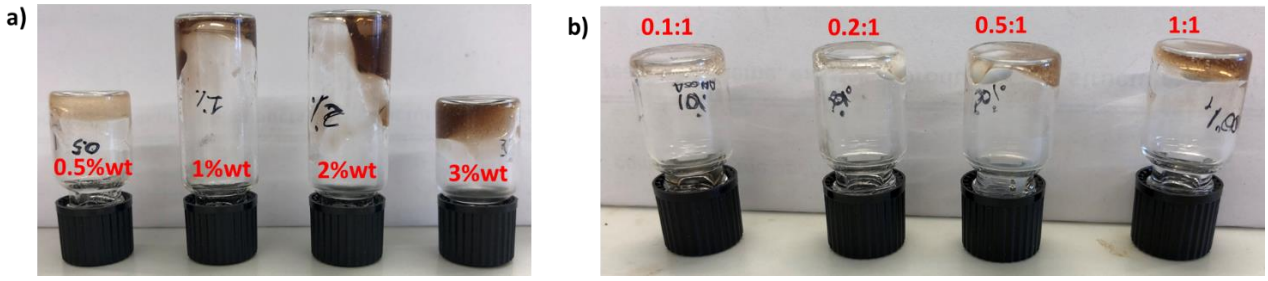

Figure 6 Inverted vial test for a) [PAA-βCD]=4 wt% + [HA-Azo]= 0.5, 1, 2, 3 wt%; and b) [PAA-βCD]=4 wt% + [HA-Azo]=2 wt% at different vol/vol ratios (0.1:1;0.2:1;0.5:1;1:1). By increasing the HA-Azo amount, gel formation time decreased going from hours (0.1:1) to a few minutes (1:1).

Rheological measurements revealed the viscoelastic properties of the HA-Azo@PAA-βCD supramolecular hydrogels. The effect of different concentrations of HA-Azo on the hydrogel mechanical behavior were compared in oscillatory rheological measurements. A strain amplitude sweep (Figure 7-A) revealed that the extent of the linear viscoelastic region (LVE) is similar for all the concentrations studied, with a breakdown of the gel structure at high share values. Initially, a lower shear was applied and constant viscosity for all the hydrogels was observed. Then, at high shear rate, a decline in viscosity occurred, indicating an irreversible disruption of the supramolecular structure under shear.

Moreover, Figure 7-A also shows how by increasing the concentration of hyaluronic acid, both the storage (G') and loss modulus (G'') increase as well. The elastic component G' dominates the viscous component G'' and the curves are parallel and almost linear, confirming the gel character of the materials. Considering the modest difference of G' and G'', the viscoelastic character of the hydrogel is limited in comparison to a permanently cross-linked polymer hydrogel. These findings suggest that stiffer gels can be obtained with a growing number of entanglements due to the supramolecular recognition between azobenzenes and cyclodextrins.

Figure 7-B reports the frequency-dependent sweep measurements over a range of oscillation frequencies at a constant oscillation amplitude and temperature. This provides more information about the colloidal forces and interactions among hydrogel components. The values for storage modulus (G') dominate the loss modulus (G'') for all the examined samples and both are frequency independent. Thus, the gels can retain their structure even at high oscillation frequencies.

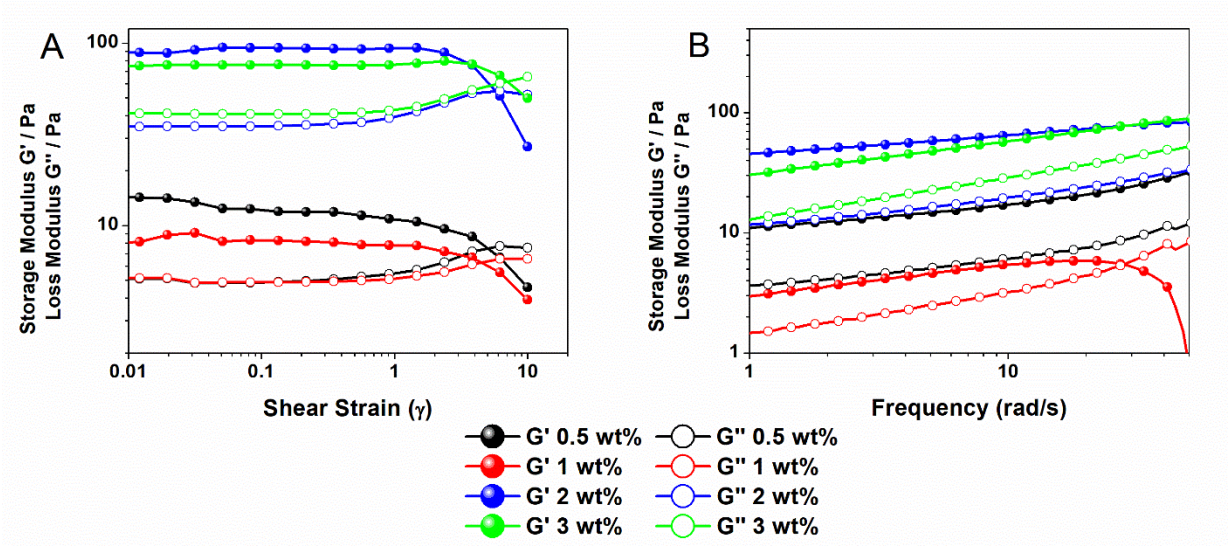

Figure 7 Oscillatory rheological measurements of the hydrogels with varying concentrations of HA-Azo (T = 20°C); ***A****) G' and G'' obtained from a strain-amplitude sweep performed at 10 rad/s;* ***B****) G' and G'' obtained from a frequency-sweep performed at 1% strain. For all samples, [PAA-βCD] = 4 wt%.*

Preliminary experiments on the mechanical properties of HA-Azo@PAA-βCD under UV irradiation suggest that the hydrogel do not undergo a sharp gel−sol transition. Probably, the high degree of association and the dynamic equilibria that are quickly established between the two polymeric

counterparts, allow for a high cross-linking density and level of entanglement in the matrix. Thus, the partial dissociation of the host-guest pairs by UV irradiation can induce a decrease of cross-linking density without gel−sol transition. However, this effect could be adequate for modulation in the release rate of eventual therapeutic cargos. Currently, further experiments are in progress to complete the hydrogel characterization and to set up the loading of therapeutic proteins on HA-Azo@PAA-βCD.

3.2 HA bioconjugate nanoplatform for drug delivery application

The combination of biopharmaceutical properties of HA and the molecular recognition ability of βCD linked to HA could generate interesting constructs with high biocompatibility and promising applications for the targeted and/or sustained delivery of drugs. Along my research activity, the entrapment of the antiviral agent Acyclovir (Acy) within the cavity of a βCD covalently grafted on HA was explored. Viral diseases affect billions of people each year worldwide, but despite a large body of knowledge about the replicative and pathogenetic mechanisms of many human viral pathogens, the therapeutic potential of current approved antiviral drugs is limited by several pharmaceutical/pharmacological issues such as narrow therapeutic indices, high dosages related to frequent administrations, low aqueous solubility, low permeability, incomplete biodistribution, and short half-life.[15, 16] A promising strategy to overcome these problems could be the development of nanoscale carriers for the delivery of antiviral drugs. Nanocarriers modify the physicochemical properties of the incorporated molecule, affecting its pharmacokinetic profile and allow for the penetration through biological barriers, enhancing the effectiveness of the drug and decreasing severe side effects.

The grafting of CD to HA has been achieved by exploiting a covalent approach via Cu(I)-catalyzed cycloaddition reaction (CuAAC) between a 6-mono-azido-β-cyclodextrin (**CDN$_3$**) and an alkyne-

terminated HA (**HA-Alk**), which involves the formation of a triazole ring in the final product **HA-CD1 (**Figure 8).

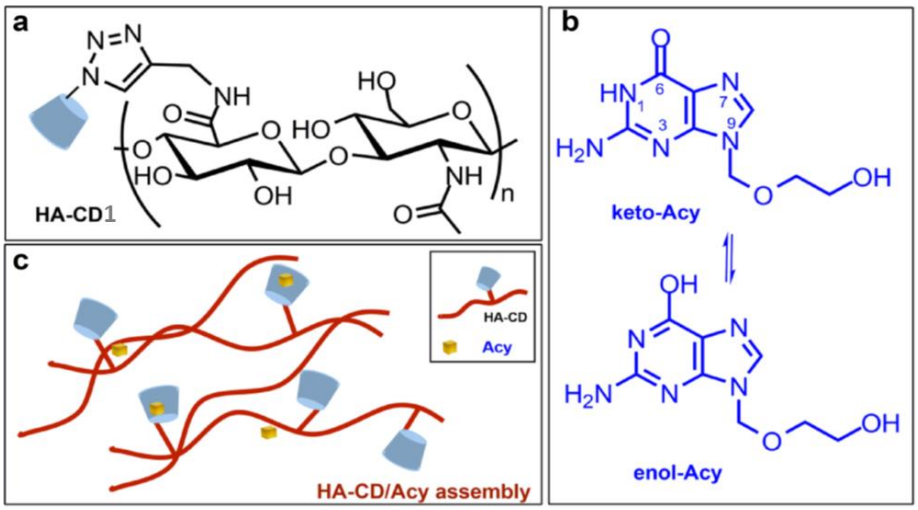

Figure 8 a) Representative structure of hyaluronic acid-β-cyclodextrin conjugate (HA-CD1); b) structures of keto- and enol tautomer of Acyclovir (Acy); c) sketched view of HA-CD1@Acy assembly.

Synthesis of HA-CD1

Alkyne fragments have been introduced into HA backbone by the "triazine activated amidation" reaction, a coupling procedure that proceeds in mild conditions (aqueous medium, room temperature and neutral pH). The cycloaddition between HA-Alk and β-CDN_3 (Scheme 4) was performed in water, in the presence of Cu(II) ions and ascorbic acid, under argon atmosphere for 4 days. Despite the long reaction time, the degree of substitution in terms of CD on HA, estimated from the integral of the ^{1}H-NMR signal of the H5 proton of the triazole ring, was ~0.7%, which is quite low, possibly because of the high steric hindrance caused by CDN_3. However, this little amount of CD was sufficient to convey new properties to HA, most importantly the capacity to entrap, deliver and release Acyclovir.

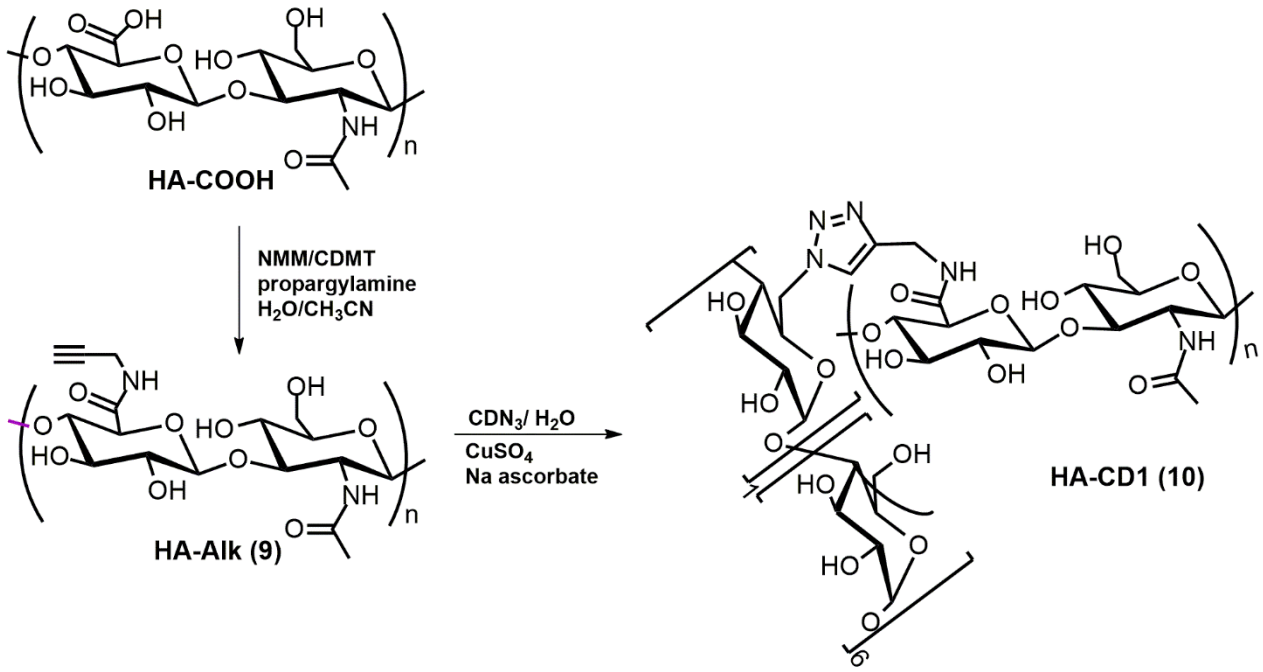

Scheme 5 Synthesis of HA-CD1

Characterization

Table 1 summarizes the physicochemical properties of HA-Alk, HA-CD1 and HA-CD1@Acy complex.

With respect to the HA-Alk precursor which aggregates were around 700 nm, HA-CD1 assemblies in aqueous solution were smaller in size (~ 350 nm) and that can be explained with an increment of hydrophilic portion and consequent improved water-dispersibility made by CD units on the polymer, compensating lipophilic alkyne moieties. The size and the hydrophilicity of the system were maintained also in the presence of Acy, in fact the HA-CD1@Acy complex after reconstitution in H_2O and PBS at pH 7.4 showed a size of ~ 320 nm. In addition, all the investigated nanoassemblies exhibited a ζ-potential of about − 45 mV, in agreement with a good stability of the assemblies in water.

Table 2 Overall properties (Mean hydrodinamic diameter, polydispersity index and ζ-potential) of nanoassemblies (HA-CD1@Acy) in comparison with synthesized derivatives (HA-Alk and HA-CD1).

System	Medium	D_H(nm ± SD)(%)[a]	PDI	ζ(mV ± SD)
HA-Alk	H_2O	698 ± 61 (91) 94 ± 17 (9)	0.17 0.36	-43 ± 2.8
HA-CD1	H_2O	367 ± 50 (90) 80 ± 9 (10)	0.27 0.22	-47 ± 3.2
HA-CD1@Acy	H_2O	317 ± 20 (91) 91 ± 18 (9)	0.13 0.39	-46 ± 2.6
	PBS, pH 7.4	331 ± 81 (100)	≤0.40	

[a]Percentage of each family of nanoassemblies are reported in parenthesis.

Complexation of Acy within HA-CD1 was further confirmed by UV/Vis spectroscopy. In fact, free Acy in water exhibited an absorption band centered at 252 nm with a shoulder around 273 nm, while the spectrum of the inclusion complex displayed an absorption band at 288 nm, bathochromically shifted of about 15 nm showing mostly a hypercromic effect (Figure 9). The band centered at minor wavelength was probably hidden by the absorption contribution given by the hyaluronic acid polymer.

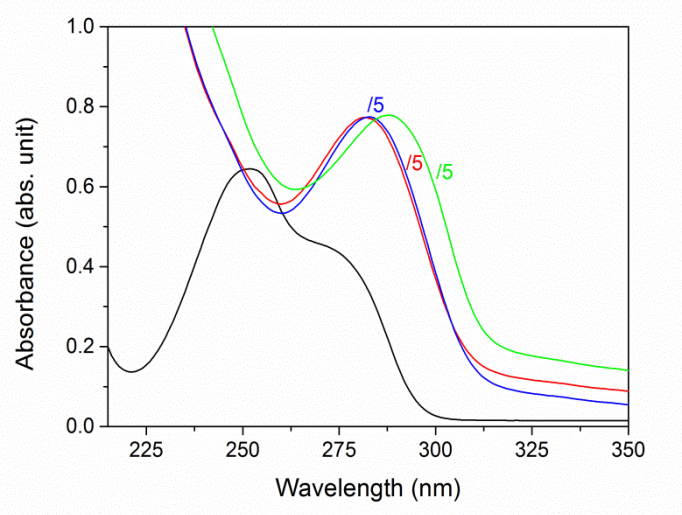

Figure 9 UV/Vis spectra of free Acy (black line) and HA-CD1@Acy inclusion complex in ultrapure water (pH= 5.2, red line), reconstituted in water (pH= 5.2, blue line) and PBS (pH=7.4, green line). In all the solutions, Acy concentration was 50 μM. For a better comparison, the HA-CD1@Acy UV/Vis spectra were divided by a factor 5.

The remarkable bathocromic and hypercromic shift of the band at higher wavelength was ascribable to the formation of stable tautomeric species of Acy,[17] i.e enolic species (Figure 8b), plausibly stabilized by HA or included into the CD cavity. This change was even more evident after reconstitution of the lyophilized complex in PBS at pH=7.4 (green trace), where the band moved to even higher wavelength, suggesting a strong entrapment into the nanoplatform, probably facilitated by the increased ionic strength in the latter medium. To further confirm the interaction of Acy with CD, a titration in the presence of Ada-OH as competitor agent has been carried out and is shown in Figure 10. Up to concentration of Ada-OH lower than Acy, the increase of absorbance at 288 nm was evident (traces b, c). This result suggests that Acy, establishing new equilibria of complexation, can be displaced from some CD cavities to other CD units or more internal domains. When all the available CD cavities were saturated by Ada-OH, increasing its concentration ([CD]/[Acy]/[Ada-OH] ≅ 3:1:10 molar ratio), a decrease of absorbance occurred (trace d), suggesting a rearrangement of the nanoassembly.

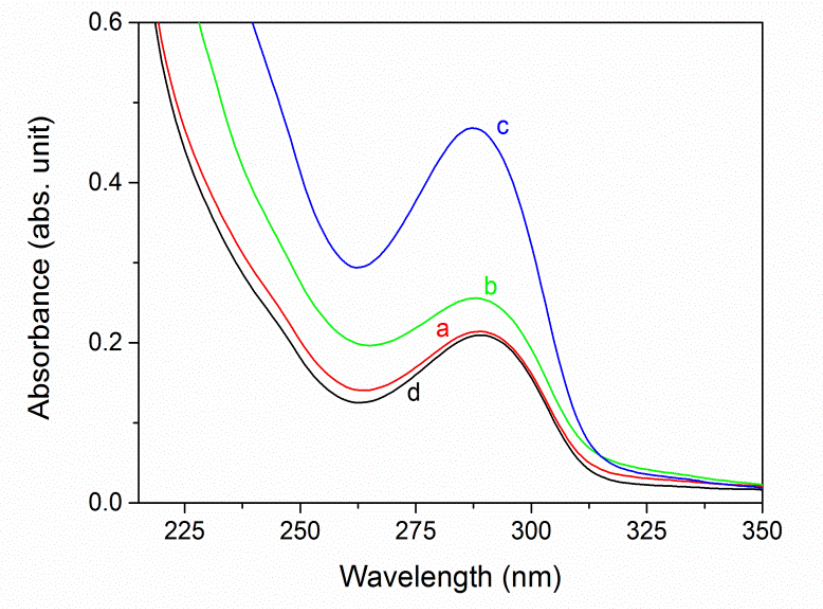

Figure 10 UV-vis spectra of HA-CD1@Acy complex ([Acy] = 2.5 μM) in ultrapure water without (trace a) and at constant amount of HA-CD1@Acy complex (0.4 mg /mL) at different [Acy]/[Ada-OH] molar ratios. Molar ratios: 1:0.2 (trace b); 1:0.4 (trace c); 1:10 (trace d).

Release profile of Acy from HA-CD1 in PBS at pH 7.4 and 37 °C was evaluated up to 10 days. As shown in Figure 11, no initial burst release was observed, and a slow release was noticed, leading to a final amount of released Acy equal to ~ 87%. It is already reported [18, 19] how the release profile of free Acy from conventional formulations in PBS (pH = 7.4, T = 37°C) is not comparable with the release from HA-CD@Acy complex, because it manifests a misleading behavior, forming detectable self-assembled species in solution (~330 nm) that could be improperly interpreted as an "apparent" delayed release.

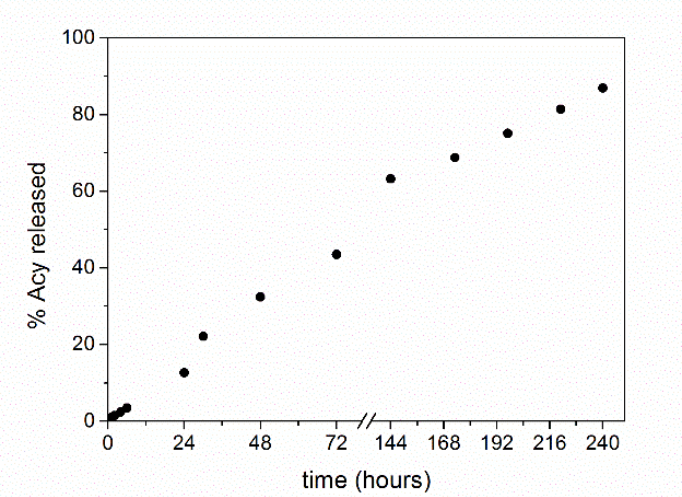

Figure 11 Release profile of Acy from HA-CD1@Acy in PBS at pH 7.4, T = 37 °C

Biological Evaluation

Biological assays to test tolerability and effectiveness of HA-CD1@Acy nanoplatform were carried out. Unconjugated HA and free Acy were used as positive controls. The cell viability was evaluated on Vero cells using bioassay kit at different concentrations (20µM, 10 µM, 5 µM, 1 µM and 0.5 µM), on the basis of ATP levels after 24 h of treatment. No cytotoxicity was detected in all tested concentrations (Figure 12).

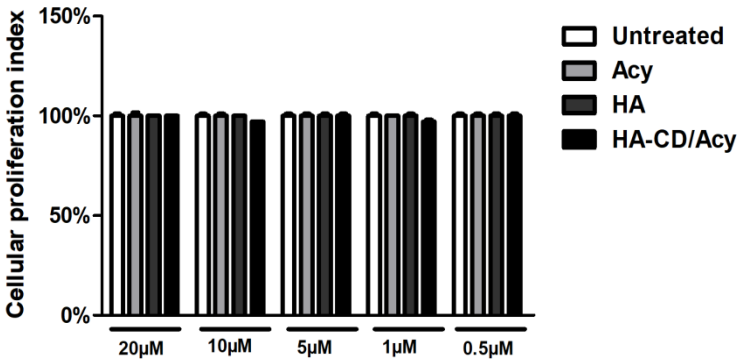

Figure 12 ***Viability assay in Vero cells.*** *The cell viability was determined on the basis of ATP levels using ViaLight™ plus cell proliferation and cytotoxicity bioassay kit (Lonza Group Ltd., Basel, Switzerland) in combination with GloMax® Multi Microplate Luminometer. Vero cells were untreated and treated with different concentrations of HA-CD1, Acy and HA-CD1/Acy (20µM, 10 µM, 5 µM, 1 µM and 0.5 µM). After 24h of treatment, the samples were collected and the luminescence value was converted in cell proliferation index (%) as described in the experimental The assay was performed as means of triplicate ± SD.*

For what it concerns the antiviral activity against HSV-1, it was evaluated *in vitro* by a standard plaque reduction assay, at five different concentrations (20µM, 10 µM, 5 µM, 1 µM and 0.5 µM), (Figure 13). The complex successfully inhibited plaque formation, without affecting cell viability and morphology. It is possible to assess that plaques were reduced either in size and number. With respect to the free Acy, the antiviral activity seems lower, probably because of the delayed mechanism of release from the complex.

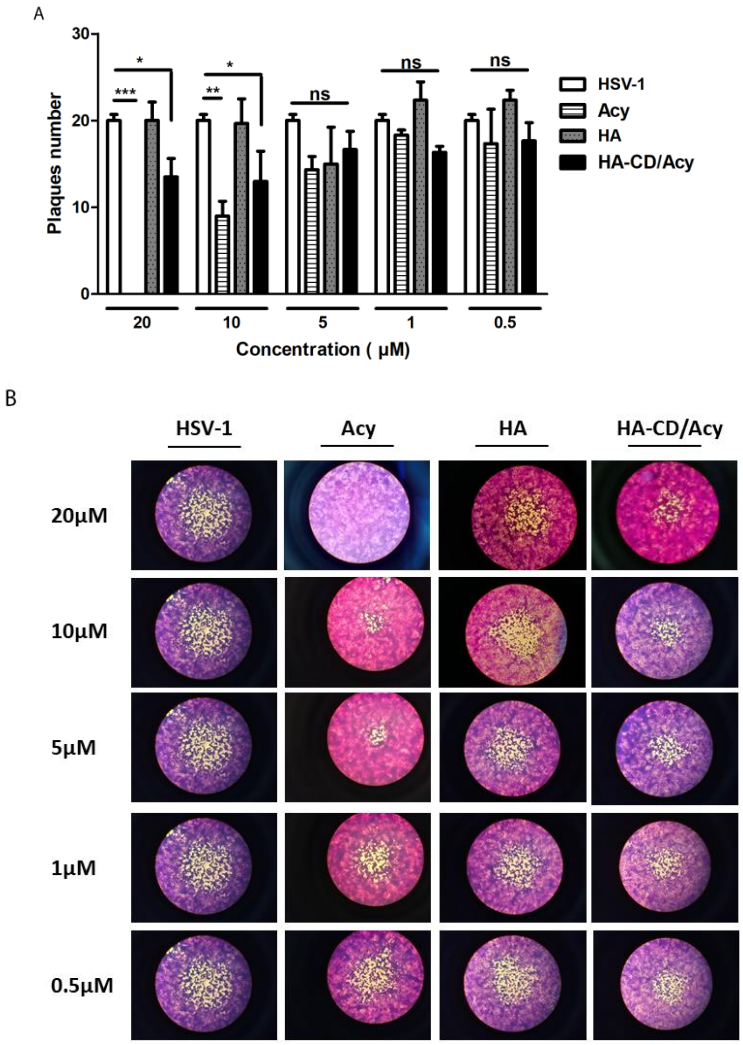

Figure 13 ***Plaque reduction assay.*** *The antiviral activity of HA-CD1@Acy was investigated by plaque reduction assay. Vero cells were infected with HSV-1 for 1 h and the virus's spread was blocked with Dulbecco's-modified Eagle's medium containing 0.8% methylcellulose in presence of HA-CD1, Acy and HA-CD1@Acy at different concentrations (20μM, 10 μM, 5 μM, 1 μM and 0.5 μM). Three days after incubation, the monolayers were fixed and stained with crystal violet. The panel A shows the antiviral activity dependent on different concentrations of Acy loaded into HA-CD1@Acy complex. The panel B shows the plaque morphology variation due to treatment with different doses of investigated complexes. Results are the mean ± SD of triplicate experiments and * indicate significant changes (p value≤0.001).*

3.3 HA conjugates

HA carboxyl units were exploited to introduce on the HA backbone hydrophobic moieties able to reversibly interact with macrocyclic structures giving novel combined biocompatible materials. Specifically, HA-TDA, HA-Ada, and HA-CD2 were synthetized. To confer to the derivatized HA polymer affinity towards CD cavities (i.e. modified CDs, polymeric CD etc.) HA-Ada and HA-TDA

derivative were prepared. HA-Ada was synthesized according the synthetic procedure reported in Scheme 5.

Synthesis of HA-Ada

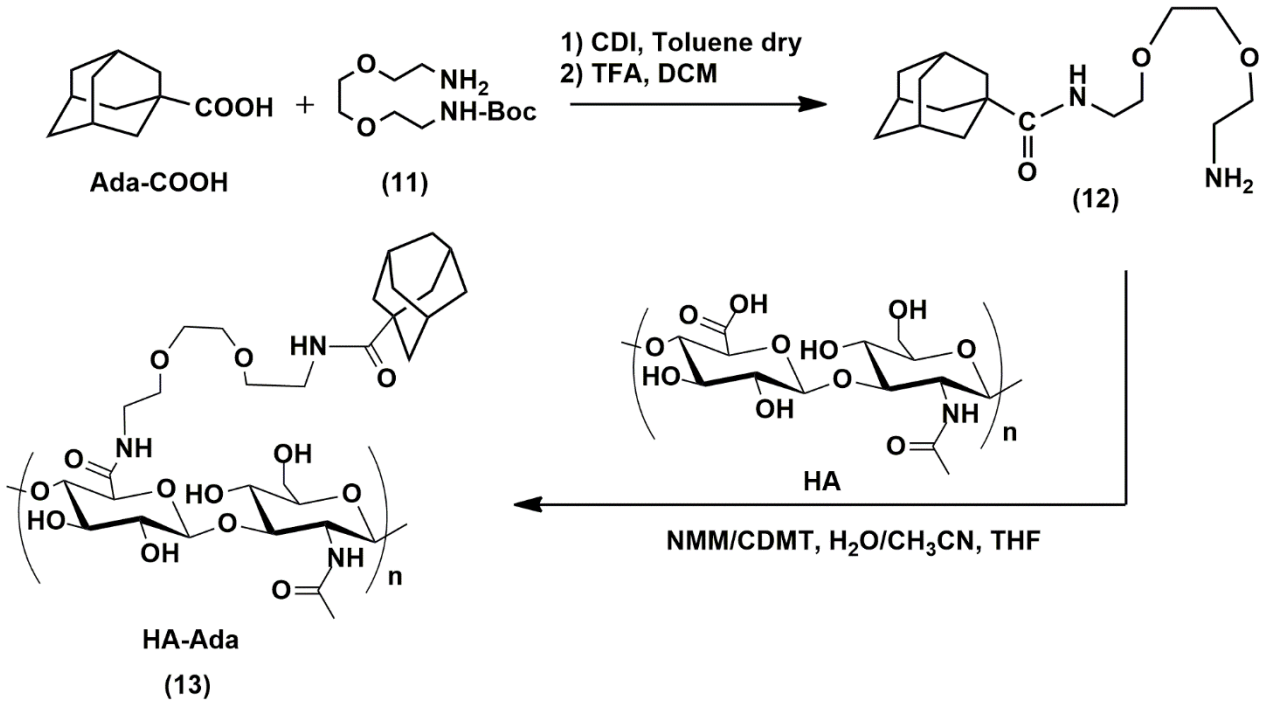

Scheme 6 Synthesis of HA-Ada

Adamantane carboxylic acid was first coupled with a mono-protected diamino aliphatic linker and the successive deprotection reaction by treatment with trifluoroacetic acid gave product (**12**), that reacted with HA carboxylate. Amide coupling reaction between (**12**) and HA-COOH was carried out at 1:1 molar ratio, leading to HA-Ada product (**13**). The degree of functionalization resulted around 30% by NMR (Figure 14). Preliminary experiments to obtain supramolecular hydrogel based on HA-Ada were carried out by using as polymeric counterparts PolyCD, HA-CD2 and PAA-βCD. No hydrogel formation was detected at the investigated conditions. However, HA-Ada will be further investigated by exploiting alternative experimental conditions (i.e. presence of gelators).

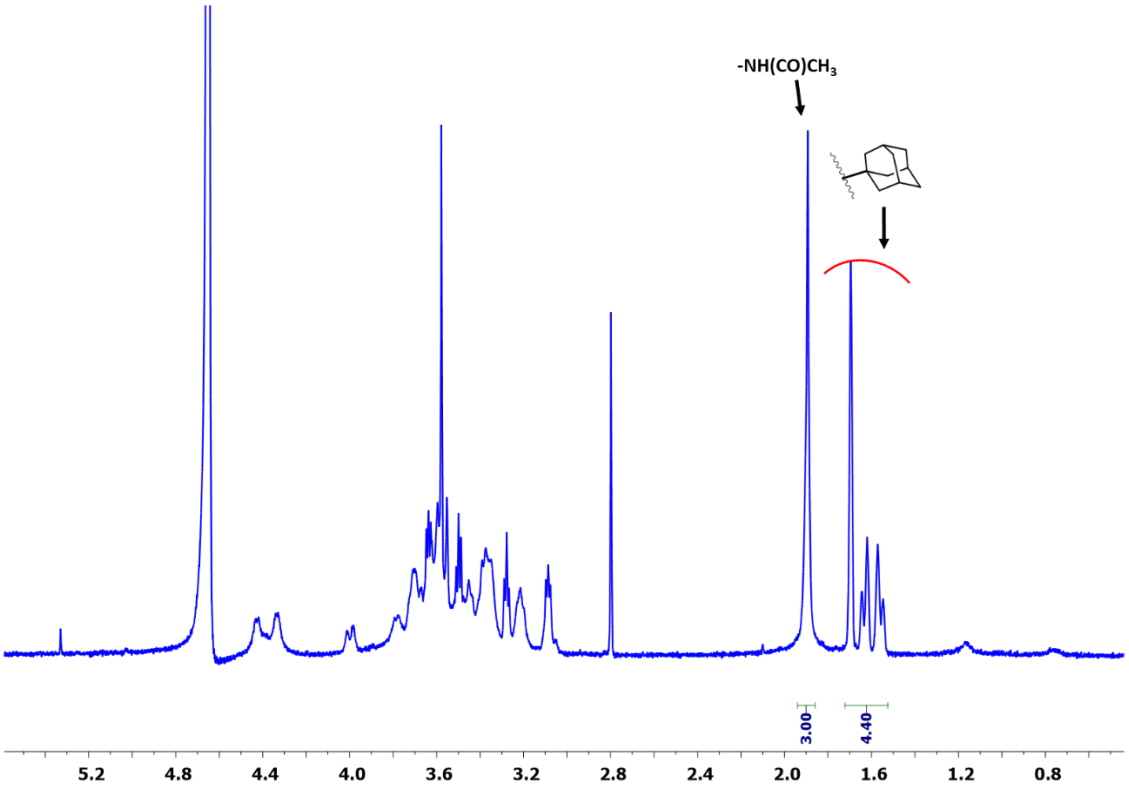

Figure 14 ^{1}H-NMR in D_2O of HA-Ada with integrated selected signals relative to HA and adamantane moiety (DS ~ 30%)

HA-TDA was prepared using different molar ratios between HA carboxylic groups and NH_2 groups of TDA (from 1:1 to 1:0.25) according to the procedure reported in Scheme 6. HA-TDA derivatives were obtained as water insoluble or poor soluble water compounds for all investigated molar ratios. The ability of HA-TDA to form supramolecular hydrogel by assembly with PolyCD was investigated in different experimental conditions. No hydrogel formation was obtained for all investigated formulations.

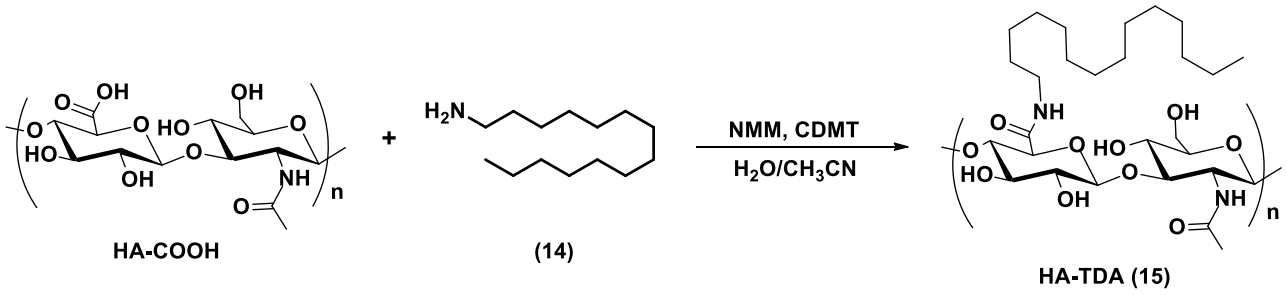

Scheme 7 Synthesis of HA-TDA

Scheme 7 reports the synthetic steps for the preparation of a novel hyaluronic acid-β cyclodextrin bioconjugate (HA-CD2), which follows the same procedure already reported for HA-CD1, but using a longer linker as spacer, the 2-(2-Propynyloxy)ethylamine, to overcome the problem of steric hindrance and thus allowing an increase of substitution degree after the *click* reaction with β-CDN_3. The degree of functionalization resulted around 21% by NMR (Figure 15).

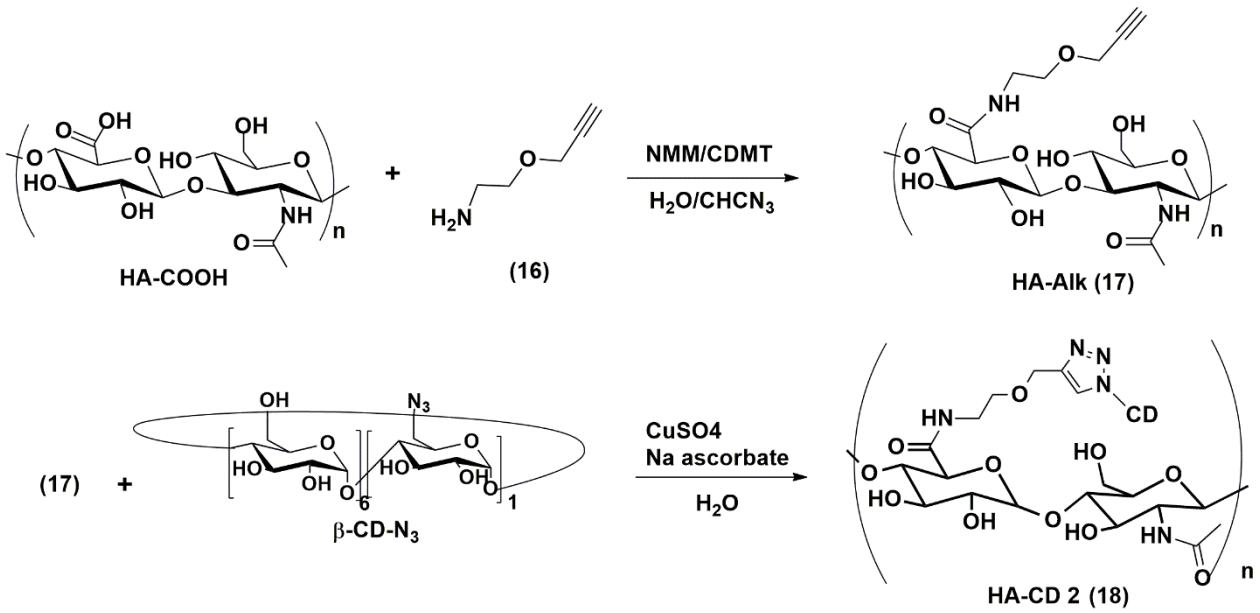

Scheme 8 Synthesis of HA-CD2

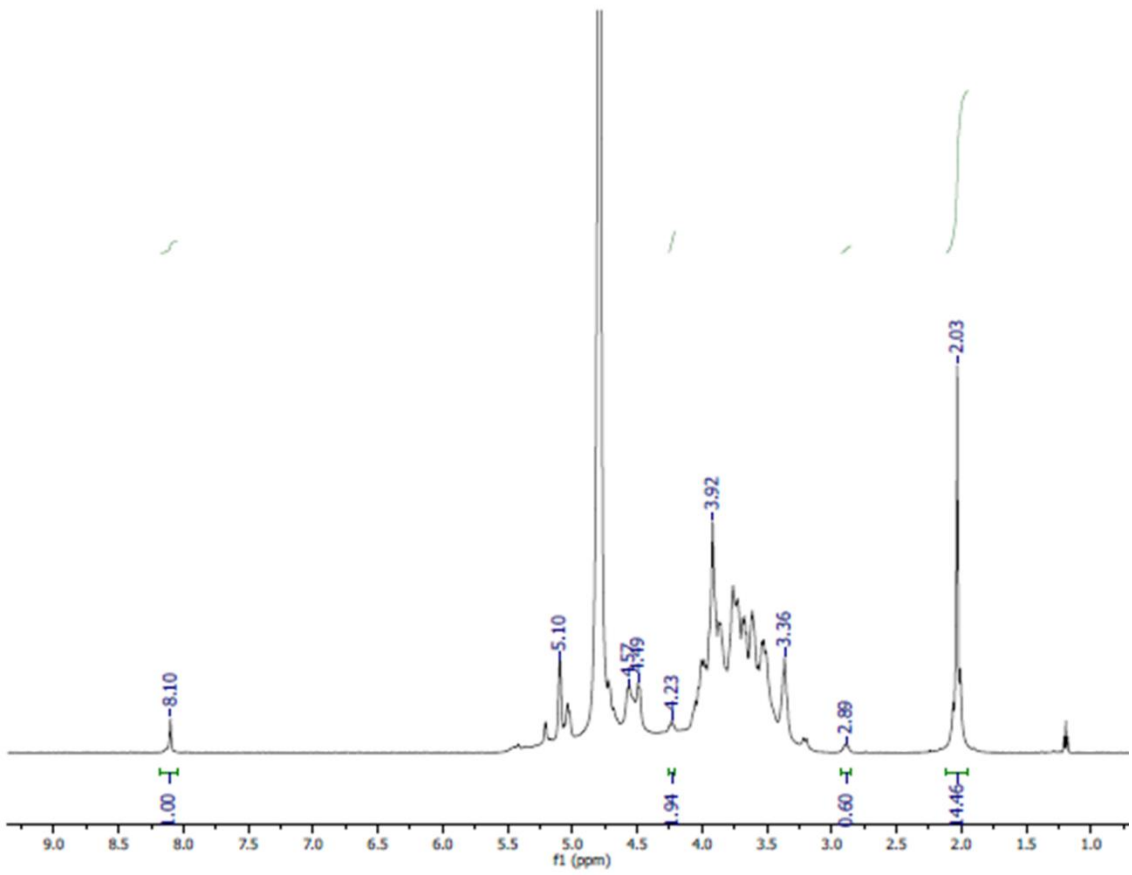

Figure 15 ^{1}H-NMR of HA-CD2 in D_2O

Experimental Section

Materials

Hyaluronic Acid sodium salt (HANa, 600-700 kDa) was kindly provided by Fidia Farmaceutici SPA, Local Unit of Noto (Italy). Mono-6-deoxy-6-azido- β-cyclodextrin (CDN_3) was synthesized according to literature method.[20] All the other reagents were of the highest commercial grade available and were used as received or were purified by distillation or re-crystallization, when necessary. All the solutions used for spectroscopic characterization were prepared in ultrapure micro-filtered water (Galenica Senese) and analysed at 298 K.

VERO cell lines (American Type Culture Collection) were grown in minimal essential medium (EMEM), supplemented with 6% fetal bovine serum (FBS) (Lonza, Belgium) and mixture 100 U/mL penicillin and 100 mg/mL streptomycin at 37°C under 5% CO_2. HSV-1 (F) is the prototype HSV-1

strain kindly provided by Professor Bernard Roizman. Virus stocks was propagated and then titrated in Vero cells.

Characterization techniques

UV/Vis spectroscopy

UV/Vis spectra were obtained on an Agilent model 8453 diode array spectrophotometer, using 1 cm and 0.5 cm path length quartz cells at r.t. (T≅ 25 °C) or, where it is specified, at T= 25°C by using a thermostatic bath. The hydrogel characterization was carried out in the laboratories of the Institute of Soft Nanoscience (Münster) using the following instrumentation: UV/Vis spectra were measured on a Jasco V-770 spectrophotometer (Jasco Deutschland GmbH, Pfungstadt, Germany) using High Precision SUPRASIL quartz glass cuvettes (Hellma Analytics GmbH, Müllheim, Germany). The spectra were recorded with Spectra Manager 2, Spectra Manager Version 2.14.06 (Jasco Deutschland GmbH, Pfungstadt, Germany). The samples were dissolved in 1 mL MilliQ water and the baseline was measured against the same solvent. Data analysis was realized using OriginPro 8.5 (ORIGINLAB Corperation, Northampton, USA).

Photoswitching experiments

Irradiation of the samples in solution was carried out with light-emitting diodes at 365 nm (UV LED Gen2 Emitter, radiant flux 1.2 W, LED Engin Inc., San Jose, California, USA) and 520 nm (LSC-G HighPower-LED, radiant flux 87 lm, Cree Inc., Durham, North Carolina, USA). Irradiation time was of 5 min per cycle.

NMR spectra were recorded on a Varian 500 and 300 MHz spectrometer at room temperature (25°C). The chemical shifts are expressed in ppm downfield from tetramethylsilane (TMS).

Size and ζ-potential measurements

The mean diameter, width of distribution (polidispersity index, PDI) and ζ-potential of the PolyCD based nanoassemblies were measured through photon correlation spectroscopy (PCS) by a Zetasizer Nano ZS (Malvern Instrument, Malvern, U.K.) at r.t. (T≅ 25°C) in ultrapure water. The measurements were performed at a 173° angle with respect to the incident beam for each dispersion. The deconvolution of the measured correlation curve to an intensity size distribution was achieved by using a non-negative least-squares algorithm. The ζ-potential values were determined using a Zetasizer Nano ZS Malvern Instrument equipped with a He−Ne laser at a power P = 4.0 mW and λ = 633 nm. The results are reported as the mean of three separate measurements on three different batches ± the standard deviation (SD).

Rheology

Rheological measurements were carried out on an Anton Paar Modular Compact Rheometer MCR 102 (Anton Paar GmbH, Graz, Austria) with Anton Paar RheoCompass V1.20.40.496 (Anton Paar GmbH, Graz, Austria) analysis software. Data processing was realized using OriginPro 8.5 (ORIGINLAB Corperation, Northampton, USA). Hydrogel samples were prepared and gelated overnight. For the measurement approximately 200 μL of the hydrogel were transferred onto the rheometer. After moving to the measuring position the sample was equilibrated for 10 min before starting the first measurement. For all measurements a CP25 (Anton Paar GmbH, Graz, Austria) spindle (25 mm plate diameter) was used.

Synthesis of 2-(2-(2-(2-Hydroxyethoxy)ethoxy)ethoxy)ethyl-4-methylbenzenesulfonate **(1)**

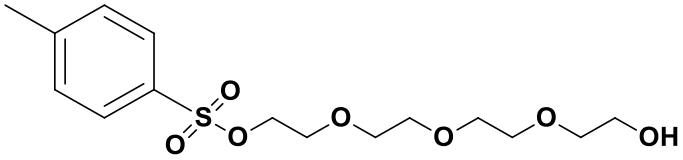

To a solution of tetraethylene glycol (22.0 g, 113 mmol, 10.3 eq.) in THF (4 mL) a solution of NaOH (690 mg, 17.1 mmol, 1.6 equiv.) in water (4 mL) was added at 0 °C. At the same temperature a solution of *p*-toluenesulfonyl chloride (2.08 g, 10.9 mmol, 1 eq.) in THF (13 mL) was added dropwise over 1 hour and stirred for 2 hours at 0 °C. The solution was poured into ice-water and the layers were separated. The aqueous layer was extracted with DCM (3 × 50 mL) and the organic layers were combined, washed with water (2 × 50 mL), dried over anhydrous $MgSO_4$, filtered and the solvent was removed under reduced pressure. The desired compound was used in the next step without further purification. Yield: 19 g (54.5 mmol, 48%) as yellow oil. **^{1}H-NMR** (400 MHz, $CDCl_3$) δ = 7.78 (d, *J* = 8.3 Hz, 2H), 7.33 (d, *J* = 8.3 Hz, 2H), 4.15 (t, *J* = 4.9 Hz, 2H), 3.72 – 3.55 (m, 14H), 2.43 (s, 3H) ppm. **^{13}C-NMR** (100 MHz, $CDCl_3$) δ = 144.93, 133.04, 129.93, 128.07, 72.56, 70.83, 70.74, 70.56, 70.42, 69.36, 68.79, 61.82, 21.75 ppm. **ESI-MS** (m/z): calculated 348.1248, found: 349.1311 $[M + H]^+$

Synthesis of (E)-2-(2-(2-(2-(4-(phenyldiazenyl)phenoxy)ethoxy)ethoxy)ethoxy)ethanol **(2)**

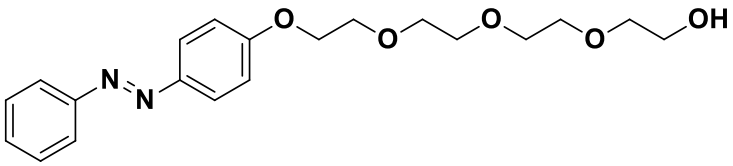

To a stirred solution of of **(1)** (5.78 g, 16.67 mmol, 1 eq.) in 150 mL of dry acetonitrile, containing K_2CO_3 (11.70 g, 84.65 mmol, 5 eq.) and catalytic amounts of LiBr, 4- phenylazophenol (3.96 g, 20 mmol, 1.2 eq.) dissolved in acetonitrile (50 mL) was added and the reaction mixture was refluxed for 3 days under argon. It was then allowed to cool to room temperature and the solvent was removed under reduced pressure. The residue was dissolved in DCM (120 mL), washed with water (100 mL)

and brine (3 × 100 mL). The organic phase was dried over $MgSO_4$ and concentrated. The residue was purified by silica gel column chromatography (EtOAc) to afford the title compound. Yield: 3 g (8 mmol, 48%) as red oil. **^{1}H-NMR** (300 MHz, $CDCl_3$) δ = 7.97 – 7.77 (m, 4H), 7.56 – 7.37 (m, 3H), 7.03 (d, J = 9.0 Hz, 2H), 4.27 – 4.17 (m, 2H), 3.94 – 3.84 (m, 2H), 3.83 – 3.63 (m, 10H), 3.62 – 3.56 (m, 2H), 2.49 (s, 1H) ppm. **^{13}C-NMR** (75 MHz, $CDCl_3$) δ = 161.39, 152.77, 147.14, 130.52, 129.15, 124.89, 122.67, 114.96, 87.44, 72.64, 70.98, 70.78, 70.70, 70.43, 69.74, 67.82, 61.86 ppm. **ESI-MS** (m/z): calculated 374.1847, found 397.1736 $[M + Na]^+$

Synthesis of 2-[2-[2-[2-[4-[(1E)-2-phenyldiazenyl]phenoxy]ethoxy]ethoxy]ethoxy]-, 1-(4-methylbenzenesulfonate) ethanol **(3)**

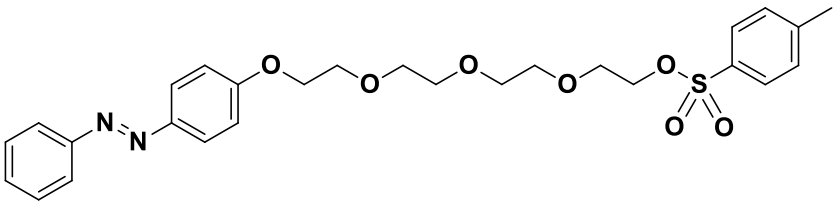

To a stirred solution of **(2)** (3.00 g, 8 mmol, 1 eq.) in CH_2Cl_2 was added NEt_3 (1,2 mL, 8 mmol, 1 eq.) and a catalytic amount of DMAP (50 mg). The mixture was stirred for 30 minutes. After that time p-toluenesulfonylchloride (2.3 g, 12 mmol, 1.5 eq.) was added dropwise at 0°C and the mixture was left stirring over 1 h at r.t. The reaction mixture was stirred overnight followed by evaporation of the solvent. The residue was redissolved in ethyl acetate and washed with water (100 mL) and brine 2 x 100 mL. The organic layer was separated and dried over $MgSO_4$. The solvent was removed under reduced pressure. The residue was subjected to silica column chromatography (EtOAc). The product was obtained as orange-brownish oil. Yield: 4,15 g, 98 %. **^{1}H-NMR** (400 MHz, $CDCl_3$): 7.89-7.84 (m, 4H); 7.76-7.74 (d, 2H); 7.48-7.45 (m, 2H); 7.42-7.40 (m, 1H); 7.29-7.27 (m, 2H); 7.00-6.98 (m, 2H); 4.18-4.16 (m, 2H); 4.13-4.10 (m, 2H); 3.86-3.83 (m, 2H); 3.68-3.54 (m, 10H); 2.37 (s, 3H). **ESI-MS** (m/z): calculated 528.1935, found 529.1933 $[M + H]^+$

Synthesis of (E)-2-(2-(2-(4-(phenyldiazenyl)phenoxy)ethoxy)ethoxy)ethyl-azide **(4)**

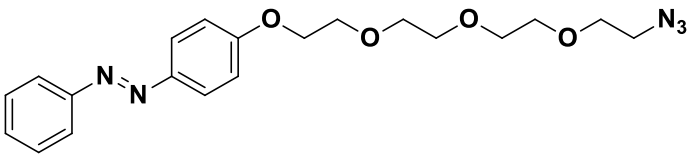

To a stirred solution of **(3)** (4.15 g, 7.86 mmol, 1 eq) in 10 mL of DMF was added NaN_3 (2.55 g, 39.3 mmol, 5 eq.) and the suspension was heated to 80°C and stirred overnight. After that, the solvent was removed *in vacuo* and the crude residue was dissolved in 100 mL of DCM and washed with water (2 x 100 mL) and with brine (2 x 100 mL). The organic layer was collected and dried over $MgSO_4$. The solvent was evaporated and the title compound was obtained as brown oil. Yield: 2.22 g, 67 %. **^{1}H-NMR** (400 MHz, $CDCl_3$): 7.90-7.86 (m, 4H); 7.46-7.43 (m, 2H); 7.43-7.41 (m, 1H); 7.02-7.00 (m, 2H); 4.21-4.18 (t, 2H, J = 4.6 Hz); 3.89-3.86 (t, 2H, J = 4.6 Hz); 3.72-3.63 (m, 10H); 3.43-3.34 (t, 2H, J = 4.6 Hz). **ESI-MS** (m/z): calculated 399.1912, found 422.1816 $[M + Na]^+$

Synthesis of 2-[2-[2-[2-[4-(2-phenyldiazenyl)phenoxy]ethoxy]ethoxy]ethoxy] ethanamine (Azo-NH_2) **(5)**

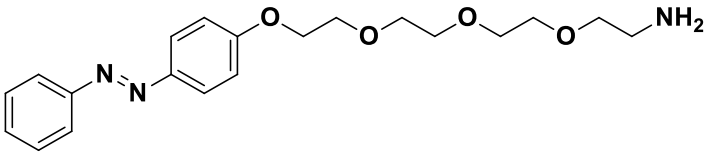

To a stirred solution of **(4)** (2.22 g, 5.5 mmol, 1 eq.) in 100 mL toluene was added PhP_3 solubilized in ~30 mL of toluene together with 150 mL HCl 2N. The solution was left stirring ad high speed overnight at r.t. The two formed phases were then separated and the aqueous layer was washed with toluene (2 x 100 mL) and basified with NaOH 5M (~50 mL) up to pH = 12. Then, the product was extracted with DCM (4 x 100 mL) and dried over $MgSO_4$ as a brown oil. Yield: 0.622 mg, 30%. **^{1}H NMR** (500 MHz, $CDCl_3$): δ 7.92–7.85 (m, 4H), 7.52–7.40 (m, 3H), 7.03 (d, 2H, J = 11.8 Hz), 4.21 (t, 2H, J = 6.0 Hz), 3.89 (t, 2H, J = 6.0 Hz), 3.80–3.61 (m, 8H), 3.51 (t, 2H, J = 6.3 Hz), 2.87 (t, 2H, J = 6.3 Hz), 2.16 (s, 2H); **^{13}C NMR** (125 MHz, $CDCl_3$): δ 161.15, 152.71, 147.04, 130.40, 129.03,

124.73, 122.57, 114.86, 70.82, 70.78, 70.58, 70.52, 69.55, 67.72, 52.10, 41.19; **ESI – MS** (m/z): calculated 373.2007, found 374.1989 $[M+H]^+$.

Preparation of hyaluronic free acid from sodium salt (HA-COOH) **(6)**

HA sodium salt 1g was dissolved in deionized water (5 mg/mL, pH=6.85) and mixed with Dowex H^+ 50W x 8–100 sulfonic resin (1 g). The resin was washed thoroughly with deionized water before use. The mixture was shaken at room temperature for 1 hr to ensure the ion exchange and then separated by centrifugation. The solution (pH = 2.85) was freeze-dried to afford 100 mg of HA in protonated form (HA-COOH).

Synthesis of HA-Azo **(7)**

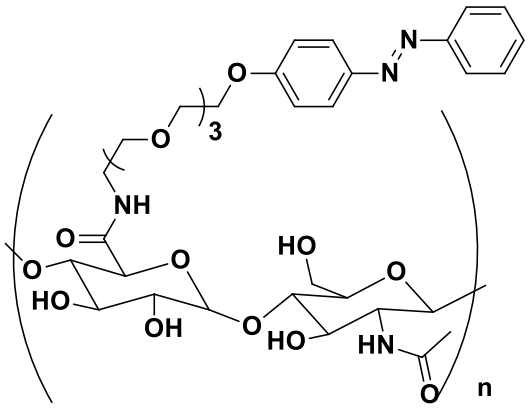

HA-COOH (200 mg, 0.5 mmol carboxylic acid) was dissolved in ~50 mL of deionized water in a 100 mL round-bottomed flask, followed by the dropwise addition of ~15 mL of acetonitrile and NMM (70 μL, 0.39 mmol, 1.5 eq.), under stirring. Then the solution was cooled down to 4°C with an ice bath and CDMT (43 mg, 0.26 mmol, 0.5 eq.) was added and stirred for 1 h at r.t. Finally, **(5)** (94 mg, 0.26 mmol, 0.5 eq.) was added to the mixture, corresponding with a 1:0.5 ratio between HA carboxyl groups and amino groups on the Azo moiety. The solution was left stirring overnight at r.t. to obtain a viscous, brownish product that, after removal of THF and ACN under vacuum, was dialyzed over water for three days (with SnakeSkin™ Dialysis Tubing, 10K MWCO, 35 mm) and lyophilized. Yield = 169 mg

Hydrogel preparation

Formulation a) Stock solutions of HA-Azo **(7)** and **PAA-βCD** were prepared in 1 mL of MilliQ water at different weight concentrations (% w/w). Then, 100 μL of both components were mixed into a 250 μL vial under gentle stirring. After leaving the vial unmoved overnight, hydrogel formation was tested by the standard inverted vial test. Formulation b) Different aliquots (10, 20, 50 and 100 μL) of HA-Azo (2 wt%) were mixed with 100 μL of PAA-βCD (4 wt%). Specifically, the vol/vol ratio of 0.1:1;0.2:1;0.5:1 and 1:1 were investigated. The gel formation time appeared to be dependent from the Azo content: when 100 μL of the two polymers were mixed at 1:1 vol/vol, the gelification process was nearly immediate (few minutes) and stirring was not even required in order to homogenize the component and drive their self-assembly.

Synthesis of hyaluronic acid alkyne conjugate (HA-Alk) **(9)**

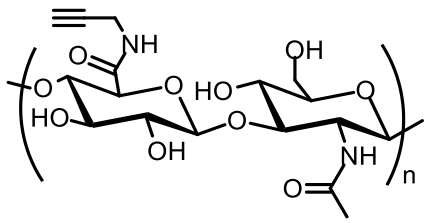

HA sodium salt (500 mg of HANa, 600-800 kD) was dissolved in 100 mL of deionized water (5 mg/mL, pH = 6.85) under sonication. Dowex H^+ 50W x 8–100 sulfonic resin was washed with deionized water for three time and then 500 mg were added to HA sodium salt solution and the reaction mixture was stirred for 1 h. The reaction mixture (pH = 3) was centrifuged (5 min, 3500 rpm) and the solution was lyophilized to give HA in protonated form. To a solution of 318 mg HA (0.83 mmol of COOH) in 20 mL of deionized water (the dissolution requires about 5-6 h under continue sonication), 8.5 mL of acetonitrile followed by 123 μL of 4-methylmorpholine (NMM) were added under stirring. The solution was cooled to 0°C and 146 mg (0.83 mmol) of 2-chloro-4,6-dimethoxy-1,3,5-triazine (CDMT) were added and stirred for 1 h at room temperature, then 53.1 μL (0.83 mmol)

of propargylamine was added and the reaction mixture was stirred for two days. Freshly washed Dowex H^+ 50W x 8–100 sulfonic resin (100 mg) was added, stirred for 5 min, then the mixture was centrifuged (5 min 3500 rpm), and the acetonitrile was removed under reduced pressure. The aqueous solution was purified by extensive cycles of dialysis (3500 Da Mw cutoff) against a mixture of ethanol and ultrapure water (20:80) and finally against ultrapure water. HA-Alk was recovered by lyophilization as a cottony white solid. The degree of substitution (DS_{100}; defined as the average number of propargyl groups per 100 disaccharide repeating unit) was calculated by the ratio between the integral of alkyne proton (m, 3.06) and the integral of one proton of HA acetyl group (s, 1.88 ppm) and turned out to be 50%. ^{1}H-NMR spectra and degree of substitution (DS) matched those reported in the literature.[21] **^{1}H-NMR**, selected signals (500 MHz, D_2O): 1.88 (s, 3H, NC(O)CH3), 3.06 (m, H, HC≡C-), 3.20-4.05 (HA sugar protons), 4.15 (m, CH_2C≡), 4.60 (m, HA anomeric protons).

Synthesis of hyaluronic acid β-cyclodextrin conjugate (HA-CD1) **(10)**

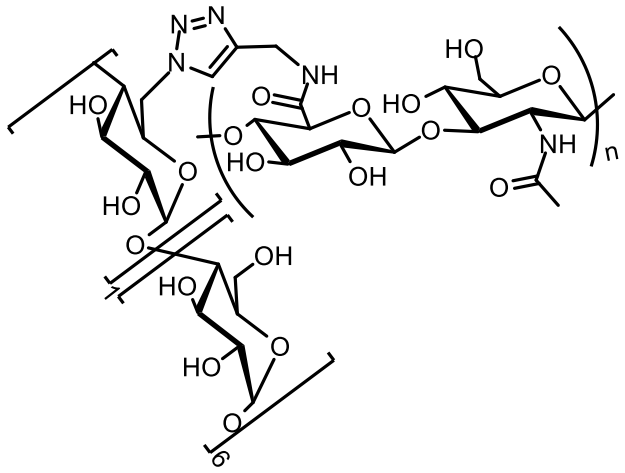

HA-Alk (172 mg, 0.172 mmol of propargyl groups) and mono-6-deoxy-6-azido-β-cyclodextrin (CDN_3) (200 mg, 0.172 mmol) were dissolved in 50 mL of water. The solution was bubbled with argon for 15 min and then $CuSO_4 \cdot 5H_2O$ (4.30 mg) and sodium ascorbate (34 mg) were added. The reaction mixture was stirred under argon atmosphere and room temperature for four days. The crude reaction mixture was purified by extensive cycles of dialysis (3500 Da Mw cutoff) against water containing ethylene-diaminetetraacetic acid (EDTA) and then ultrapure water. Finally, the product

was recovery by lyophilization as a cottony solid and characterized by ^{1}H-NMR spectroscopy. The degree of substitution (DS_{100}) was determined by the integration of the triazole proton peak at 7.88 ppm and the acetyl proton peak at 1.90 ppm. The DS_{100} turned out to be 0.7% corresponding to 2.2 mg % w/w of CD content. **^{1}H-NMR**, selected signals, (500 MHz, D_2O): 1.90 (s, 3H, NC(O)CH3), 3.06(m, unreacted HC≡C-), 3.20-3.75(HA sugar protons), 3.48(m, H4, CD), 3.52(m, H2, CD), 3.73(m, H5, CD) 3.75(m, H6, CD), 3.83(m, H3, CD), 4.15 (m, unreacted CH_2C≡), 4.30-4.36 (m, H1, HA), 4.41-4.44 (m, H1, HA), 4.95(m, H1, CD), 7.88(s, H5 triazole).

Preparation of HA-CD1@Acy assemblies

HA-CD1@Acy complex was prepared dissolving 20.3 mg of HA-CD1 (CD = 0.39 μmol) in 2.5 mL of water under sonication for 10 minutes. A stock solution of 2 mM of Acyclovir in water was prepared and an aliquot of 62.5 μL (Acy = 0.13 μmol) was added to HA-CD1 dispersion in order to obtain HA-CD1@Acy complex with 1:0.3 [CD:Acy] molar ratio. The mixture was stirred (250 rpm) and left to equilibrate for 5 days at 10-15°C, pH = 5.5. The final dispersion was freeze-dried and a weighed amount was redissolved both in water and PBS at pH = 7.4 for the characterization of the system. The assembly, reconstituted in water, showed drug loading (DL) and entrapment efficiency (EE%) of ~ 0.14 % and ~100 %, respectively as determined by UV/Vis spectroscopy. DL and EE were calculated according to the previously reported equations (Chapter 2, Experimental Section).

Competition experiments in the presence of 1-adamantanol (Ada-OH) were carried out preparing different batches with constant amount of HA-CD1@Acy complex ([HA-CD1] = 0.4 mg/mL) at different [Acy]/[Ada-OH] molar ratios. ([Acy]/[Ada-OH] molar ratios: 1:0.2; 1:0.4; 1:10). After adding the Ada-OH, the dispersions were mixed by vortex and analyzed at room temperature through UV/Vis spectroscopy.

Synthesis of N-(2-(2-(2-aminoethoxy)ethoxy)ethyl)adamantane-1-carboxamide **(12)**

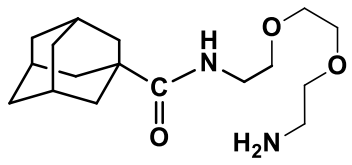

Adamantyl carboxylic acid (360 mg, 2 mmol, 1 eq.) was added to a round-bottom flask containing dry toluene (20 mL) and fitted with a reflux condenser, a dry Argon inlet, and a magnetic stirrer. The solution was heated to 60 °C and stirred. CDI (324 mg, 2 mmol, 1 eq.) was added to the solution and stirred until the CO_2 evolution had ceased. The solution was heated for a further 30 min and purged with argon. N-Boc-2,2'-(ethylenedioxy)diethylamine (500 mg, 2 mmol, 1 eq.) was added to the solution and allowed to stir at 60 °C for a further 2 h and then cooled to room temperature. The reaction mixture was concentrated in vacuo, and the remaining clear liquid was dissolved in dichloromethane and washed three times with water (3 x 10 mL). The washed dichloromethane (DCM) solution was dried with anhydrous Na_2SO_4, filtered, and concentrated. Then, the intermediate product (250 mg, 0.6 mmol) was deprotected with 1.8 mL of trifluoroacetic acid (TFA) in DCM (1.2 mL), added dropwise in ice bath and left stirring overnight. The reaction mixture was washed with a solution of KOH (10%) and the organic phases were dried, filtered, and concentrated. Yield: 100 mg, 16%; **^{1}H-NMR** (500 MHz, $CDCl_3$): δ 7.62 (s, 1H), 6.16 (s, 2H), 3.58 (s, 4H) 3.51 – 3.38 (m, 6H), 2.84 (t, 2H), 2.12 – 1.63 (m, 15H); **^{13}C-NMR** (125 MHz, $CDCl_3$): δ 178.2, 72.81, 69.87, 41.70, 40.44, 39.09, 36.43, 27.86;

Synthesis of HA-Ada **(13)**

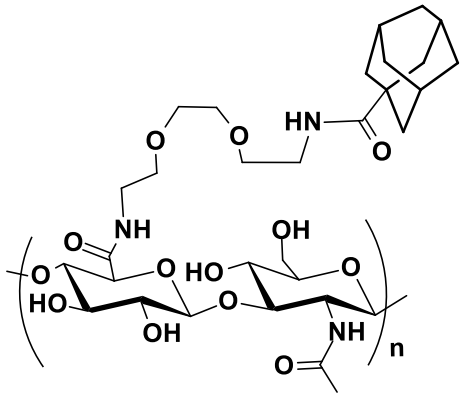

HA-COOH (100 mg, 0.13 mmol carboxylic acid) was dissolved in ~3 mL of deionized water in a 100 mL round-bottomed flask, followed by the dropwise addition of ~2 mL of acetonitrile, ~1.5 mL of THF and NMM (36 μL, 0.39 mmol, 1.5 eq.), under stirring. Then the solution was cooled down to 4°C with an ice bath and CDMT (23 mg, 0.13 mmol, 1 eq.) was added and stirred for 1 h at r.t. Finally, **(11)** (40 mg, 0.13 mmol, 1 eq.) was added to the mixture, corresponding with a 1:1 ratio between HA carboxyls and amino groups. The solution was left stirring overnight at r.t. to obtain a white product that, after removal of THF and ACN under vacuo, was dyalized over water for three days and finally liophilized. Yield 90 mg

Synthesis of HA-TDA **(15)**

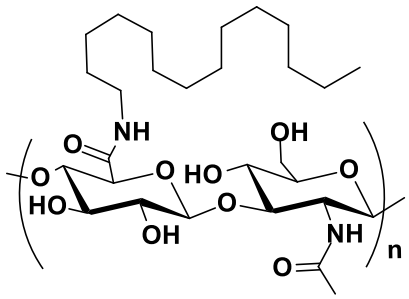

The synthesis was carried out at different molar ratios HA-COOH/TDA. Below is reported the preparation of poor soluble HA-TDA obtained using 1:0.5 as HA-COOH/TDA.

HA-COOH (100 mg, 0.13 mmol carboxylic acid) was dissolved in 6 mL of deionized water in a 50 mL flask. Therefore 4 mL of THF and 2 mL of acetonitrile were added dropwise while stirring,

together with NMM (36 μL, 0.39 mmol, 1.5 eq.). The solution was then cooled to 4°C, and 11.5 mg (0.06 mmol, 0.5 eq.) of CDMT were added and stirred for 1 hr at room temperature. Afterward the solution was mixed with 14 mg (0.06 mmol) of tetradecylamine (TDA), corresponding to a 1:0.5 ratio between HA carboxyl groups and TDA amine groups, and stirred for 48 h. Acetonitrile and THF were removed under reduced pressure and the precipitate was washed with ethanol, water and finally centrifuged several times. In the end the solid product was freezed and lyophilized as well as the supernatant. NMR spectra (Figure 16) of HA-TDA from 1:0.5 molar ratio was performed after hydrolysis with HCl and following dialysis.

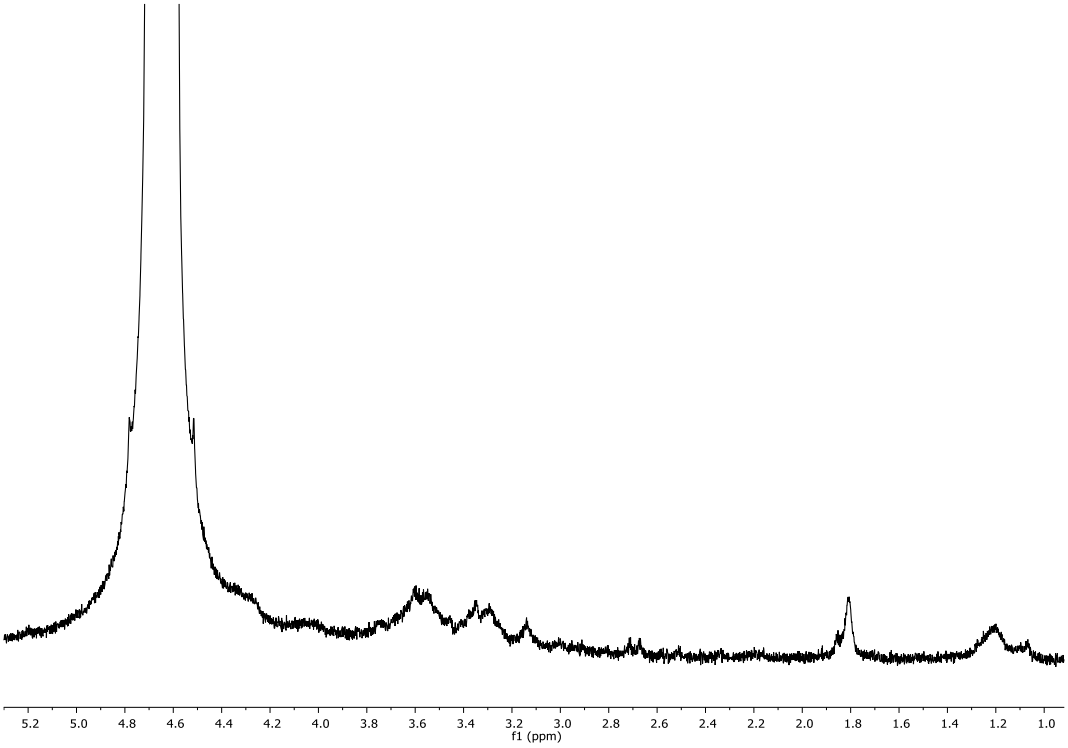

Figure 16 ^{1}H-NMR of HA-TDA (1:0.5) in D_2O after HCl hydrolysis and dialysis

References

1. Highley, C. B.; Prestwich, G. D.; Burdick, J. A., Recent advances in hyaluronic acid hydrogels for biomedical applications. *Current Opinion in Biotechnology* **2016,** *40*, 35-40.

2. Kim, D.-Y.; Lee, S.-A.; Park, M.; Choi, Y.-J.; Kang, S.-W.; Jeong, K.-U., Multi-responsible chameleon molecule with chiral naphthyl and azobenzene moieties. *Soft Matter* **2015,** *11* (15), 2924-2933.

3. Beharry, A. A.; Woolley, G. A., Azobenzene photoswitches for biomolecules. *Chemical Society Reviews* **2011,** *40* (8), 4422-4437.

4. Chen, L.; Zhao, X.; Lin, Y.; Su, Z.; Wang, Q., Dual stimuli-responsive supramolecular hydrogel of bionanoparticles and hyaluronan. *Polymer Chemistry* **2014,** *5* (23), 6754-6760.

5. Pang, J.; Gao, Z.; Zhang, L.; Wang, H.; Hu, X., Synthesis and Characterization of Photoresponsive Macromolecule for Biomedical Application. *Front Chem* **2018,** *6* (217), 217.

6. Bortolus, P.; Monti, S., cis .dblharw. trans Photoisomerization of azobenzene-cyclodextrin inclusion complexes. *The Journal of Physical Chemistry* **1987,** *91* (19), 5046-5050.

7. Deka, S. R.; Yadav, S.; Mahato, M.; Sharma, A. K., Azobenzene-aminoglycoside: Self-assembled smart amphiphilic nanostructures for drug delivery. *Colloids and Surfaces B: Biointerfaces* **2015,** *135*, 150-157.

8. Voskuhl, J.; Sankaran, S.; Jonkheijm, P., Optical control over bioactive ligands at supramolecular surfaces. *Chemical Communications* **2014,** *50* (96), 15144-15147.

9. Zhao, W.; Li, Y.; Zhang, X.; Zhang, R.; Hu, Y.; Boyer, C.; Xu, F.-J., Photo-responsive supramolecular hyaluronic acid hydrogels for accelerated wound healing. *Journal of Controlled Release* **2020,** *323*, 24-35.

10. Rosales, A. M.; Rodell, C. B.; Chen, M. H.; Morrow, M. G.; Anseth, K. S.; Burdick, J. A., Reversible Control of Network Properties in Azobenzene-Containing Hyaluronic Acid-Based Hydrogels. *Bioconjugate Chemistry* **2018,** *29* (4), 905-913.

11. Hesler, M.; Schwarz, D. H.; Dähnhardt-Pfeiffer, S.; Wagner, S.; von Briesen, H.; Wenz, G.; Kohl, Y., Synthesis and in vitro evaluation of cyclodextrin hyaluronic acid conjugates as a new candidate for intestinal drug carrier for steroid hormones. *European Journal of Pharmaceutical Sciences* **2020,** *143*, 105181.

12. Micale, N.; Piperno, A.; Mahfoudh, N.; Schurigt, U.; Schultheis, M.; Mineo, P. G.; Schirmeister, T.; Scala, A.; Grassi, G., A hyaluronic acid–pentamidine bioconjugate as a macrophage mediated drug targeting delivery system for the treatment of leishmaniasis. *RSC Advances* **2015,** *5* (116), 95545-95550.

13. Serrano-Aroca, Á., Latest Improvements of Acrylic-Based Polymer Properties for Biomedical Applications. In *Acrylic Polymers in Healthcare*, 2017.

14. Nakahata, M.; Takashima, Y.; Yamaguchi, H.; Harada, A., Redox-responsive self-healing materials formed from host–guest polymers. *Nature Communications* **2011,** *2* (1), 511.

15. Lembo, D.; Donalisio, M.; Civra, A.; Argenziano, M.; Cavalli, R., Nanomedicine formulations for the delivery of antiviral drugs: a promising solution for the treatment of viral infections. *Expert opinion on drug delivery* **2018,** *15* (1), 93-114.

16. Prasad, M.; Lambe, U. P.; Brar, B.; Shah, I.; J, M.; Ranjan, K.; Rao, R.; Kumar, S.; Mahant, S.; Khurana, S. K.; Iqbal, H. M. N.; Dhama, K.; Misri, J.; Prasad, G., Nanotherapeutics: An insight into healthcare and multi-dimensional applications in medical sector of the modern world. *Biomedicine & pharmacotherapy = Biomedecine & pharmacotherapie* **2018,** *97*, 1521-1537.

17. Plass, M.; Kristl, A.; H. Abraham, M., Spectroscopic investigation of the tautomeric equilibria in the guanine derivatives of acyclovir. *Journal of the Chemical Society, Perkin Transactions 2* **1999,** (11), 2641-2646.

18. Iannazzo, D.; Mazzaglia, A.; Scala, A.; Pistone, A.; Galvagno, S.; Lanza, M.; Riccucci, C.; Ingo, G. M.; Colao, I.; Sciortino, M. T.; Valle, F.; Piperno, A.; Grassi, G., β-Cyclodextrin-grafted on multiwalled carbon nanotubes as versatile nanoplatform for entrapment of guanine-based drugs. *Colloids Surf B Biointerfaces* **2014,** *123*, 264-270.

19. Piperno, A.; Zagami, R.; Cordaro, A.; Pennisi, R.; Musarra-Pizzo, M.; Scala, A.; Sciortino, M. T.; Mazzaglia, A., Exploring the entrapment of antiviral agents in hyaluronic acid-cyclodextrin conjugates. *Journal of Inclusion Phenomena and Macrocyclic Chemistry* **2019,** *93* (1), 33-40.

20. Nielsen, T. T.; Wintgens, V.; Amiel, C.; Wimmer, R.; Larsen, K. L., Facile synthesis of β-cyclodextrin-dextran polymers by "Click" chemistry. *Biomacromolecules* **2010,** *11* (7), 1710-1715.

21. Borke, T.; Winnik, F. M.; Tenhu, H.; Hietala, S., Optimized triazine-mediated amidation for efficient and controlled functionalization of hyaluronic acid. *Carbohydr Polym* **2015,** *116*, 42-50.

Chapter 4

This chapter describes the preparation of Gold@Silver core-shell nanoparticles (Au@Ag NPs) using cationic poly-cyclodextrin (PolyCD) or Hyaluronic Acid (HA) or Hyaluronic Acid modified with β-cyclodextrins (HA-CD2) as polymeric coating. Herein, the preliminary results about the physicochemical properties of these systems as well as their interaction with selected Raman reporters (RaRs) are discussed. They are proposed as SERS-Tags for diagnostic purposes and specifically for the recognition of exosomes in blood samples in liquid biopsy (Figure 1). Exosomes are a sub-group of cell-derived nanovesicles (30-100 nm) involved in the regulation of many biological processes that recently have aroused growing interest due to their involvement in cancer growth and progression. This research project is currently ongoing in collaboration with Prof Simion Astilean and Dr Alexandru Hada from the Interdisciplinary Research Institute in BioNano-Sciences, Babes-Bolyai University (Romania).

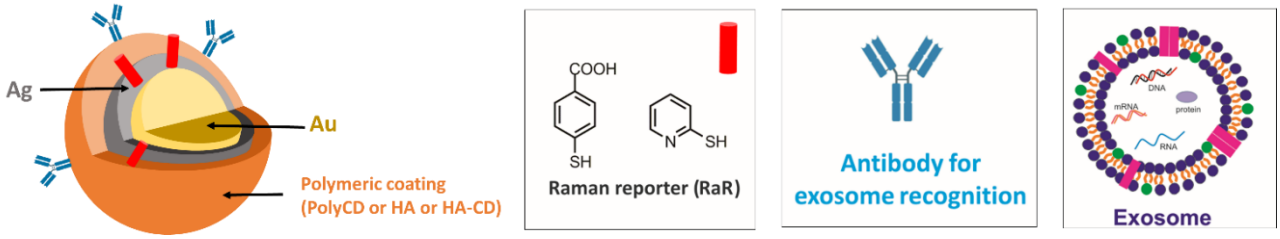

Figure 1 Sketched representation of materials used for the preparation of polymer-coated Gold@Silver core-shell nanoparticles (Au@Ag NPs).

4.1 Synthesis and characterization of Gold@Silver core-shell nanoparticles

Noble metal nanoparticles, particularly gold and silver (AuNPs, AgNPs) have attracted increasing interest in the last decades for the development of new biosensors and/or for the improvement of existing biosensing techniques, in order to fulfill the increasing demand for more specific and highly sensitive biomolecular diagnostics. These nanomaterials show unique physicochemical properties at nanoscale level with respect to their respective microparticles or bulk materials. Indeed, one of the most common nanotechnology-based approaches for application in biomedical fields makes use of NPs, due to their simplicity, high surface-to-volume ratio, ease of surface functionalization and extreme analytical sensitivity that makes them ideal for biosensors development as well as for *in vivo* sensing /imaging for disease diagnosis and monitoring along with the therapeutic treatment. [1-3]

Surface plasmon resonance is a physical phenomenon that occurs when the frequency of the electromagnetic radiation resonates with the collective oscillation of the conduction electrons of the noble-metal nanoparticles. This effect manifests as an intense UV/Vis absorption band, the so-called plasmonic band, whose position can be influenced by particles size, shape, surrounding environment and degree of association. In our research groups different polymers,[4] porphyrin[5] and cycodextrin[6, 7] based motifs were utilized to stabilize noble metal NPs with potential in biomedical applications. Surface enhanced Raman spectroscopy (SERS) exploits the large local field enhancements that occur near the NPs surface due to plasmon excitation to amplify the Raman scattering signal of the molecules located at or near the metallic surface. This effect has been recently exploited for the development of a new kind of optical contrast agents called SERS-Tags, complex nanoconstructs

constituted by: i) a plasmonic nanoparticle, ii) a Raman active molecules bound to the surface of the nanoparticle which should provide a strong and discernible SERS signal, iii) an external organic or inorganic layer to guarantee stability and biocompatibility.[8] In our strategy, the polymer coatings (PolyCD, HA and HA-CD2) act as stabilizers and reducing agents towards Au^{3+}, providing an environmental-friendly approach for the preparation of noble-metal core-shells.

Results and discussion

The ability of PolyCD, HA or HA-CD2 biomaterials to stabilize Gold@Silver core-shell was investigated. They were selected due to a series of unique characteristics such as biocompatibility and the presence in their molecular structure of several amino/hydroxyl groups and other functionalities that can simultaneously act as reductants and stabilizers, avoiding the use of classical reducing agents. Different experimental conditions (i.e. temperature, time, metal ions concentration) were investigated to set up the best preparation protocol. The synthetic approach for the production of AuNPs consists in two phases: i) addition of tetrachloro-auric(III) acid (10^{-3} M) to an aqueous solution of the polymer (2 mg/mL), maintained at constant temperature (60-70°C); ii) three successive additions of $AgNO_3$ aliquots (10^{-1} M) into the solution containing the colloidal polymer-coated AuNPs and ascorbic acid (r.t.). The reactions were monitored by UV/Vis analysis, following the evolution of the typical plasmon resonance absorption peaks. Right after the addition of $HAuCl_4$, the solutions slowly began to change from colorless to purple, suggesting that Au^{3+} was effectively reduced, forming AuNPs within 3-5 hours.
Figure 2 reports the UV spectra of AuNPs and Au@Ag NPs coated with PolyCD. The polymer was purified by dialysis and lyophilized before the use. The experiments were carried out on PolyCD hydrochloride salt (PolyCD $NH3^+$ Cl^-) and PolyCD containing free NH_2 groups (PolyCD-NH_2). The absorption band typical of monodisperse spherical AuNPs was detected at 526-527 nm. The successive additions of $AgNO_3$ aliquots lead to a change of the extinction spectra with the formation

of a higher and broader absorption band at 403-408 nm (Figure 2), due to the localized surface plasmon resonance (LSPR) effect that occurs at the interface between the Au-core and the Ag-shell. The shape of the band and the intensity of this phenomenon are both controlled by the size and shape of the gold core, as well as the thickness of the silver shell.[9-11]

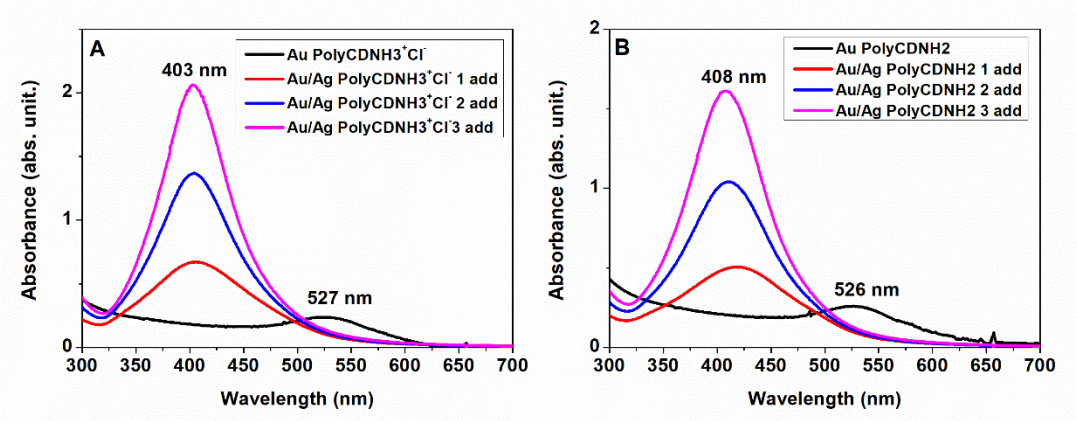

Figure 2 UV/Vis spectra of AuNPs vs. Au@Ag NPs coated by PolyCD hydrochloride salt ($PolyCDNH_3^+Cl^-$) (A) and PolyCD free NH_2 ($PolyCDNH_2$) (B). (d = 0.2 cm)

To investigate the colloidal stability of PolyCD Au@Ag NPs, DLS and zeta-potential measurements were carried out (Table 1 and Figure 3).

Table 3 DLS and ζ-potential measurements of AuNPs and Au@Ag NPs in water

Sample	Mean D_H (nm ± SD)[a](%)[b]	PDI	ζ (mV ± SD)
AuNPs ($PolyCDNH_3^+Cl^-$)	38.10 ± 17 (75) 247 ± 33 (21)	≥ 0.4	21.7 ± 6
AuNPs ($PolyCDNH_2$)	31.29 ± 11 (64) 294 ± 27 (35)	≥ 0.4	16.7 ± 6
Au@Ag NPs ($PolyCDNH_3^+Cl^-$)	48.51 ± 22 (98)	≥ 0.4	23.4 ± 7
Au@Ag NPs ($PolyCDNH_2$)	51.42 ± 30 (97)	≥ 0.4	22.6 ± 7

[a]SD was calculated on three different batches. [b] Mean size with corresponding intensity % distribution (only main populations).

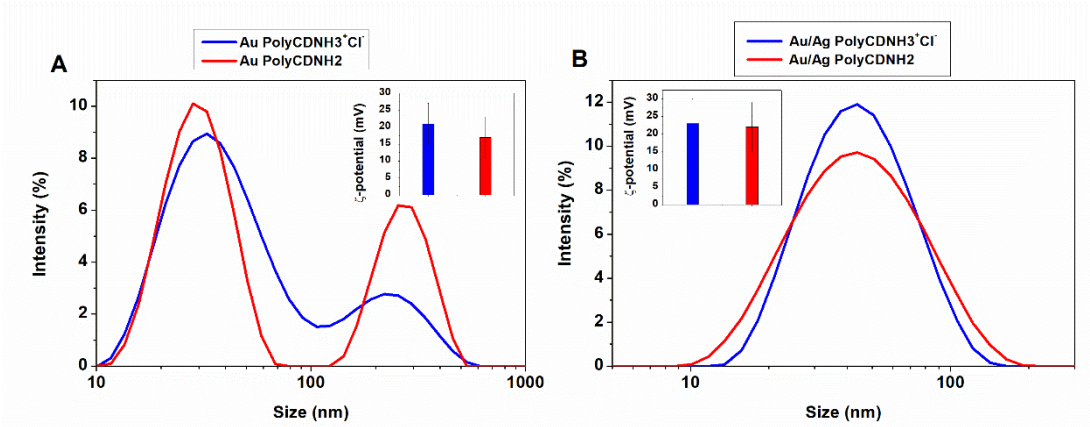

*Figure 3 Size (or D_H) distribution of **A)** AuNPs coated by PolyCDNH$_3^+$Cl$^-$ (blue trace) and PolyCDNH$_2$ (red trace) in ultrapure water at r.t.; **B)** Au@Ag NPs core-shell coated by PolyCDNH$_3^+$Cl$^-$ (blue trace) and PolyCDNH$_2$ (red trace) in ultrapure water at r.t. In the insets the respective ζ potential ± SD.*

PolyCD AuNPs showed two populations with a mean diameter (D_H) in the range of 31-38 nm (main population), and 247-294 nm (minor population). The respective Au@Ag NPs core-shell showed a single population with a mean diameter (D_H) in the range of 48-51 nm. Interestingly, both AuNPs samples gave rise to unique population of small Au@Ag NPs core-shell (Figure 3).

AuNPs and Au@Ag NPs obtained from PolyCD hydrochloride salt had a strong positive ζ-potential (*i.e*, +21.7 and +23.4 mV respectively). AuNPs and Au@Ag NPs obtained from PolyCD with free amino groups (sample treated with $NaHCO_3$ before the dialysis) as expected, showed lower positive ζ-potential values (*i.e*, +16.7 and +22.6 mV respectively) than NPs obtained from PolyCDNH$_3^+$Cl$^-$. From our experiments performed to set up the preparation of Au@Ag NPs emerged that the purity of PolyCD could affect the formation of core-shell. Some experiments carried out on commercially not-purified batches failed. However, our first experiments were carried out on non-purified PolyCD. Figure 4 reports UV/Vis spectra of AuNPs and Au@Ag NPs obtained from PolyCD hydrochloride salt not dialyzed and the NPs obtained from Hyaluronic Acid (HA) and Hyaluronic Acid modified with cyclodextrin (HA-CD2).

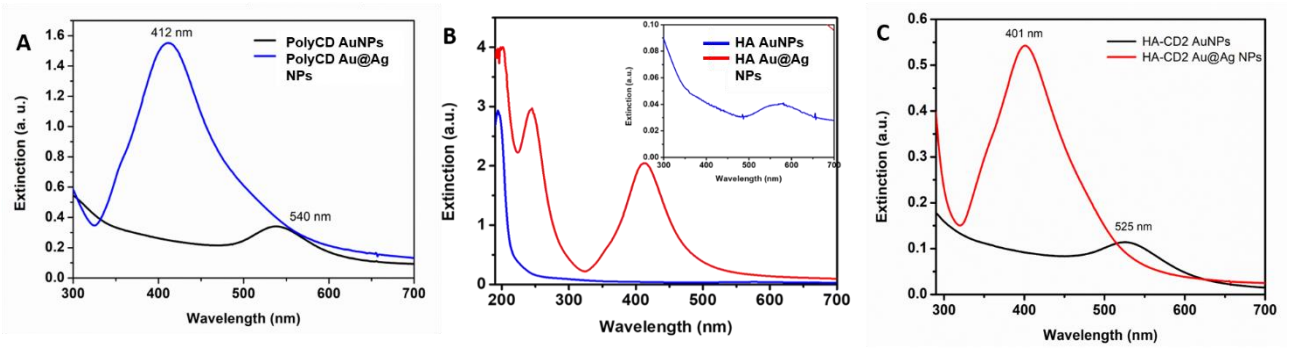

*Figure 4UV/Vis spectra of Au vs. Au@Ag NPs coated by **A)** PolyCD, **B)** HA and **C)** HA-CD2 (d = 0.2 cm)*

In view of their exploitation as SERS contrast agents for biosensing, the polymer-coated NPs were additionally modified with selected reporter molecules, 4-Mercaptopyridine (Pyr-SH) and p-mercaptobenzoic acid (4MBA). These Raman active molecules bond metal surface by thiol group, providing to the NPs a peculiar Raman fingerprint. According to our project purpose, this advantageous property is exploitable, after proper conjugation of an antibody on the nanoparticle's surface, to reveal the presence of specific exosome-derived antigens in complex biological samples such as blood.

Figures 5-7 illustrate the extinction spectra of the different colloidal dispersions recorded before and after SERS tagging, specifically: PolyCD with Pyr-SH and 4MBA (Figure 5), HA with Pyr-SH (Figure 6) and HA-CD with Pyr-SH and 4MBA (Figure 7). After the addition of the reporter, the extinction spectra for all the nanoparticles exhibited a red shift due to the local increase of refractive index. This change evidences that the coating allows the reporters to penetrate and diffuse through the polymer matrix to finally attach onto the metallic surface via sulfur-gold/silver bonding. The stability of the construct to aggregation phenomena was also tested with different centrifugation cycles (CRF) after different incubation time intervals.

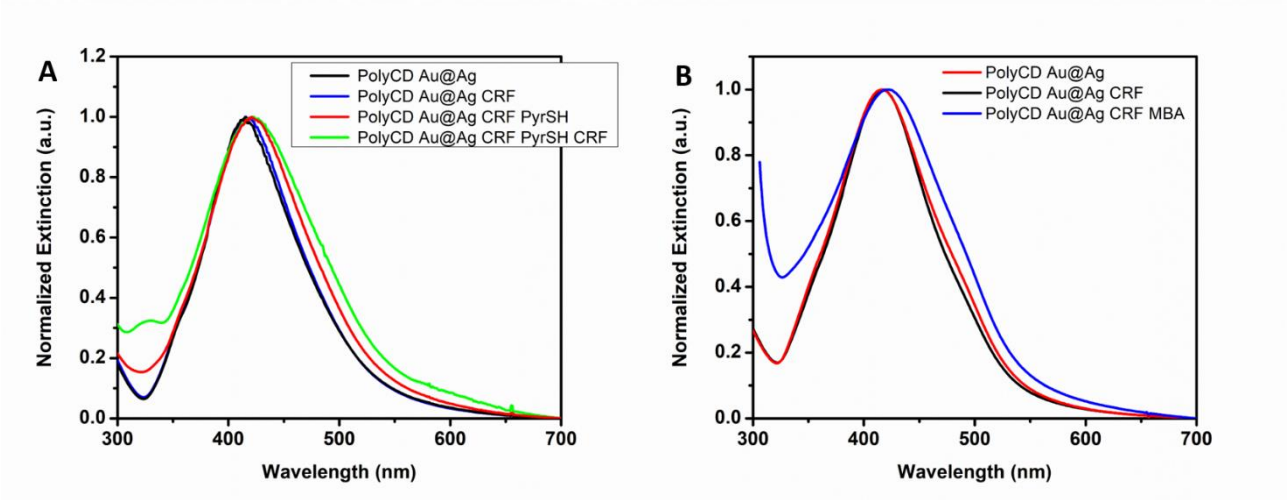

Figure 5 ***A)*** *Normalized extinction spectra of PolyCD Au@Ag NPs (blue), after the first centrifugation and redispersion in water (black), incubation with PyrSH (red) and after the second centrifugation and redispersion in water (red);* ***B)*** *Normalized extinction spectra of PolyCD Au@Ag NPs (red), PolyCD Au@Ag NPs after centrifugation (black) and centrifuged PolyCD Au@Ag NPs marked with 4MBA (blue); (d = 0.2 cm)*

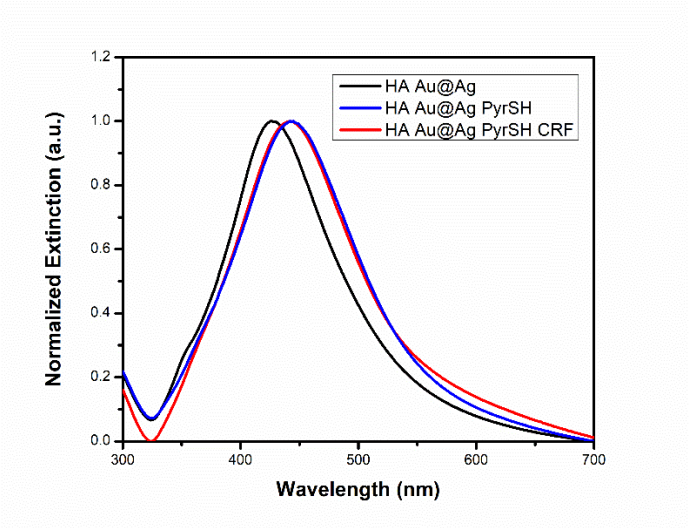

Figure 6 Normalized extinction spectra of HA Au@Ag NPs (blue), after the first centrifugation and redispersion in water (black), incubation with PyrSH (red) and after the second centrifugation and redispersion in water (red) (d = 0.2 cm)

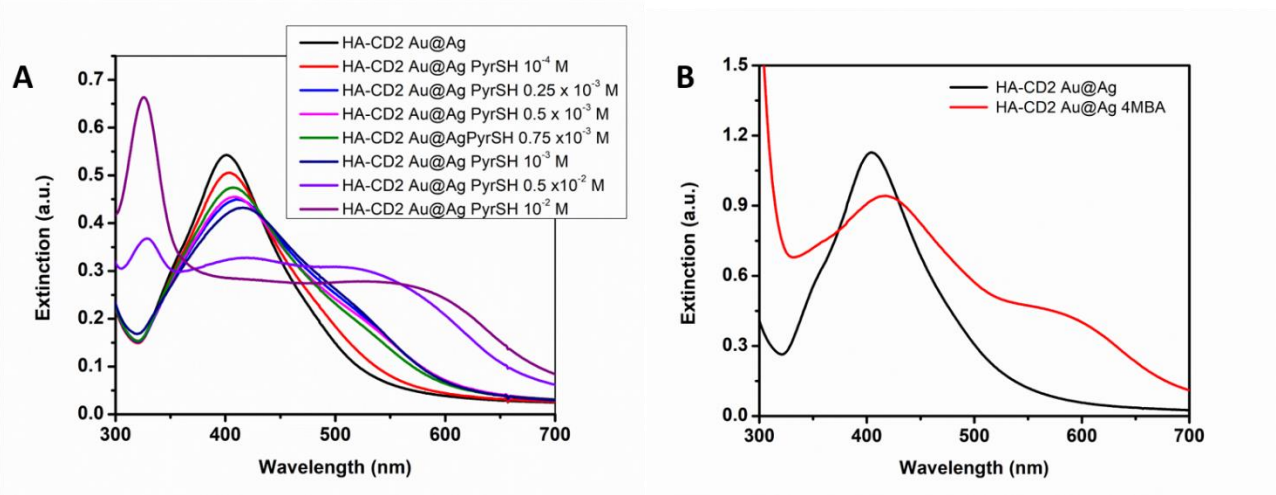

Figure 7 ***A)*** *Extinction spectra of HA-CD2 Au@Ag NPs incubated with different concentrations of PyrSH;* ***B)*** *The extinction spectra of HA-CD2 Au@Ag NPs before (black) and after (red) the incubation with 4MBA. (d = 0.2 cm)*

CONCLUSIONS

Our preliminary results suggest that polymers based on cyclodextrin or on hyaluronic acid are promising biomaterials for the preparation of Au@Ag NPs. Specifically, the synthesis, the characterization and the interaction with selected RaRs of Au@Ag NPs obtained from PolyCD, HA, and HA-CD2 were investigated. Nanoparticles with better performance in terms of stability and sensibility will be employed as SERS-Tag for exosomes recognition.

Experimental Section

Materials

Tetrachloro-auric acid ($HAuCl_4$), silver nitrate ($AgNO_3$) and all other reagents were purchased from Sigma-Aldrich (Milan, Italy). All the solutions used for spectroscopic characterization were prepared in ultrapure micro-filtered water (Galenica Senese) and analysed at 298 K. NMR, UV/Vis, Size and ζ-potential measurements were carried out in the same modalities and equipments described in the Experimental Section of Chapter 2 and 3. HA-CD2 was prepared according to the synthetic procedure

reported in Chapter 3. PolyCD was purchased by Cyclolab as reported in Chapter 1. Three samples of PolyCD have been used: i) commercial untreated PolyCD, ii) PolyCD dialyzed against water for one week and iii) PolyCD pre-treated with $NaHCO_3$ for 30 min and dialyzed against water for one week. Dialysis membrane cutoff was 3500 kDa. All samples were finally lyophilized.

Preparation of PolyCD-coated Au@Ag NPs

A stock aqueous solution of PolyCD AuNPs was prepared by dissolving 3 mL of 10^{-3} M $HAuCl_4$ and 18 mL of PolyCD (2 mg/mL) in ultrapure water and letting the solution stir for 3 h at 60-70°C. The progress of the reaction was monitored via UV/Vis measurement by the increase of intensity of the typical plasmon resonance absorption peak of AuNPs at ~530 nm. Then, 5 mL of the latter pinkish solution were added with 30 µL of 10^{-1} M of ascorbic acid and three successive aliquots (10 µL) of 10^{-1} M $AgNO_3$ to obtain PolyCD Au@Ag core-shell as an orange clear solution. After each $AgNO_3$ addition, the mixture was kept under magnetic stirring at room temperature (20-25°C) for 1h. Ag^+ reduction was monitored following the gradual increase of the characteristic plasmonic resonance absorption band in the range 390-420 nm of the UV/Vis spectrum.

Preparation of HA-coated Au@Ag NPs

A stock aqueous solution of HA Au NPs was prepared by dissolving 1.5 mL of 10^{-3} M $HAuCl_4$ and 9 mL of HA (2 mg/mL) in ultrapure water and letting the solution stir for 5 h at 60-70°C. The typical plasmon resonance absorption peak of AuNPs was detected at ~550 nm. Then, 5 mL of the latter pinkish solution were added with 30 µL of 10^{-1} M of ascorbic acid and three successive aliquots (10 µL) of 10^{-1} M $AgNO_3$ to obtain HA Au@Ag core-shell as an orange clear solution. After each $AgNO_3$ addition, the mixture was kept under magnetic stirring at room temperature (20-25°C) for 1h. Ag^+ reduction was monitored following the gradual increase of the characteristic plasmonic resonance absorption band in the range 390-420 nm of the UV/Vis spectrum.

Preparation of HA-CD2 coated Au@Ag NPs

A stock aqueous solution of HA-CD AuNPs was prepared by dissolving 0.75 mL of 10^{-3} M $HAuCl_4$ and 4.5 mL of HA (2 mg/mL) in ultrapure water and letting the solution stir for 1.5 h at 65°C. The typical plasmon resonance absorption peak of AuNPs at ~550 nm. Then, 5 mL of the latter pinkish solution were added with 30 μL of 10^{-1} M of ascorbic acid and three successive aliquots (10 μL) of 10^{-1} M $AgNO_3$ to obtain HA-CD Au@Ag core-shell as an orange clear solution. After each $AgNO_3$ addition, the mixture was kept under magnetic stirring at room temperature (20-25°C) for 45 min. Ag^+ reduction was monitored following the gradual increase of the characteristic plasmonic resonance absorption band in the range 390-420 nm of the UV/Vis spectrum.

SERS Labeling

490 μL of PolyCD, HA and HA-CD were incubated at room temperature for 1 h with 10 μL of 10^{-3} M solution of two selected Raman-active molecules, respectively: PolyCD Au@Ag NPs with 4-Mercapto pyridine (Pyr-SH), HA Au@Ag with 4-Mercaptobenzoic acid (4MBA) and HA-CD Au@Ag NPs with both. The resulting labeled core-shell nanoparticles underwent several centrifugation steps at high speed (5000 rpm x 10 min) and were redispersed in ultrapure water after every cycle.

References

1. Doria, G.; Conde, J.; Veigas, B.; Giestas, L.; Almeida, C.; Assunção, M.; Rosa, J.; Baptista, P. V., Noble metal nanoparticles for biosensing applications. *Sensors* **2012,** *12* (2), 1657-1687.

2. Jain, P. K.; Huang, X.; El-Sayed, I. H.; El-Sayed, M. A., Noble Metals on the Nanoscale: Optical and Photothermal Properties and Some Applications in Imaging, Sensing, Biology, and Medicine. *Accounts of Chemical Research* **2008,** *41* (12), 1578-1586.

3. Zhang, Z.; Lin, P.-C., Chapter 7 - Noble metal nanoparticles: synthesis, and biomedical implementations. In *Emerging Applications of Nanoparticles and Architecture Nanostructures*, Barhoum, A.; Makhlouf, A. S. H., Eds. Elsevier: 2018; pp 177-233.

4. Scala, A.; Piperno, A.; Hada, A.; Astilean, S.; Vulpoi, A.; Ginestra, G.; Marino, A.; Nostro, A.; Zammuto, V.; Gugliandolo, C., Marine bacterial exopolymers-mediated green synthesis of noble metal nanoparticles with antimicrobial properties. *J Polymers* **2019,** *11* (7), 1157.

5. Mineo, P.; Abbadessa, A.; Mazzaglia, A.; Gulino, A.; Villari, V.; Micali, N.; Millesi, S.; Satriano, C.; Scamporrino, E., Gold nanoparticles functionalized with PEGylate uncharged porphyrins. *Dyes and Pigments* **2017,** *141*, 225-234.

6. Mazzaglia, A.; Trapani, M.; Villari, V.; Micali, N.; Merlo, F. M.; Zaccaria, D.; Sciortino, M. T.; Previti, F.; Patanè, S.; Scolaro, L. M., Amphiphilic Cyclodextrins as Capping Agents for Gold Colloids: A Spectroscopic Investigation with Perspectives in Photothermal Therapy. *The Journal of Physical Chemistry C* **2008,** *112* (17), 6764-6769.

7. Trapani, M.; Romeo, A.; Parisi, T.; Sciortino, M. T.; Patanè, S.; Villari, V.; Mazzaglia, A., Supramolecular hybrid assemblies based on gold nanoparticles, amphiphilic cyclodextrin and porphyrins with combined phototherapeutic action. *RSC Advances* **2013,** *3* (16), 5607-5614.

8. Hada, A. M.; Potara, M.; Suarasan, S.; Vulpoi, A.; Nagy-Simon, T.; Licarete, E.; Astilean, S., Fabrication of gold-silver core-shell nanoparticles for performing as ultrabright SERS-nanotags inside human ovarian cancer cells. *Nanotechnology* **2019,** *30* (31), 315701.

9. He, W.; Wang, Y.; Lv, Y.; Xiao, Q.; Ye, L.; Cai, B.; Qin, C.; Han, X.; Cai, T.; Yin, L., Denatured protein stabilized drug nanoparticles: tunable drug state and penetration across the intestinal barrier. *Journal of Materials Chemistry B* **2017,** *5* (5), 1081-1097.

10. Zhu, J., Surface Plasmon Resonance from Bimetallic Interface in Au–Ag Core–Shell Structure Nanowires. *Nanoscale Research Letters* **2009,** *4* (9), 977.

11. Zhang, C.; Chen, B.-Q.; Li, Z.-Y.; Xia, Y.; Chen, Y.-G., Surface Plasmon Resonance in Bimetallic Core–Shell Nanoparticles. *The Journal of Physical Chemistry C* **2015,** *119* (29), 16836-16845.

Publications:

1. Trapani, M.; Mazzaglia, A.; Piperno, A.; Cordaro, A.; Zagami, R.; Castriciano, M.A.; Romeo, A.; Monsù Scolaro, L. Novel Nanohybrids Based on Supramolecular Assemblies of Meso-tetrakis-(4-sulfonatophenyl) Porphyrin J-aggregates and Amine-Functionalized Carbon Nanotubes. *Nanomaterials* **2020**, *10*, 669.

2. Cordaro, A.; Neri, G.; Sciortino, M.T.; Scala, A.; Piperno, A. Graphene-Based Strategies in Liquid Biopsy and in Viral Diseases Diagnosis. *Nanomaterials* **2020**, *10*, 1014.

3. Cordaro, A.; Zagami, R.; Malanga, M.; Venkatesan, J.K.; Alvarez-Lorenzo, C.; Cucchiarini, M.; Piperno, A.; Mazzaglia, A. Cyclodextrin Cationic Polymer-Based Nanoassemblies to Manage Inflammation by Intra-Articular Delivery Strategies. *Nanomaterials* **2020**, *10*, 1712.

4. Nazanin Kordestani, Hadi Amiri Rudbari, Zohreh Fateminia, Guy Caljon, Louis Maes, Placido Mineo, Annalaura Cordaro, Antonino Mazzaglia, Angela Scala, Nicola Micale. Antimicrobial and Antiprotozoal Activities of Silver Coordination Polymers Derived from the Asymmetric Halogenated Schiff Base Ligands. (accepted for publication in *Applied Organometallic Chemistry*, **2020**)

5. Francesco Valle, Silvia Tortorella, Angela Scala, Annalaura Cordaro, Marianna Barbalinardo, Fabio Biscarini, Antonino Mazzaglia. Amphiphilic cationic cyclodextrin nanovesicles: a versatile cue for guiding cell adhesion. (accepted for publication in *Nanoscale Advances*, **2020**)

6. Piperno, A., Zagami, R., Cordaro, A. *et al.* Exploring the entrapment of antiviral agents in hyaluronic acid-cyclodextrin conjugates. *J Incl Phenom Macrocycl Chem* **2018,** *93***,** 33–40.

Communications at meetings and conferences:

1. Annalaura Cordaro, Roberto Zagami, Angela Scala, Antonino Mazzaglia, Anna Piperno. *"Hyaluronic acid as delivery platform for regenerative medicine applications".* I Convegno DOCTOCHEM – UNIME, Messina, 22 giugno 2018 (oral communication)

2. Annalaura Cordaro, Serena M. Torcasio, Angela Scala, Anna Piperno, Giovanni Grassi, Roberto Zagami, Antonino Mazzaglia, Placido G. Mineo, Rosamaria Pennisi, Maria Musarra Pizzo, Maria Teresa Sciortino. *MicroRNA Nanocarrier Based on Graphene Engineered with Cationic Cyclodextrins*. Congresso congiunto delle sezioni Sicilia e Calabria 2018, Catania, 9-10 febbraio 2018 (poster presentation, PO27 p. 73)

3. Annalaura Cordaro, Roberto Zagami, Milo Malanga, Anna Piperno, Antonino Mazzaglia. *Hydrogels based on hyaluronic acid/cyclodextrin assemblies for regenerative medicine.* Italian National Conference on Materials, Science and Technology, Bologna, 22-26 ottobre 2018 (poster presentation, PO19 p. 182).

4. Annalaura Cordaro. *Supramolecular assemblies as therapeutic scaffolds for tissue regeneration*. Workshop di Istituto CNR-ISMN, Cinisi, 12-14 dicembre 2018 (flash communication)

5. Annalaura Cordaro, Roberto Zagami, Angela Scala, Antonino Mazzaglia, Anna Piperno. *Supramolecular nanoassemblies based on hyaluronic acid and polymeric cyclodextrins as therapeutic platforms*. Congresso congiunto delle sezioni Sicilia e Calabria 2019, Palermo, 1-2 marzo 2019 (oral communicatotion, OC16 p. 42)

6. Annalaura Cordaro, Antonino Mazzaglia, Roberto Zagami, Angela Scala, Anna Piperno. *Supramolecular assemblies as injectable hydrogel for ostheoartritis treatment***.** 4th International Symposium on Organic Chemistry (CISOC), Bologna, 16-17 aprile 2019 (poster presentation, PC13 p. 91).

7. Annalaura Cordaro, Roberto Zagami, Milo Malanga, Angela Scala, Anna Piperno, Antonino Mazzaglia. *Cyclodextrin-based nanoassemblies as therapeutic scaffolds for the treatment of inflammatory diseases***.** 4th International School on Cyclodextrins, Milano, 10-12 giugno 2019 (poster presentation, P15)

8. A. Cordaro, R. Zagami, A. Scala, A. Mazzaglia, A. Piperno. *Nanoplatforms based on hyaluronic acid and β-cyclodextrins for the treatment of osteoarticular diseases*. II Convegno DOCTOCHEM – UNIME, Messina, 5 luglio 2019 (oral communication)

9. Annalaura Cordaro, Roberto Zagami, Eva Fenyvesi, Milo Malanga, Angela Scala, Magali Cucchiarini, Carmen Alvarez-Lorenzo, Anna Piperno and Antonino Mazzaglia. *Novel cyclodextrin-based nanoplatforms for the treatment of osteoarthritis*. 6th European Conference on Cyclodextrins (EUROCD 2019) – Santiago de Compostela (Spain), 2-4 ottobre 2019 (flash communication F25; poster PO 25)

Awards:

Premio poster da parte di "Giotto Biotech S.r.L" al convegno "4th International Symposium on Organic Chemistry (CISOC)", Bologna 16-17 Aprile 2019

Participation in research projects:

- MatISSE "Materiali innovativi e sostenibili per la Salute e l'Energia"
- BiLiGeCT "Biopsie Liquide per la gestione clinica dei tumori"
- "Drug delivery: veicoli per un'innovazione sostenibile"

Ringraziamenti

Sono poche le occasioni in cui si ha la possibilità di dire pubblicamente “grazie” ad una lunga serie di persone che, in modo più o meno decisivo, mi hanno aiutato ad arrivare al termine di questo percorso.

Innanzitutto voglio ringraziare i miei relatori, la cui guida costante ed i preziosi consigli sono stati per me un supporto essenziale, non soltanto dal punto di vista lavorativo e professionale, ma anche personale.

Ringrazio inoltre tutti i gruppi di ricerca e i laboratori senza i quali il concreto svolgimento di questo lavoro non sarebbe stato possibile, in particolare il CNR-ISMN, sedi operative di Messina e Palermo, che grazie al progetto MatISSE mi ha concesso di entrare a far parte, seppur per breve tempo, di questa realtà; in ultimo, ringrazio il mio team e i colleghi dell’Università di Messina.

Infine un doveroso grazie va alla mia famiglia e a tutti quegli amici che ci sono sempre stati.

Spero che questo lavoro di tesi non sia per me un punto di arrivo, bensì di partenza.

“Success doesn’t rush. The greatest reward is the journey!” (O. Wilde)